GPO PRICE $ _____

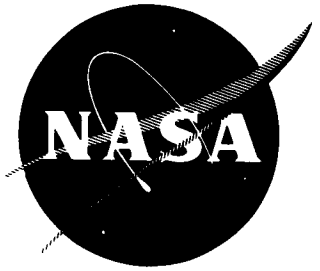
CFSTI PRICE(S) $ _____

Hard copy (HC) 3.00

Microfiche (MF) .65

ff 653 July 65

NASA CR-54871



THIOKOL 260-SL CASE DEVELOPMENT PROGRAM

prepared for

NATIONAL AERONAUTICS AND SPACE ADMINISTRATION

CONTRACT NAS 3-6285

FACILITY FORM 602

N68-16477 (ACCESSION NUMBER)

52 (PAGES)

CR-54871 (NASA CR OR TMX OR AD NUMBER)

1 (THRU)

(CODE)

08 (CATEGORY)

MAR 1968

RECEIVED

NASA STI FACILITY

INPUT BRANCH

THIOKOL CHEMICAL CORPORATION

Space Booster Division

Brunswick, Georgia

CR-54871

260-SL CASE DEVELOPMENT PROGRAM

18 JAN 1966

Distribution of this report is provided in the interest of information exchange. Responsibility for the contents resides in the author or organization that prepared it.

Prepared Under Contract No. NAS 3-6285 By
THIOKOL CHEMICAL CORPORATION
Space Booster Division
Brunswick, Georgia

for Lewis Research Center

NATIONAL AERONAUTICS AND SPACE ADMINISTRATION

NOTICE

This report was prepared as an account of Government sponsored work. Neither the United States, nor the National Aeronautics and Space Administration (NASA), nor any person acting on behalf of NASA:

A.) Makes any warranty or representation, expressed or implied, with respect to the accuracy, completeness, or usefulness of the information contained in this report, or that the use of any information, apparatus, method, or process disclosed in this report may not infringe privately owned rights; or

B.) Assumes any liabilities with respect to the use of, or for damages resulting from the use of any information, apparatus, method or process disclosed in this report.

As used above, "person acting on behalf of NASA" includes any employee or contractor of NASA, or employee of such contractor, to the extent that such employee or contractor of NASA, or employee of such contractor prepares, disseminates, or provides access to, any information pursuant to his employment or contract with NASA, or his employment with such contractor.

Requests for copies of this report should be referred to

National Aeronautics and Space Administration
Office of Scientific and Technical Information
Attention: AFSS-A
Washington, D.C. 20546

TABLE OF CONTENTS

		Page
List of Illustrations		iv
List of Tables		vii
I	SUMMARY AND CONCLUSIONS	1
II	OBJECTIVES	2
III	TOOLING	4
IV	FABRICATION	16
	A Fabrication Sequence	16
	1 Domes	16
	2 Y-Rings	20
	3 Cylinder Sections	20
	B Materials	
	1 Plates	20
	2 Forgings	28
	3 Material Properties	28
	4 Welding	30
	5 Thermal Processing	58
	6 Machining, Drilling, and Tapping	66
V	NONDESTRUCTIVE TESTING	69
	A Procurement Inspection	69
	1 Plate	69
	2 Forgings	69
	3 Processing Material	69
	4 Critical Tooling	70

TABLE OF CONTENTS (Cont'd)

		Page
B	Fabrication and Process Quality Control	70
1	General Defects	70
2	Surface Acceptance Criteria	70
3	Laminar Defects	70
4	Nonlaminar Defects	76
5	Radiographic Equipment and Procedure	76
6	Ultrasonic Equipment and Procedures	77
7	Discussion	78
VI	HYDROTEST	82
A	Summary	82
B	Purpose and Objectives	82
C	Test Configuration	82
D	Hydrotest Tooling and Handling Equipment	82
1	Hydrotest Adapter	82
2	Piston	83
3	Hydrotest Tower	83
4	Handling Equipment	83
5	Pressurization System	85
E	Instrumentation	85
1	Pressure Measurements	85
2	Strain Measurements	88
3	Accelerometers	88
F	Test Procedure	89
1	Test Procedure Documents	89
2	Deviations from Specified Procedure	89

TABLE OF CONTENTS (Cont'd)

		Page
G	Comparison of Predicted Performance with Test Data	89
	1 Pressure	89
	2 Strain and Stress	89
APPENDIX - NASA Failure Report		100

LIST OF ILLUSTRATIONS

Figure		Page
1	Longitudinal Section of Motor 260-SL-1	3
2	Formed 260-SL Forward Gore in Finishing Die Set	10
3	Fixture for Machining OD Welds on 260-SL Gores	11
4	Use of Folding-Leg Spider and Belly Band Fixtures on 260-SL Case Sections	12
5	Forward and Upper 260-SL Case Segments on Mandrel Positioned for Circumferential Welding	13
6	Inside and Outside Surfaces Welding Fixture Supporting 156-2C-1 Case Dome during Welding Operations	14
7	156-2C-1 Cylindrical Section Showing Spider and Mandrel Arrangement	15
8	Exploded View of 260-SL-1 Case	17
9	Revised 260-SL Case Y-Ring Configuration	21
10	Typical Micropitting of Plate Parent Material following Re-Solution Annealing (100 X)	27
11	Joint Configurations for 0.477-In. and 0.73-In. Submerged Arc Weld Specimens	32
12	Net Fracture Stress versus Crack Length of 0.73-In. Qualification Submerged Arc Welds (Code No. PA-1 through PA-4)	33
13	Comparative Fracture Toughness Values for 3/4-in.-Thick Panel and Mockup Welds	35
14	Titanium Content of Weld versus Fracture Toughness	36
15	Comparison of Weld Bead Configuration Using Straight Polarity and Reverse Polarity Techniques	38
16	Round and Flat Test Specimen Configurations	40
17	Crack Size Versus Net Fracture Stress in Aged 0.48- and 0.73-in. Thick Submerged Arc Welds	41
18	Transverse Section of 1/2-In. Thick, Two-Pass Submerged Arc Weld Using Improved Weld Parameters (2 X)	43

LIST OF ILLUSTRATIONS (Cont'd)

Figure		Page
19	Transverse Section of 3 [illegible]. Thick, Two-Pass Submerged Arc Weld Us[illegible]mproved Weld Parameters (2 X)	43
20	Crack Size versus Net Fracture Stress in Submerged Arc Welds Made Using Low-Titanium Weld Wire	44
21	Typical Weld Joint Configurations for 260-SL Cases	45
22	Fracture Toughness Evaluation of Multipass TIG Qualification Weld	48
23	Weld Crack Located in the Longitudinal Microspecimen (Mag: 100X and Etchant: Kroll's Reagent)	49
24	Transverse Section of 3/4-In. Thick, Two-Pass Submerged Arc Weld (2 X)	52
25	Transverse Section of 3/4-In. Thick, Two-Pass Submerged Arc Weld Repaired Using Multipass Weld Method (2 X)	52
26	Crack Size versus Net Fracture Stress of Specimens Taken from Heat-Affected Zone of TIG Repair Weld	53
27	Fracture Toughness Evaluation of Vertical-Submerged-Arc Qualification Weld	55
28	Effect of Solution Annealing Temperature on Aged Tensile Properties of 18-Percent Nickel Maraging Steel (250-ksi Grade)	59
29	Y-Ring Segment Dimensions Taken during Component Shrinkage Evaluation	60
30	Scrap Plate Dimensions Taken During Component Shrinkage Evaluation	61
31	Weld Fracture Toughness and Yield Strength versus Aging Temp	64
32	Fracture Toughness of Locally Aged Welded Panels	65
33	Drilling 156-2C-1 Case Joint Ring	67
34	Machining 260-SL-1 Case Aft Attach Flange in Aged Condition	68

LIST OF ILLUSTRATIONS (Cont'd)

Figure		Page
35	Diagram of Typical Fabrication and Inspection Flow	79
36	260-SL-1 Case in Hydrotest Tower	84
37	Schematic Diagram of Pressurization System	86
38	Location of Strain Gages	87
39	Planned and Actual Pressure Cycles	90
40	Predicted Strain and Stress Levels	91
41	Forward Dome Stresses	94
42	Forward Y-Ring Stresses at 500 PSIG	95
43	Cylinder Stresses	96
44	Aft Y-Ring Stresses at 500 PSIG	98
45	Nozzle Attach Flange Stresses	99

LIST OF TABLES

Table		Page
I	Tooling Drawings for 260-SL Cases	5
II	Identification of 260-SL-1 Case Components	18
III	Typical Mechanical Properties of a Four-Inch-Thick Rolled Plate	23
IV	260-SL-1 Case Aft Attach Flange Tensile Properties	24
V	260-SL-1 Case Aft Attach Flange Impact Properties	24
VI	Tensile Test Results of Various 1-7/8-Inch Thick Plate Conditioning Cycles (Phase I)	25
VII	Tensile Properties of 260-SL-1 Case Parent Material Specimens after Production Aging	29
VIII	Joint Design and Typical Welding Data for Welding the Carbon-Steel Segment Test Panels	34
IX	Improved Weld Parameter Data for Two-Pass Submerged-Arc Welds Parametric Investigation	39
X	Weld Parameters of TIG Qualification Weld	47
XI	Bead Sequence and Welding Data of Multipass TIG Welds Repair Investigation	51
XII	Weld Parameters of Vertical-Submerged-Arc Qualification Weld	54
XIII	Mechanical and Fracture Toughness of 260-SL-1 Production Aged Welds	56
XIV	Electric versus Kerosene Furnace Tensile Specimen Test Results	63
XV	Material Discrepancies during 260-SL-1 Case Fabrication	71
XVI	Welding Wire Discrepancies for 260-SL-1 Case	75
XVII	Dimensional Discrepancies Found in 260-SL-1 Case	81
XVIII	Measured Strains and Stresses at 500 PSIG	93

I. SUMMARY AND CONCLUSIONS

The 260-SL-1 case was designed and fabricated using the monolithic roll-and-weld fabrication concept. The case material selected and used was air melt, 18-percent nickel maraging steel (250-ksi grade).

Hydrostatic pressure test of the case resulted in a catastrophic failure at approximately 56 percent of proof pressure. Failure was initiated at one or both of two weld defects in a longitudinal seam in the aft cylinder. (See Appendix - NASA Failure Report.)

Work in conjunction with failure analysis shows that submerged arc welding as performed under this program does not provide adequate fracture toughness for large rocket motor cases using 250-ksi grade maraging steel.

Evaluation of all test data generated in the case material acceptance phase indicated that the maraging steel which meets essential requirements of specification SB-SP-174, using either air melt or vacuum arc remelt techniques, can be produced on a production basis.

A review of all the tests performed in this program shows that the most useful tests employed in determining usability of materials were (1) partial-thickness-crack (PTC) tensile tests, (2) metallographic examination, and (3) the standard mill tests (tensile, elongation, chemistry, cleanliness, ultrasonic, etc.). However, a review of related programs indicates that the slow bend test more adequately defines the material fracture toughness than the partial-thickness-crack tensile test and should be used in future programs in lieu of PTC tests.

Banding of 250 grade 18-percent nickel maraging steel was common and was associated with retained austenite bands which usually contain massive bands of inclusions (primary titanium carbonitrides). If heavy, closely connected inclusions are present, the material will crack when fatigued at relatively few cycles and medium (160,000 psi) stress levels. In addition, the presence of many inclusions will cause the material to delaminate when locally heated to near the fusion temperature.

The soft tooling used controlled part contour within expected limits. More recent studies of the effect of contour on stresses do, however, indicate the desirability of using hard tooling to improve contour.

II. OBJECTIVES

The general objective of the 260-inch diameter motor demonstration program was to demonstrate the feasibility of fabricating a 260-inch diameter solid rocket motor case using state-of-the-art fabrication techniques. The technology gained was to be directly applicable to the development of full length, 260-inch diameter (or larger) motors. This program was conducted initially for the Air Force per contract AF 04(695)-351; and continued under National Aeronautics and Space Administration contract NAS 3-6285.

Initially, the 260-inch motor demonstration program was preceded by the design, fabrication, and testing of a 156-inch diameter segmented case made from 0.48-in. and 0.73-in. thick, 18-percent nickel maraging steel (250-ksi grade). This case, fabricated by Excelco Developments, Inc. using the TIG (tungsten electrode, inert gas) welding process, withstood hydrotest pressures of 960 psig and a maximum static firing pressure of 727 psia.

Design, fabrication, and testing of the 260-SL-1 case was intended to be a minimum risk, conservative program based on a case safety factor of 1.3. The 260-SL-2 case was then to be fabricated using the same general dimensions and techniques, but having thinner case walls to reduce the safety factor from 1.3 to 1.2. A longitudinal cross-section of the 260-SL-1 motor is shown in Figure 1. The following tasks and problem areas were also to be resolved during the 260-inch diameter motor demonstration program:

1. Design and stress analysis of a pressure vessel of the large solid booster class
2. Procurement of plate and forgings having adequate properties
3. Development and determination of welding and weld repair procedures and schedules
4. Determination of optimum thermal processing cycles
5. Development of nondestructive techniques and procedures
6. Design and fabrication of soft tooling

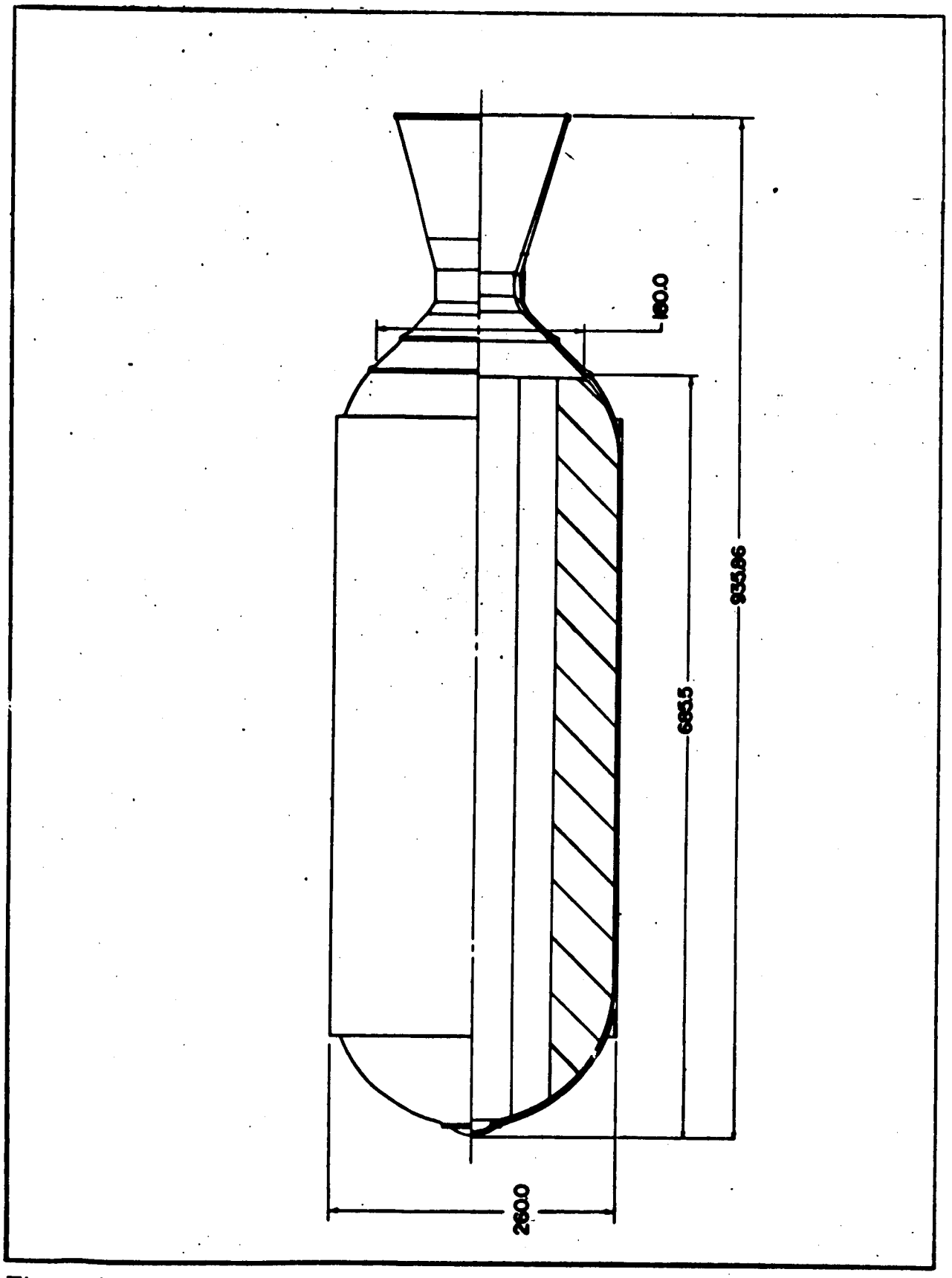


Figure 1 - Longitudinal Section of Motor 260-SL-1

III. TOOLING

The original case tooling concept for 260-inch diameter case fabrication called for hard, refined, and elaborate tooling. However, because of funding limitations, this concept was changed. The 260-inch tooling was then designed much the same as the soft tooling used successfully for fabrication of the 120-inch and 156-inch diameter cases.

There are approximately 100 top drawings concerning 260-inch case tools and planning for tools. A complete listing of these drawings by number and titles is included as Table I. Figures 2 through 5 show some of the major items of tooling used for 260-inch diameter case fabrication. For comparison, Figures 6 and 7 show comparable 156-inch diameter case tooling.

Using this tooling, the following typical tolerances were achieved in fabricating the 260-SL cases:

Longitudinal weld mismatch	
Dome	0.015 in.
Cylinder	0.010 to 0.020 in.
Circumferential weld mismatch	0.020 to 0.025 in.
Nominal out-of-contour at	
Longitudinal cylinder welds	0.062 in.
Longitudinal gore welds	0.045 in.

The techniques and soft tooling used to fabricate the 260-SL cases were sufficient to produce a dimensionally acceptable product. However, the out-of-contour condition encountered in some welds needs to be improved. Longitudinal weld control can be improved after welding by either rolling the cylinder or by forming the weld area in a press brake.

The soft tooling used controlled part contour within expected limits. More recent studies of the effect of contour on stresses do, however, indicate the desirability of using hard tooling to improve contour.

TABLE I

TOOLING DRAWINGS FOR 260-SL CASES

Drawing No.	Drawing Title	Applicable Case 260-SL-1	260-SL-2
ST 10501B	Finishing Die for Head Gore Arrangement	X	X
ST 10502B	Finishing Die for Head Gore Details	X	X
ST 10503A	Roughing Die for Head Gore Arrangement	X	X
ST 10504A	Roughing Die for Head Gore Details	X	X
ST 10505B	Spreader Beams for Lift Flat Plate and Half Shell	X	X
ST 10506A	Soft Nose Lifting Clamp	X	X
ST 10507C	Strongbacks for Clamping Shell Plates on 40-ft Planer	X	X
ST 10508B	Belly Band	X	X
ST 10509A	Support Fixture for Chip Side Gore Plates	X	X
ST 10510	Side Beam Track and Stand	X	X
ST 10511	Folding Spider Arrangement	X	
ST 10512B	Folding Spider Details	X	
ST 10513A	Stiff Leg Spider Arrangement and Details	X	
ST 10514D	Layout Mold for Gore Plates (Sheet 1)	X	X
ST 10515C	Layout Mold for Gore Plates (Sheet 2)	X	X
ST 10516C	Layout Mold for Gore Plates Strongbacks	X	X
ST 10517A	Lifting Rollers for Cylindrical Sections	X	X
ST 10518A	Lifting Rollers for Cylindrical Sections	X	X
ST 10519B	Hydrostatic Test - Test Tower Structure Steel Erection Plan	X	X
ST 10520	Hydrostatic Test Arrangement	X	X
ST 10521A	Assembly Mandrel	X	
ST 10522A	Mandrel Bearing	X	X
ST 10523	Gore Layout Fixture Angle Plate Extension	X	X
ST 10524	Forward Enclosure Assembly Outside Weld Arrangement	X	X
ST 10525A	Aft Enclosure Assembly Outside Weld Arrangement	X	X
ST 10526A	Forward and Aft Enclosure Assembly Weld Fixture	X	X
ST 10527D	Forward and Aft Enclosure Assembly Fixture F-1 for External Weld Arrangement and Details	X	X
ST 10528B	Forward and Aft Enclosure Assembly Fixture F-2 for External Weld Arrangement and Details	X	X
ST 10529	Forward and Aft Enclosure Assembly Fixture F-1 and F-2	X	
ST 10530A	Forward and Aft Enclosure Assembly Fixture F-1, F-2, F-3 Clamping Ring and Brackets	X	X
ST 10531A	Aft Enclosure Assembly Fixture F-3 for External Weld	X	X
ST 10532	Lifting Beam and Spreaders for Hand Motor Case	X	X
ST 10533	Longitudinal Weld Pre Y-Ring	X	
ST 10534	Y-Ring Longitudinal Weld Support Fixture	X	
ST 10535	Y-Ring Longitudinal Weld Support Fixture	X	
ST 10536	Aligning Fixture for Spiders, Arrangement	X	
ST 10537B	Aligning Fixture for Spiders Details	X	X

TABLE I (Cont'd)

TOOLING DRAWINGS FOR 260-SL CASES

Drawing No.	Drawing Title	Applicable Case 260-SL-1	260-SL-2
ST 10538B	Hydrostatic Test-Test Tower Skirt Support	X	X
ST 10539	Weld Gore Joints Inside, General Arrangement	X	X
ST 10540B	Fixture for Weld Gore	X	X
ST 10541B	Fixture for Weld Gore	X	X
ST 10542	Fixture for Weld Gore Joints, Inside Details of Support Band	X	X
ST 10543A	Fixture for Weld Gore	X	X
ST 10544	Weld Gore Joints, Inside Bearing Support	X	X
ST 10545	Aft Gore Assembly Lift Ring-Positioner Pig Jack Stands	X	
ST 10546A	Forward Gore Assembly - Lifting Ring	X	X
ST 10547	Nozzle Attach Flange, Longitudinal Weld	X	X
ST 10548A	Nozzle Attach Flange, Longitudinal Weld Support Fixture	X	X
ST 10549	Nozzle Attach Flange, Longitudinal Weld Support Fixture	X	X
ST 10551B	Forward Closure Attach Ring and T Template	X	X
ST 10552	Vent Subarc Water Cooled Nozzle	X	X
ST 10553	Circumferential Joint Insulation Arrangement	X	X
ST 10554A	Clamp Block for Gore Plate Layout Fixture	X	X
ST 10555	Trace and Check Temperature for Aft Nozzle Attach Flange	X	X
ST 10600	Equalizer and Links Lift Motor Case	X	X
ST 10601	Forward Enclosure Inside Circumferential Weld Support Fixture	X	X
ST 10602	Forward Closure and Attach Flange	X	X
ST 10603B	Forward Closure Attach Ring Machining Fixture	X	X
ST 10604	Aft Enclosure Inside Circumferential Weld Support Fixture	X	X
ST 10605	Y-Ring Machining Fixture	X	X
ST 10606	Mandrel Pedestal	X	X
ST 10607	Assembly Turning Rolls - Arrangement	X	X
ST 10608B	Hydrostatic Test - Test Tower - Upper and Lower Block Details	X	X
ST 10609	Extension Beams on Manipulator	X	X
ST 10610	Nozzle Attach Flange - Machining	X	X
ST 10611A	Nozzle Attach Flange - Machining	X	X
ST 10612	Forward and Aft Enclosure Machining at Equator	X	X
ST 10613	Weld Inside Circumferential Joint - Flux Recovery Unit Support	X	X
ST 10614C	Nozzle Attach Ring Trace and Check Temperature	X	
ST 10615	Assembly Turning Rolls Details	X	X
ST 10616	Side Beam Weld Fixture	X	X
ST 10617	Side Beam Weld Fixture - Details	X	X
ST 10618	Side Beam Weld Fixture - Detail and Section	X	
ST 10619B	Hydrostatic Test - Test Tower Sheave, Arrangement and Details	X	X
ST 10620A	Tie Bolts, Align - Blocks Welds Skirt Assembly	X	X
ST 10621	Inside Circumferential Joint Weld Head Control	X	X

TABLE I (Cont'd)

TOOLING DRAWINGS FOR 260-SL CASES

Drawing No.	Drawing Title	Applicable Case 260-SL-1	260-SL-2
ST 10622A	Trunnion Stand, General Arrangement	X	X
ST 10623C	Trunnion Stand, Details	X	X
ST 10624C=	Forward and Aft Centering Ring	X	X
ST 10625	Location for Gore Layout Fixture, Arrangement and Details	X	X
ST 10626B	Hydrostatic Test - Test Tower Structural Steel Girders and Eye Bar Details	X	X
ST 10627A	Dies for Gripping Tensile Test Specimen	X	X
ST 10628	Hydrostatic Test - Test Tower - Structural Steel Column and Beam Details	X	X
ST 10629	Weld Inside Circumferential Joint with Mandrel, General Arrangement	X	X
ST 10630	Inside Circumferential Joint with Mandrel Reel and Track	X	X
ST 10631A	Inside Circumferential Joint with Mandrel Arm and Details	X	X
ST 10632	Weld Inside Circumferential Joint with Mandrel Wire Handling Reel	X	X
ST 10633A	Inside Circumferential Joint with Mandrel Gear Box and Details	X	X
ST 10634	Weld Inside Circumferential Joint with Mandrel Column and Miscellaneous Details	X	X
ST 10635	Weld Inside Circumferential Joint with Mandrel Roller, Arrangement and Details	X	X
ST 10636A	Mandrel Guide Pedestal, Arrangement	X	X
ST 10637A	Mandrel Guide Pedestal, Details	X	X
ST 10638	Turning Stand, Arrangement and Details	X	X
ST 10639A	Containers for A-Blanks and Specimens	X	X
ST 10640	Cylindrical Leveling Block, Arrangement and Details	X	X
ST 10641	Machining of Gore Plate Meridians, General Arrangement	X	X
ST 10642A	Machining of Gore Plate Meridians, Support Fixture	X	X
ST 10643A	Machining of Gore Plate Meridians	X	X
ST 10644	B-Containers of Blanks and Specimens	X	X
ST 10645	Hydrostatic Test - Test Tower - Structural Steel - "X" Brace Details	X	X
ST 10646	Hydrostatic Test - Test Tower Foundation - Reinforcing Steel Details	X	X
ST 10647	D-Containers for Blanks and Specimens	X	X
ST 10648	Lifting Beam for Removing Seam Weld Clamp Arrangement and Details	X	X
ST 10649C	Hydrostatic Test - Test Tower - Foundation Concrete and Imbedded Details	X	X
ST 10650	Hydrostatic Test - Test Tower Structural Sections and Details	X	X
ST 10651A	Gore Plate Annealing Fixture	X	X
ST 10652	Plant Engineers' Tooling Drawing (Sheet 1)	X	X
ST 10653	Plant Engineers' Tooling Drawing (Sheet 2)	X	X
ST 10654	Plant Engineers' Tooling Drawing (Sheet 3)	X	X
ST 10655	Plant Engineers' Tooling Drawing (Sheet 4)	X	X
ST 10656	Plant Engineers' Tooling Drawing (Sheet 5)	X	X

TABLE I (Cont'd)

TOOLING DRAWINGS FOR 260-SL CASES

Drawing No.	Drawing Title	Applicable Case 260-SL-1	260-SL-2
ST 10657	Plant Engineers' Tooling Drawing (Sheet 6)	X	X
ST 10658	Plant Engineers' Tooling Drawing (Sheet 7)	X	X
ST 10659	Plant Engineers' Tooling Drawing (Sheet 8)	X	X
ST 10660	Tooling Plan Drawings (Sheet 1)	X	X
ST 10661	Tooling Plan Drawings (Sheet 2)	X	X
ST 10662	Tooling Plan Drawings (Sheet 3)	X	X
ST 10663	Tooling Plan Drawings (Sheet 4)	X	X
ST 10664	Tooling Plan Drawings (Sheet 5)	X	X
ST 10665	Tooling Plan Drawings (Sheet 6)	X	X
ST 10666	Tooling Plan Drawings (Sheet 7)	X	X
ST 10667	Tooling Plan Drawings (Sheet 8)	X	X
ST 10668	Tooling Plan Drawings (Sheet 9)	X	X
ST 10669A	Forward and Aft Sections Lifting Rig	X	X
ST 10670	Alteration to Finishing Die for Head Gore	X	X
ST 10671	Sleeve for Lifting Mandrel	X	X
ST 10672	Outside Circumferential Weld Fixture	X	X
ST 10673	Outside Circumferential Weld Fixture	X	X
ST 10674	Forward Closure and Attach Flange Drill Rig (Sheet 1)	X	X
ST 10675	Forward Closure and Attach Flange Drill Rig (Sheet 2)	X	X
ST 10676	Forward Closure and Attach Flange Drill Rig (Sheet 3)	X	X
ST 10677J	Hydrotest Nozzle Adapter Assembly and Details	X	X
ST 10678B	Hydrotest Piston, Arrangement and and Details	X	X
ST 10680	Forward Subassembly - Item 5, Tracing and Checking Templates		X
ST 10681B	Arrangement and Details for Drilling Nozzle	X	X
ST 10682	Mandrel Dolly, Arrangement and Details	X	X
ST 10683C	Hydrostatic Test - Test Tower - Girder	X	X
ST 10684A	Nozzle Attach Flange Drill Rig (Sheet 1)	X	X
ST 10685A	Nozzle Attach Flange Drill Rig (Sheet 2)	X	X
ST 10686	Hydrotest Main Hoist Winch Foundation	X	X
ST 10687	Spider with Folding Segments	X	X
ST 10688A	Nozzle Assembly Lifting Sheaves	X	X
ST 10690	Hydrotest Tower - Grit Blast Platform Arrangement	X	X
ST 10691	Hydrotest Tower - Grit Blast Platform Details	X	X
ST 10692A	Forward Closure Attach Ring	X	X
ST 10693	Arrangement for Mandrel Removal	X	X
ST 10694	Case Loaded on Railroad Car	X	X
ST 10696	Fixture for Welding Skirt Assembly, Arrangement	X	X
ST 10697	Fixture for Welding Skirt Assembly, Details	X	X
ST 10698	Hydrostaging Instrumentation and Inspection	X	X
ST 10699	Motor Case Transporting Center Sub-assembly	X	X
ST 10707D	Hydrostatic Test Layout Pump and Piping	X	X
ST 10708F	Hydrostatic Test Pumping Station	X	X
ST 10709E	Hydrostatic Test Tower Piping		

TABLE I (Cont'd)

TOOLING DRAWINGS FOR 260-SL CASES

Drawing No.	Drawing Title	Applicable Case 260-SL-1	260-SL-2
ST 10710C	Hydrostatic Test Tower Piping Plan and Electrical	X	X
ST 10711C	Hydrostatic Test, Miscellaneous	X	X
ST 10712	Tracing and Checking Template for Aft Nozzle and Aft Ring	X	X
ST 10714	Lifting Spider, Forward Gore Assembly	X	X
ST 10716	Lifting Rig for Handling Forward and Aft Enclosure Assembly	X	X
ST 10717	Nozzle Attach Flange Drill Rig (Sheet 1)	X	X
ST 10718	Nozzle Attach Flange Drill Rig (Sheet 2)	X	X
ST 10719	Hydrotest Main Hoist Electrical Equipment	X	X
ST 10720	Forward Closure Weld Fixture	X	X
ST 10721	Hydrotest Access Ladder to Staging	X	X
ST 10722A	Nozzle Attach Ring Check Template		X
ST 10723	Protective Covering Foundation	X	X
ST 10724A	Wiring for Strain Gages	X	X
ST 10725	Roof for Protective Covering and Details	X	X
ST 10726	Protective Covering Bracking, Arrangement	X	X
ST 10727	Protective Covering Bracking, Details	X	X
ST 10728	Protective Covering, Arrangement	X	X
ST 10729	Protective Covering Opening for Motor Case	X	X
ST 10756	Cribbing for Transporting Sub-assemblies	X	X
ST 10757	Nozzle Attach Flange Drill Rig (Sheet 3)	X	X
ST 10800A	Name Plate for Tooling Equipment	X	X

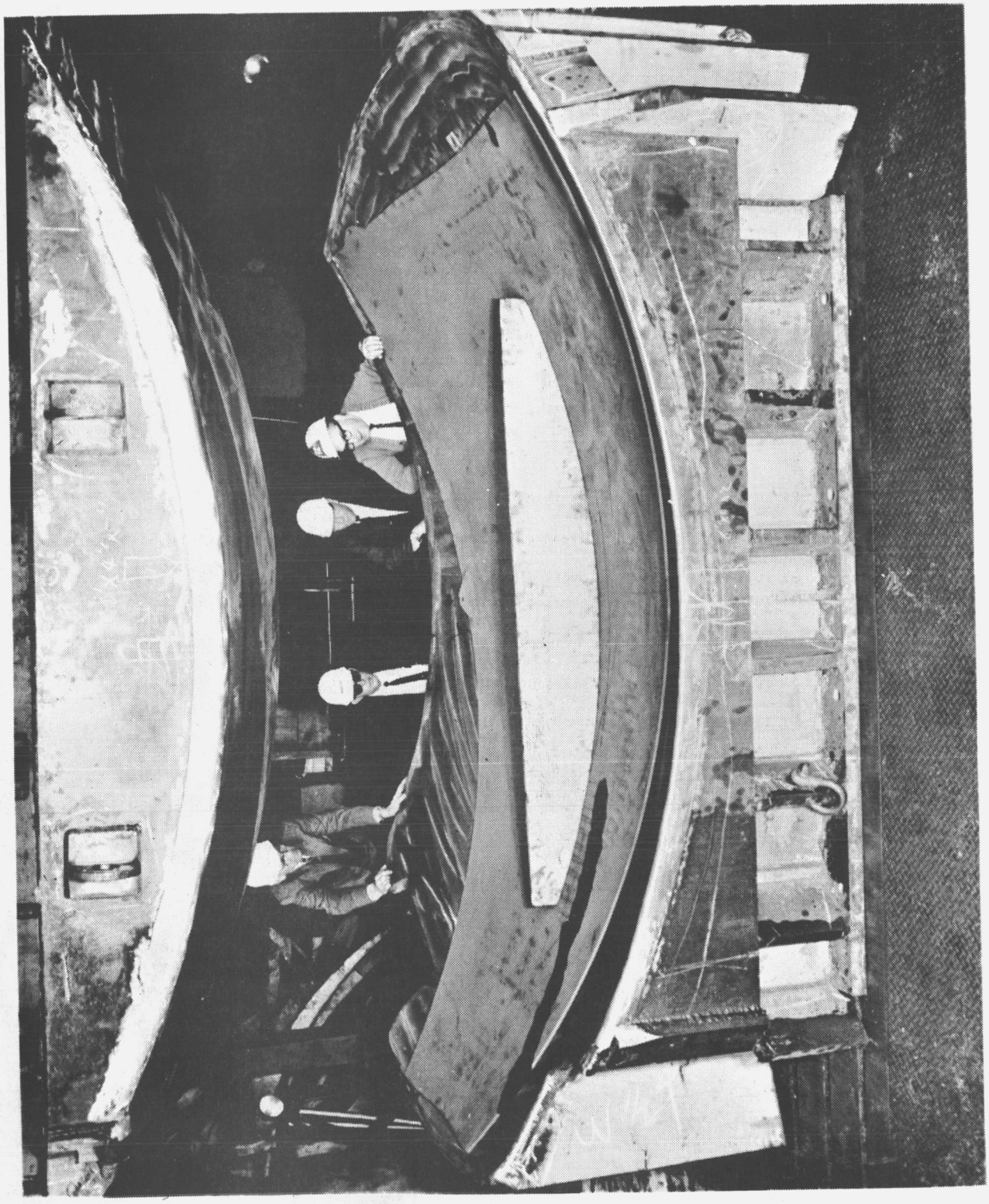


Figure 2 - Formed 260-SL Forward Gore in Finishing Die Set

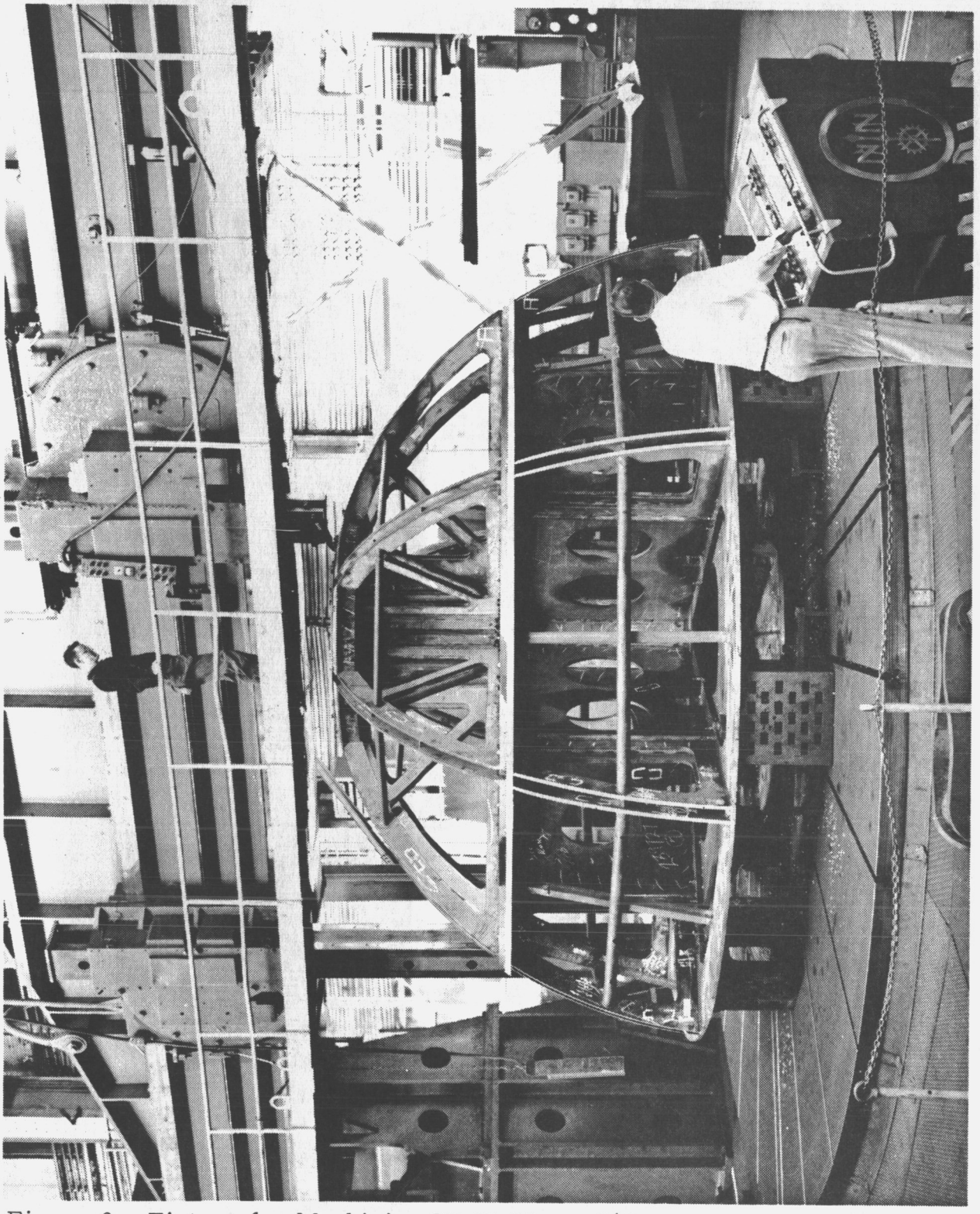


Figure 3 - Fixture for Machining OD Welds on 260-SL Gores

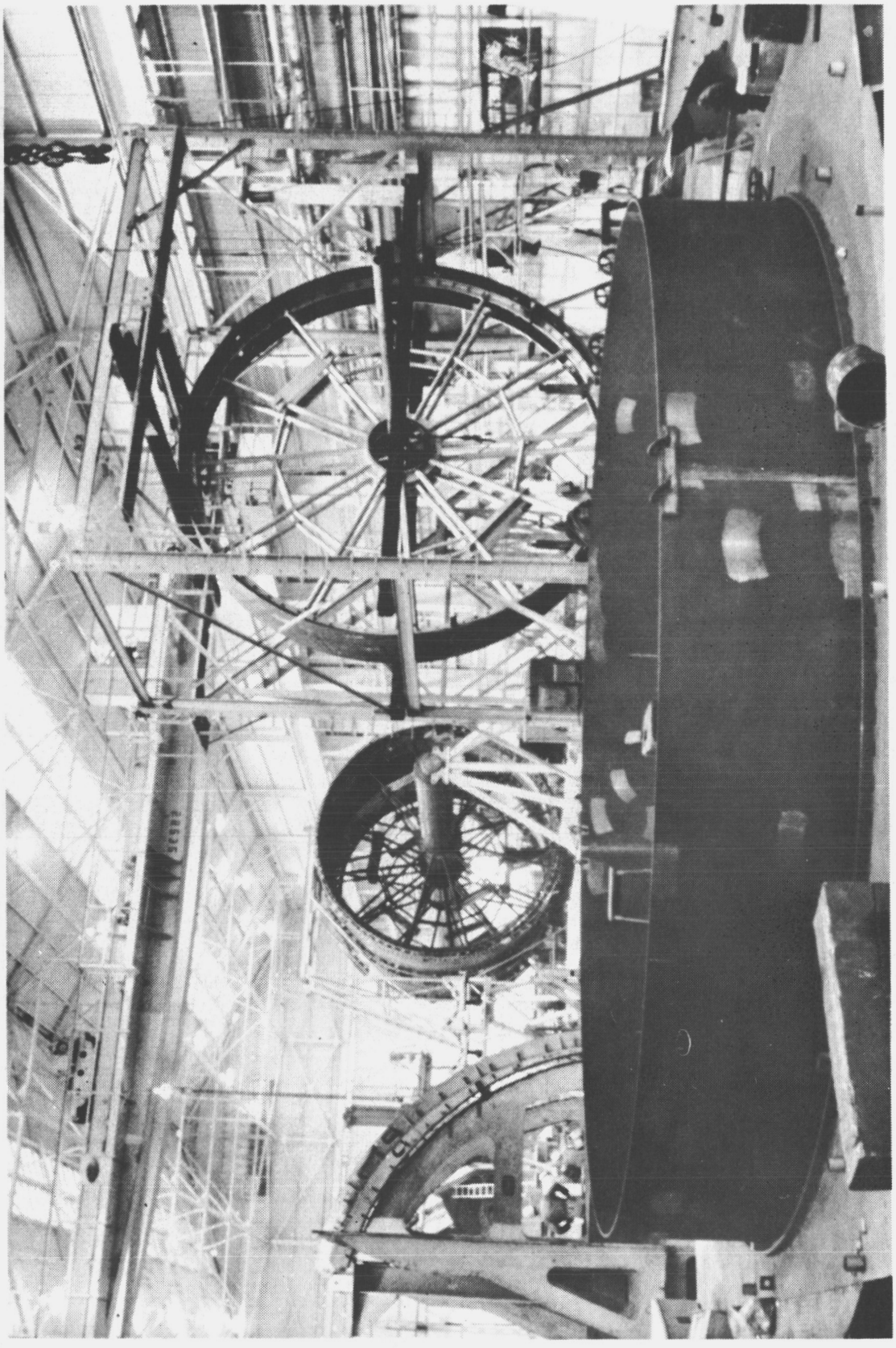


Figure 4 - Use of Folding-Leg Spider and Belly Band Fixtures on 260-SL Case Sections

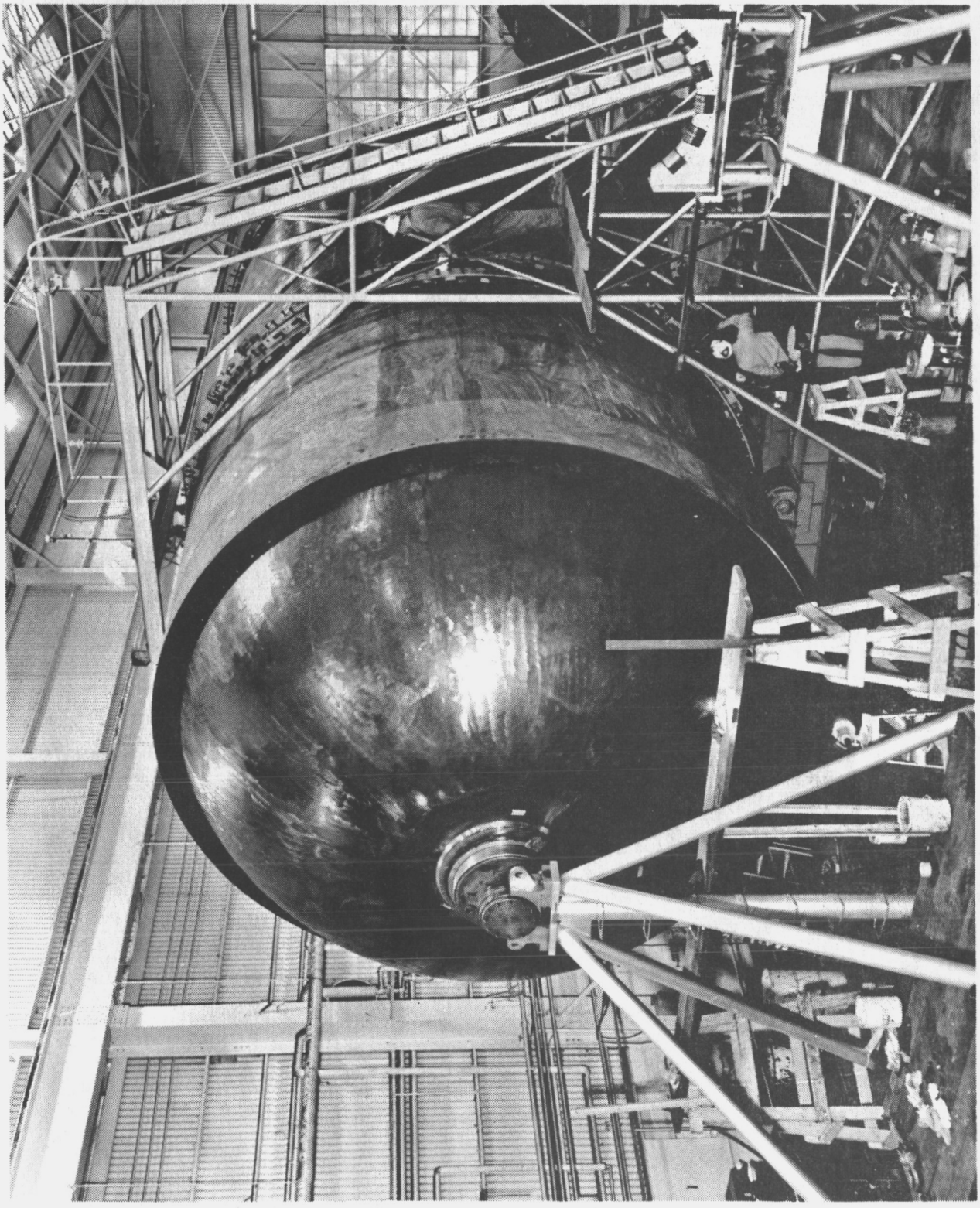


Figure 5 - Forward and Upper 260-SL Case Segments on Mandrel Positioned for Circumferential Welding

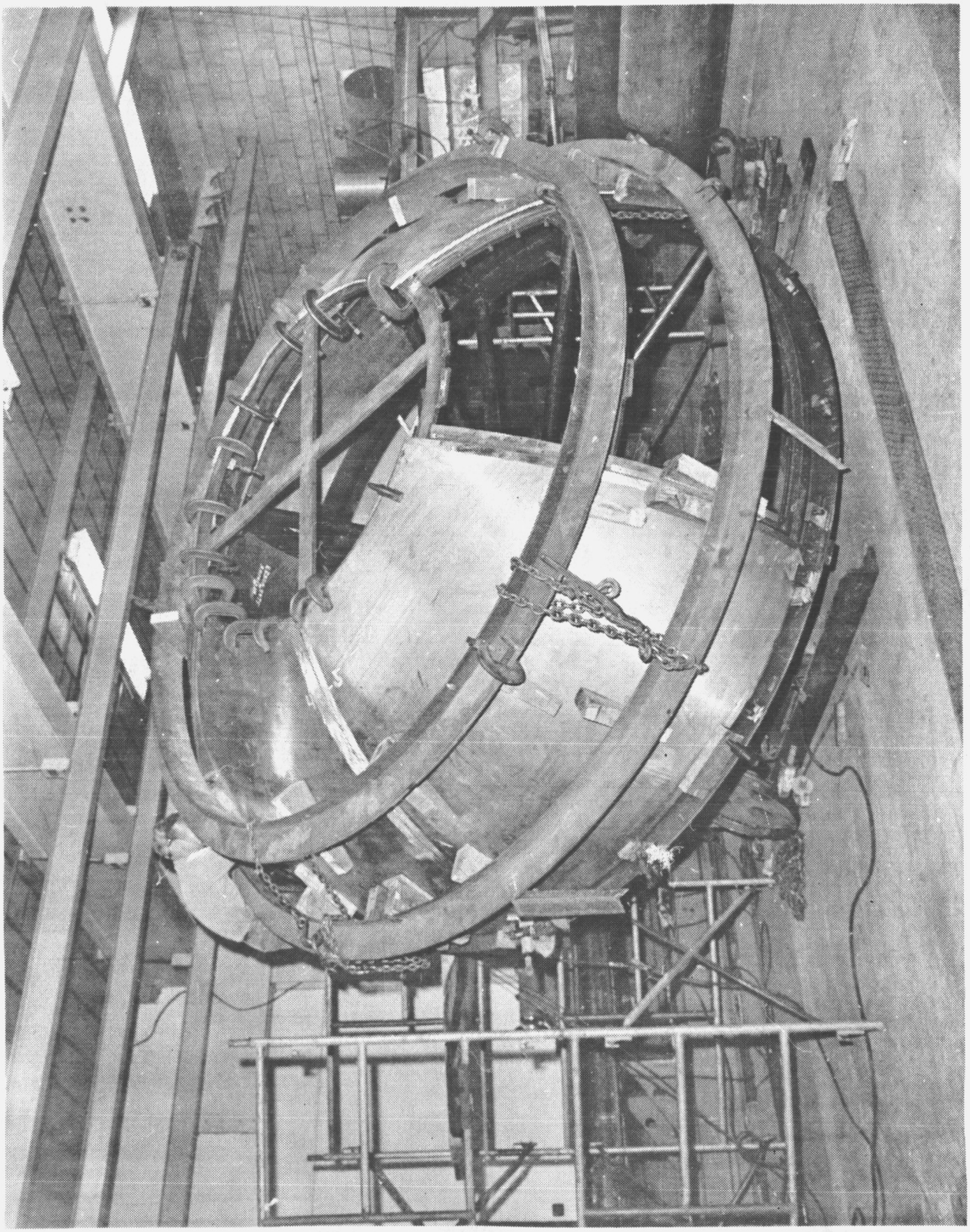


Figure 6 - Welding 156-2C-1 Dome Supported by ID and OD Welding Fixtures

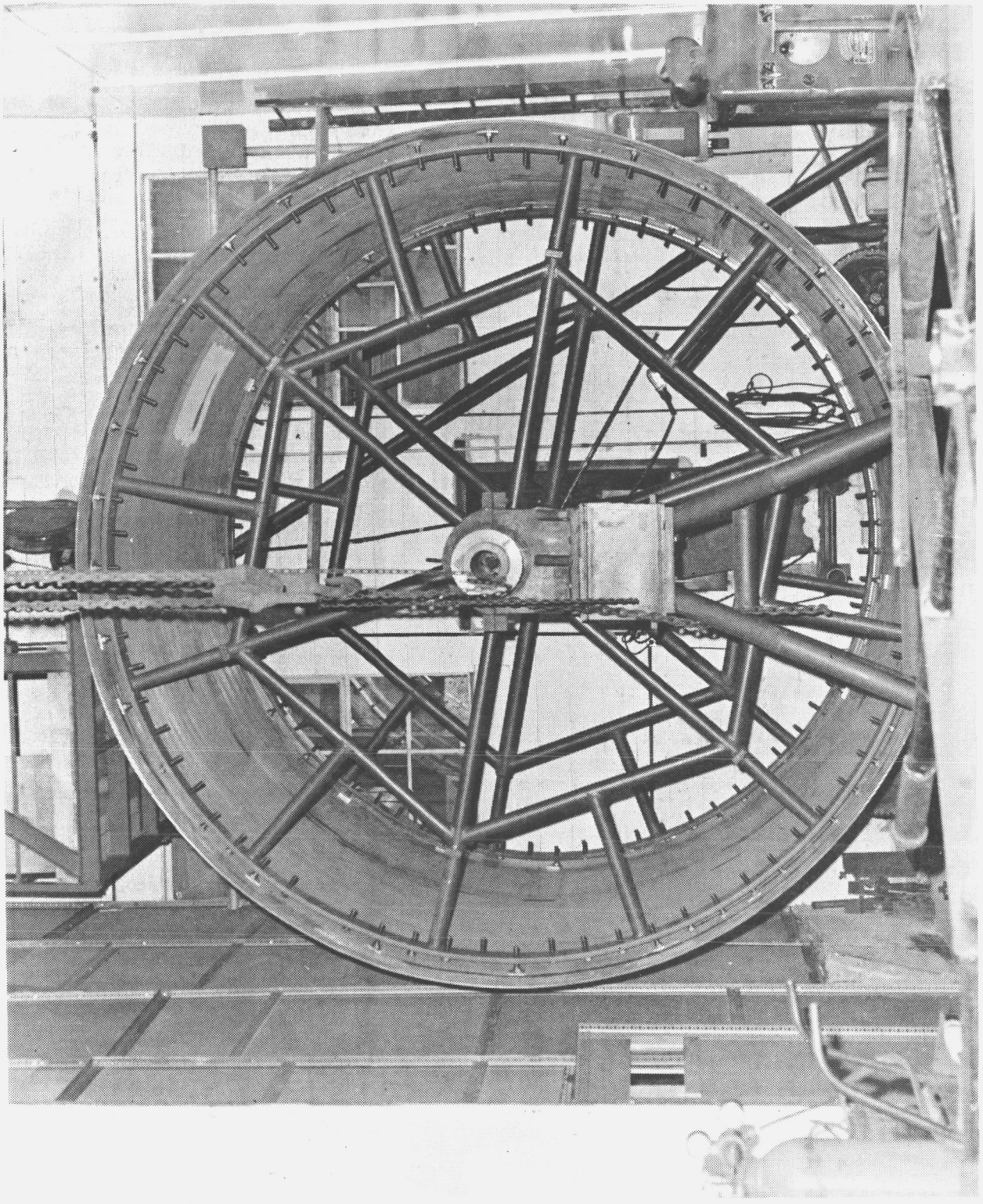


Figure 7 - 156-2C-1 Cylindrical Section Showing Spider and Mandrel Arrangement

IV. FABRICATION

The 260-SL-1 case was fabricated and aged in three segments because of furnace size limitations. Segments were subsequently girth-welded together, after which the girth welds were aged locally. An exploded view of the 260-SL-1 case is shown in Figure 8. The plate and heat identification numbers of each case component are presented in Table II.

A. FABRICATION SEQUENCE

The forward subassembly consisted of a forward attach flange, dome, Y-ring, skirt, and cylinder section. The center subassembly consisted of two cylindrical sections. The aft subassembly consisted of a cylinder section, Y-ring, skirt dome, aft attach flange extension, and aft attach flange.

Final assembly was accomplished on a mandrel with the forward and center subassemblies being welded together, after which the weld was locally aged. Then the aft subassembly was welded to the center subassembly, after which that weld was locally aged also.

The head subassembly contained a polar opening 40.04 inches in diameter to facilitate motor manufacturing and inspection. A closure and closure cap for this opening was provided to complete the basic case. This closure was fabricated from plate formed and welded to attachment flanges which had been machined from forged plate. The 6-in. diameter closure cap was machined from forged plate.

State-of-the-art fabrication techniques and soft tooling were used throughout the sequence of fabrication. Following is a brief description of the fabrication of major case subcomponents:

1. Domes

The hemispherical heads were fabricated by welding eight gores to form hemispherical shells. Forming of the gores was accomplished with two sets of forming dies: roughing dies and finishing dies. Full-size gore plates were cold worked to a 7-ft, 11.5-in. inside radius in the roughing die. The plates were then transferred to the finishing die where they were cold formed to near the finished radius. Upon completion of this operation, the gores were placed in an oven and heated to the annealing temperature. When the plates had been at annealing temperature for one hour, they were removed from the oven and placed in the finishing dies. The dies were closed with a moderate closing pressure to form the gores to final contour. The gores were allowed to air cool to room temperature before being removed from the dies. This fabrication technique produced gores to within 0.010 inch of specified contour.

The aft dome was fabricated using two strakes of gores. An adapter transition piece between the aft gores and aft attach flange. The 1 1/4-in. thick

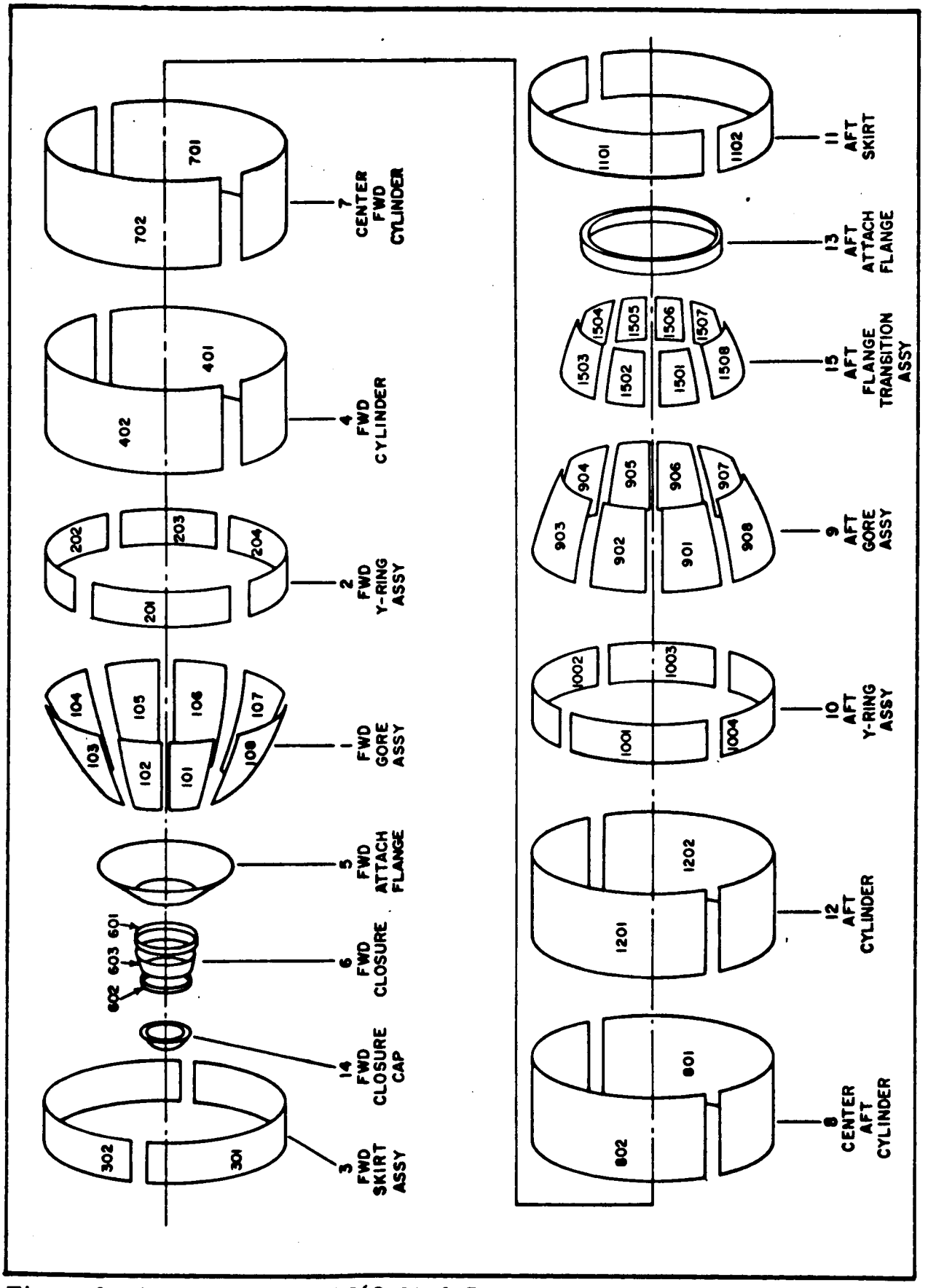


Figure 8 - Exploded View of 260-SL-1 Case

TABLE II

260-SL-1 CASE COMPONENTS IDENTIFICATION

Assembly Nomenclature	Assembly No.	Part No.	Plate No.	Heat No.
Forward skirt	3	301	195997	X50388
		302	195997	X50388
Forward closure cap	14	14	4B	X53540
Forward closure	6	601	4B	X53540
		602	3A	X53541
		603	12(979A1)	X53674
Forward attach flange	5	5	3A	X53541
Forward gore assembly	1	101	193029A	X53085
		102	193025B	X53085
		103	193026A	X53085
		104	195996A	X53088
		105	193029B	X53085
		106	193026B	X53085
		107	195996B	X53088
		108	156897A	X53013
Forward Y-ring assembly	2	201	3A	X53540
		202	3A	X53540
		203	2A	X53541
		204	2A	X53541
Forward cylinder	4	401	W41701	X53471
		402	241372	X53201
Center forward cylinder	7	701	196003	X53088
		702	195999	X53088
Center aft cylinder	8	801	41704	X53471
		802	41703	X53471
Aft cylinder	8	1201	193091	X53085
		1202	224411	X53158
Aft Y-ring assembly	10	1001	3A	53540
		1002	3A	53540
		1003	3A	53540
		1004	2A	53541

TABLE II (Cont'd)

260-SL-1 CASE COMPONENTS IDENTIFICATION

Assembly Nomenclature	Assembly No.	Part No.	Plate No.	Heat No.
Aft gore assembly	9	901	193029A	X53085
		902	193025B	X53085
		903	193026A	X53085
		904	195996A	X53088
		905	193029B	X53085
		906	193026B	X53085
		907	195996B	X53088
		908	156897A	X53013
Aft flange transition assy	15	1501	N-1	50236-1
		1502	N-1	50236-1
		1503	N-1	50236-1
		1504	N-1	50236-1
		1505	N-1	50236-1
		1506	N-1	50236-1
		1507	N-1	50236-1
		1508	N-1	50236-1
Aft attach flange	13	13	AAS/N2	--
Aft skirt	11	1101	193027	X53065
		1102	193027	X53065

transition section was made from eight gores formed in the same dies as the fore and aft gores. After being formed, this section was machined on the outside to the proper thickness to mate with the gores and the aft attach flange.

2. Y-Rings

Y-rings were used to provide attachments for the thrust skirts, and provide a transition for joining the thicker cylinder sections to the thinner dome sections. Each Y-ring was fabricated from forged plate that was rolled to diameter and welded using the vertical submerged arc (VSA) process.

Early in the program, the Y-rings were modified to provide a register for the fore and aft skirts. This was done to decrease tooling requirements and to provide alignment of the skirt and dome. Detailed review of the case design stress analysis indicated a need for skirt-to-Y-ring design revision as indicated in Figure 9.

3. Cylinder Sections

Each cylinder section (one each in the fore and aft subassemblies and two in the center subassembly) was made from two rolled plates joined by two longitudinal welds. The standard procedure of press braking the ends to eliminate trimming after rolling was used.

B. MATERIALS

The plate and forgings for these cases were procured in accordance with Space Booster Division material specification SB-SP-174. The steel mills would not initially produce plate or forgings to the technical requirements deemed necessary by Space Booster Division. Therefore, material inspection was performed to the more stringent fabrication specification SB-SP-4. The specific inspection criteria requirements not agreed upon were (1) minimum properties at the lower aging temperature (835°F versus 900°F); (2) banding evaluation as a rejection criterion; (3) internal soundness testing level and rejection criteria; and (4) surface testing and finish requirements. The greatest difficulty was in ultrasonic testing. The standard mill practice was to use a 36-deg transducer angle for shear wave testing; whereas in the development of the ultrasonic specification, it was determined that a 48-deg transducer angle gave better results. The main objection from the steel mill was that shear wave indications which are acceptable when found with a 36-deg transducer angle are rejectable when a 48-deg transducer angle is used. This inspection procedure resulted in plate passing the mill and purchase requirements, and then being rejected for use in the case during receiving inspection. This situation has never been fully resolved with the major supplier.

1. Plates

a. Plate Processing

In the design of the thick case sections, the best approach appeared to be forming and welding thick plate to the general shape and then machining to

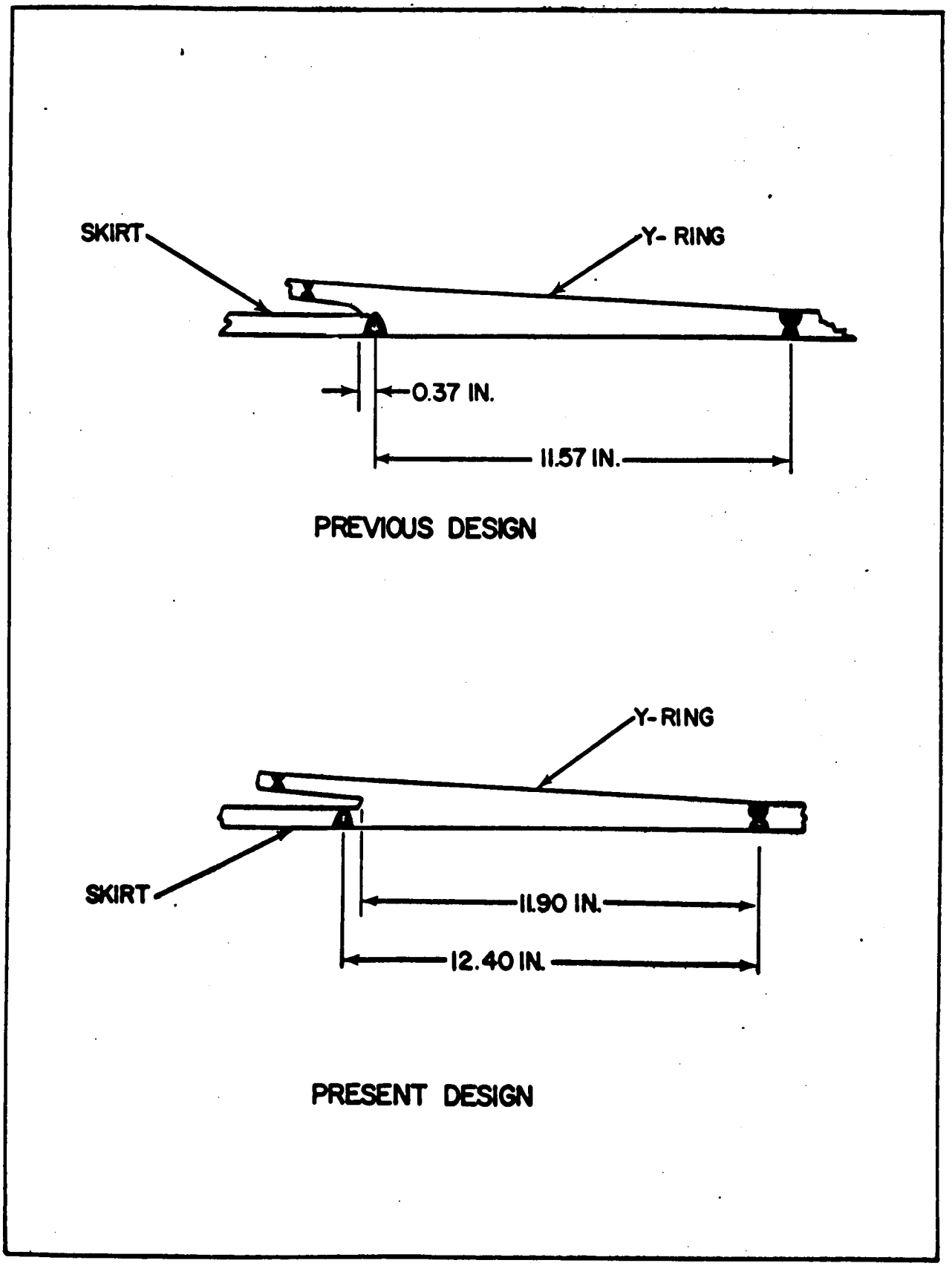


Figure 9 - Revised 260-SL Case Y-Ring Configuration

final contour. The first problem encountered was in obtaining thick sections that met the strength and ductility requirements in three directions. The through-thickness direction had the poorest properties. In some tests, bars failed at extremely low strength levels (130 ksi) with no measurable elongation. Table III contains typical mechanical properties of a 4-in.-thick air melt rolled plate. The low strength and lack of ductility were largely caused by severe segregation banding. This condition was most prevalent in sections of three and four inches thick. For this reason, all such thick-plate sections were replaced by forgings.

The axial direction of a rolled ring forging corresponds to the through-thickness direction of a rolled plate. However, the properties from the axial direction of the forgings were better than the through-thickness properties of thick plate. The properties shown in Tables IV and V for the aft attach flange were typical for the case forgings.

In thinner plate sections (approximately two inches thick), this weaker through-thickness condition in some cases was improved by thermal treatment as shown in Table VI. Consequently, the forge-prepared plate material for the Y-rings (1-7/8 inches thick) was annealed after being VSA welded longitudinally.

In the cases where thermal treatment improved ductility, the initial difficulty appeared to be caused by grain orientation instead of banding. Thermal treatment had some beneficial effects on banded plates. However, this improvement was not sufficient to make badly banded material acceptable.

Acceptance testing of both 3/4- and 1/2-in. thick plate revealed that when tested transverse to the direction of final rolling, the fracture toughness (W/A) and ductility were lower than when tested longitudinally. Metallographic examination indicated that this condition was most likely caused by preferential grain orientation. The mill had annealed the material in the range of 1500 to 1650 F for one hour. The plate was subsequently solution annealed for an additional time in an attempt to improve properties. Following is a presentation of typical properties achieved during re-solution annealing:

Specimen Orientation	0.2-% Yield Tensile Strength (ksi)	Ultimate Tensile Strength (ksi)	Elongation (%)	Reduction of Area (%)	W/A (in. lb/in.^{2})	Annealing Treatment
Longitudinal	253.0	263.0	10.0	46.0	730	Mill anneal
Transverse	260.0	268.0	10.0	32.0	492	1600 F; aged at 900 F for 3 hrs
Longitudinal	274.0	283.0	8.7	35.0	872	Re-annealed
Transverse	274.0	281.0	7.7	31.5	822	1550 F; aged at 900 F for 3 hrs
Longitudinal	248.0	258.0	11.2	48.0	890	Re-annealed
Transverse	252.0	260.0	10.7	38.0	864	at 1650 F; aged at 900 F for 3 hrs

TABLE III

TYPICAL MECHANICAL PROPERTIES
OF A 4-IN. -THICK AIR MELT ROLLED PLATE

Specimen Axis	0.2 % Yield Tensile Stress (ksi)	Ult. Tensile Stress (ksi)	Elongation (%)	Reduction of Area (%)
Longitudinal	252	265	7	32.6
Longitudinal	249	259	6	20.2
Longitudinal	246	257	6	19.6
Longitudinal	246	258	5	17.7
Longitudinal	238	252	7	23.6
Longitudinal	242	252	9	46.5
Longitudinal	244	255	7	22.7
Transverse	244	257	7	37.6
Transverse	242	254	7	35.9
Transverse	226	259	4	13.5
Transverse	242	261	4	15.6
Transverse	248	259	5	21.6
Transverse	256	264	7	31.6
Transverse	239	254	9	41.9
Through-thickness	☆	161	1	35.6
Through-thickness	☆	130	0	35.5
Through-thickness	☆	117	0	35.6
Through-thickness	☆	116	0	35.6
Through-thickness	☆	148	0	35.6
Through-thickness	☆	127	0	35.5
Through-thickness	☆	127	0	35.6

☆Broke without yielding

TABLE IV

260-SL-1 CASE AFT ATTACH FLANGE TENSILE PROPERTIES

Specimen Axis	Aging Time (hr)	0-Deg Location				180-Deg Location			
		0.2% Yield Tensile Stress (ksi)	Ultimate Tensile Stress (ksi)	1-In. Area Elongation (%)	Reduction of Area (%)	0.2% Yield Tensile Stress (ksi)	Ultimate Tensile Stress (ksi)	1-In. Area Elongation (%)	Reduction of Area (%)
Circumferential	3	228.6	240.2	10	52	231.4	241.4	10	51
		230.6	240.6	10	54	228.6	239.0	10	54
	12	251.0	261.9	10	50	250.6	261.6	10	51
		251.0	262.0	10	51	251.6	262.8	11	53
Axial	3	231.4	242.0	8	37	230.6	240.6	8	42
		230.7	242.0	8	38	230.7	241.2	9	41
	12	249.8	260.4	7	33	249.2	261.3	8	38
		250.6	261.2	6	27	249.0	260.6	8	38

NOTE: Specimens were solution heat treated for a double cycle at 1650 F for 10 hours and air cooled. The specimens were then aged at 900 F for indicated times and subsequently tested at room temperature.

TABLE V

260-SL-1 CASE AFT ATTACH FLANGE IMPACT PROPERTIES

Specimen Axis	0-Deg Location		180-Deg Location	
	Crack Depth (in.)	W/A (in. lb/in.^{2})	Crack Depth (in.)	W/A (in. lb/in.^{2})
Circumferential	0.030	768	0.060	845
	0.040	904	0.030	904
	0.020	1203	0.045	1144
Axial	0.035	674	0.035	735
	0.050	682	0.040	714
	0.060	722	0.035	800

NOTE: Specimens were solution heat treated for a double cycle at 1650 F for 10 hours and air cooled. The specimens were then aged at 900 F for three hours and tested at room temperature.

TABLE VI

TENSILE TEST RESULTS OF VARIOUS 1-7/8-IN. THICK PLATE CONDITIONING CYCLES (PHASE I)

Type Bar	Specimen Orientation	0.2-% Offset Yield Tensile Strength (ksi)	Ultimate Tensile Strength (ksi)	Elongation (%)	Reduction of Area (%)
AS-RECEIVED AND AGED AT 900 F FOR 3 HR					
R-1	Transverse	269.5	273.5	6.0	39.4
R-1	Transverse	275.0	277.0	7.0	37.9
R-1	Longitudinal	268.0	271.5	8.0	42.5
R-1	Longitudinal	274.0	277.5	8.0	41.9
R-4	Through-thickness	250.0	254.5	0	0
R-4	Through-thickness	240.0	242.5	<1.0	6.1
R-4	Through-thickness	243.0	245.0	2.0	18.1
R-4	Through-thickness	231.0	232.5	<1.0	15.7
R-4	Through-thickness	234.0	238.5	<1.0	9.7
ANNEALED AT 1620 F AND AGED AT 900 F FOR 3 HR					
R-1	Transverse	241.5	245.5	10.0	48.1
R-1	Transverse	243.0	246.5	10.0	45.3
R-1	Transverse	244.5	248.5	9.0	47.3
R-1	Transverse	244.5	248.0	9.0	49.3
R-1	Longitudinal	240.0	245.0	9.0	49.8
R-1	Longitudinal	244.5	249.0	10.0	45.7
R-1	Longitudinal	241.5	246.5	☆	49.3
R-1	Longitudinal	241.5	246.5	9.0	48.5
R-4	Through-thickness	214.0	239.5	2.0	13.3
R-4	Through-thickness	--	236.0	0	0
R-4	Through-thickness	234.0	237.5	1.0	7.3
R-4	Through-thickness	234.0	238.0	1.0	7.3
R-4	Through-thickness	240.0	243.5	☆	10.9
R-4	Through-thickness	--	218.0	☆	0

☆Broke outside of gage mark

As indicated, re-solution annealing reduced the variation in test values and improved the W/A values by approximately 30 to 50 percent. Based on the results, all cylinder plates for the 260-SL-1 case were re-solution annealed by the mill; and the gore plates were re-annealed in the forming process.

Re-solution annealing resulted in two changes (1) it produced a more equi-axed grain structure eliminating the grain directionality caused by rolling and (2) insured that the maximum amount of material was in solution available for transformation to martensite.

A side effect of this process was pitting or "snowflake bursts." The pits were caused by a localized, accelerated corrosion of the plate surface, which was catalyzed by sub-surface inclusions of foreign matter. Typical photomicrographs proved that the condition was confined to the plate surface and not associated with cracking (Figure 10).

Immediate changes were made to eliminate the pitting. All plate was re-annealed and then ground to a dye-penetrant, flaw-free surface. Also, the steel mills changed heating practices to preclude the possibility of molybdenum-catalyzed oxidization of the grain boundaries, as it was hypothesized that the pitting could have resulted from this condition.

All 260-SL-1 plate material was made by the air melt process except the 1-1/4-in.-thick aft gore extension plates, which were made from vacuum arc remelted steel.

b. Plate Surface Condition

The original purchase requisition specified the plate surface to be in the as-rolled condition. However, as-rolled plate surface had excessive scale and scab as well as pitting, even after more than normal mill conditioning. Therefore, all plate material was subsequently ground.

All plates were surface ground in the flat condition except for the gore plates and two of the cylinder plates which had already been formed. These plates were surface ground to a dye-penetrant, flaw-free surface. The surface finish, except in areas where extensive hand grinding was required, was approximately equal to a 63 RMS or better finish.

Surface finishing by hand grinding was required for the gores and two cylinder plates because forming had been accomplished with the surface in the as-rolled, mill-ground condition. These plates were hand-disc ground to a surface finish approximately equal to a 125 RMS or better.

c. Plate and Gore Forming

A forming study was conducted at the beginning of the program to determine the respective forming characteristics of 18-percent nickel maraging steel (250-ksi grade), HY-80 steel, and 4340 steel. The maraging steel was in the annealed condition, the HY-80 steel in the quench and tempered condition, and the 4340 steel in the normalized condition. It was determined that the maraging steel has more springback than HY-80 steel, requiring approximately 15 percent as much forming to produce the same configuration as HY-80 steel.

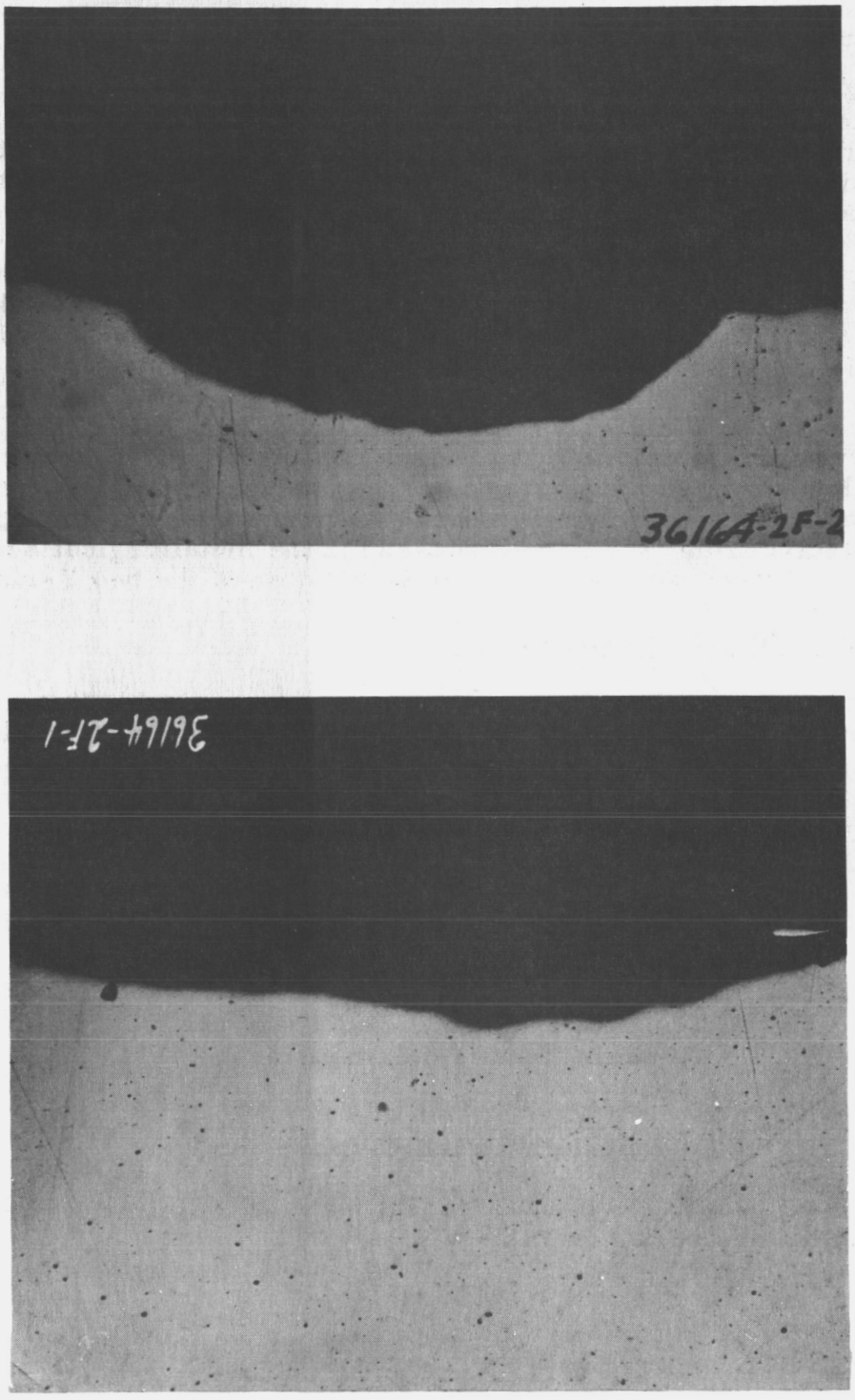


Figure 10 - Typical Micropitting of Plate Parent Material following Re-Solution Annealing (100 X)

These springback criteria were analyzed to determine the necessary contour in the final set of contour dies. The gore material was re-annealed before the gores were formed. Therefore, instead of being final formed at room temperature, these gores were final set from the annealing temperature in modified dies. The contour control using this method was within 0.010 inch.

2. Forgings

A ring-rolled forging was used for the aft attach flange. The properties of this forging in the radial direction were better than the through-thickness properties of thick plate. The relationships between properties and test direction, and properties and finish-forge temperature, and thermal treatment are covered in the metallurgical section of this report.

Mandrel forged rings - One mandrel forged ring was used for the small end flange of the hydrotest adapter. This forging was a thick-walled, approximately 10 inches, as-forged ring. The forging was machined to the required dimensions.

Forge prepared plate - This process consisted of upset forging an ingot and then slabbing by forging prior to rolling to final gage. The process was used in an attempt to improve the short transverse properties of thick sections. The results of the work are discussed in the metallurgical section of this report. Forged plate was used in fabrication of the two Y-rings.

3. Material Properties

Selection of materials for the 260-SL case were made after a complete evaluation of both chemical and physical properties of each plate and forging. Tests conducted were as follows:

1. Chemical analysis
2. Microcleanliness
3. Grain size
4. Hardness
5. Uniaxial tensile
6. Uniaxial tensile delamination
7. Precracked Charpy V (forgings only)
8. Critical crack length (plate only)

Mechanical properties of case parent material specimens aged with the case assemblies are shown in Table VII.

TABLE VII

TENSILE PROPERTIES OF 260-SL-1 CASE PARENT MATERIAL SPECIMENS AFTER PRODUCTION AGING

Plate, Heat	Type Test Bar	Yield Tensile Strength (ksi)	Ultimate Tensile Strength (ksi)	Gage Elongation (%)	Reduction of Area (%)	Part Description and Number
FORWARD SUBASSEMBLY						
3A, X53541	R-	246.0*	256.5*	6.0	25.4*	Fwd attach flange 9
195997, X53088	R-	222.0*	230.0*	13.0	45.7	Fwd skirts 301, 302
193026A, X53085	R-5	244.3	298.9	11.0	32.5	Fwd gore 103
193025B, X53085	Represented by plate 193026A					Fwd gore 102
193029A, X53085	R-5	247.3	255.2	10.0	31.4	Fwd gore 101
193029B, X53085	R-5	250.8**	256.8**	10.0	35.8	Fwd gore 105
195996B, X53088	R-5	212.0**	223.8**	14.0	41.3	Fwd gore 107
195996A, X53088	Represented by plate 195996B					Fwd gore 104
193026B, X53085	Represented by plate 193026A					Fwd gore 106
156997A, X53013	Represented by plate 156897A					Fwd gore 108
3A, X53540	R-1	226.0*	236.5*	9.0	46.6	Fwd Y-ring 201, 202
2A, X53541	R-1	228.0*	237.0*	10.0	49.2	Fwd Y-ring 203, 204
041701, X53471	R-2	238.5	247.5	10.0	46.9	Cylinder 401
241372, X53201	R-2	237.0	245.0	10.0	46.1	Cylinder 402
CENTER SUBASSEMBLY						
196003, X53088	R-2	243.0	247.5	11.0	53.6	Cylinder 701
195999, X53088	R-2	246.0***	251.0	9.0	43.3	Cylinder 702
041704, X53471	R-2	261.0***	264.0***	10.0	46.5	Cylinder 801
041703, X53471	R-2	224.5*	231.0*	9.0	44.9	Cylinder 802
AFT SUBASSEMBLY						
193031, X53085	R-2	237.5	244.0	9.0	45.7	Cylinder 1201
224411, X53158	R-2	257.5*	265.0*	9.0	33.9	Cylinder 1202
3A, X53540	R-1	224.0*	234.5*	9.0	43.4	Y-ring 1001, 1002, 1003
2A, X53541	R-1	231.0	241.0	11.0	50.0	Y-ring 1004
193027, X53085	R-2	246.0	253.0	10.0	45.7	Skirt 1101, 1102
193029A, X53085	No test					Aft gore 901
193025B, X53085	R-5	247.6	255.1	10.0	30.0	Aft gore 902
193026A, X53085	Represented by plate 193026B					Aft gore 903
195996A, X53088	R-5	220.9*	229.8*	15.0	37.2	Aft gore 904
193029B, X53085	No test					Aft gore 905
193026B, X53085	R-5	245.8	255.3	11.0	35.0	Aft gore 906
195996B, X53088	Represented by plate 195996A					Aft gore 907
156897A, X53013	R-5	221.4*	227.9*	13.0	42.2	Aft gore 908
N-1, X50236-1	R-1	234.0*	243.5*	10.0	44.9	Gore ext 1501 thru 1508
2AA	R-3 (radial)	223.2*	231.6*	4.0	21.7	Aft attach flange 13
2AA	R-3 (circ)	218.4*	228.8*	10.0	54.5	Aft attach flange 13
2AA	R-3 (axial)	223.2	228.0	8.0	43.2	Aft attach flange 13
FORWARD CLOSURE						
4B, X53540	R-1	240.0	247.0	9.0	40.1	Aft attach flange
3A, X53541	R-1	230.5	238.0	5.0	19.9	Fwd attach flange
127979A1, X53674	R-5	237.8	245.7	10.0	30.0	Membrane
FORWARD CLOSURE CAP****						
4B, X53540	R-1	233.0	241.5	1.0	8.9	--
	R-1	225.0	234.0	1.0	9.6	--
	R-1	233.0	239.0	--	7.7	--

NOTES: 1. All specimens were B-type bars aged during the same production aging cycle as the case subassemblies.

*These values do not meet the 230.0 to 240.0-ksi requirement established for a 900-F, 3-hr aging cycle. However, these specimens do meet the requirements for a 835-F, 3-to-4-hr age cycle.

**The NFS bar with a 0.232-in. long crack has a gross fracture stress of 225.2 ksi, exceeding the revised 835-F aging cycle requirements. Preproduction welded bars from either side of the plate had yield strengths of 225.6 and 220.6 ksi, exceeding yield strength of parent bars.

***Plate was mill-annealed at 1510 F instead of 1575 F.

****Part has already been hydrotested at 960 psig.

4. Welding

Welding of 250-ksi grade maraging steel was not well developed at the start of the Air Force 623A Program, of which the Space Booster Division effort was a part. TIG welding had been accomplished on a limited amount of material up to 1-inch thickness(by Excelco Developments, Inc., in particular) and MIG and submerged-arc welding to an even lesser extent.

The Space Booster Division's subcontractor originally proposed to use the MIG process for welding the case. However, because of promising laboratory results at Newport News Shipbuilding and Dry Dock Company, and for the reasons enumerated later, a decision was made to develop the submerged-arc process for use on the 260-inch case program.

Development work had been accomplished by the case subcontractor on the MIG process for welding under a NASA development contract. The subcontractor had concurrently conducted company-funded development effort on the submerged-arc process. MIG welding was considered deficient in that the process was prone to mechanical difficulties, such as gas back-up requirements, weld "splatter" dropping from the nozzle causing metallic (oxide) inclusions and excessive porosity.

As will be discussed in subsequent sections, three primary welding methods were ultimately employed on the case. Submerged-arc (SA) was used for 3/4-in, and thinner plate with one exception, vertical submerged-arc (VSA) was used for the 1-7/8-in. thick Y-ring material, and automatic TIG welding was used for the one-sided skirt to Y-ring weld (the exception noted above).

TIG welding was generally used for repairs not involving removal of a complete pass. Prior to using TIG for weld repair, attempts were made to use manual, fine wire MIG welding process for repair welding of the hydrotest adapter; however, this method was soon abandoned because of excessive porosity in the repair welds.

a. Submerged-Arc Welding

The submerged-arc welding process was selected for general use based on such qualities as speed of welding, amount of metal deposited, freedom from porosity, number of passes required (all welds two-pass), and heat transfer from electrode to flux. Unlike the TIG and MIG processes which use gas as a shielding medium, the submerged-arc process uses flux to shield the metal transfer. Also, in submerged-arc welding there is no true arc such as with the TIG and MIG welding methods. Instead, the heat transfer is between the filler wire and the flux, causing a molten flux condition covered by an unmelted flux overburden. The method of feeding the wire and of current transfer to the wire in submerged-arc welding are the same as in MIG welding. Submerged-arc welding, unlike either MIG or TIG welding, is strictly an automatic process and cannot be used for manual welding. The welding head is maintained stationary, and the parts to be welded are passed under the head.

Preliminary studies had indicated weld difficulties when weld wire with high titanium content was used. This condition could have been caused partially

by flux reactions. However, when Linde 105 Lo-Sil flux was used with a wire containing a nominal 1.20 percent titanium, the welding characteristics were good. The reaction of the flux with the molten filler metal reduced the 1.20-percent titanium of the wire to approximately 0.60-percent titanium in the bead.

Figure 11 shows joint configuration and parameters for typical weld qualification panels for both 3/4- and 1/2-inch nominal thickness material. Figure 12 is a graph of net fracture stress as a function of crack length and shows the average mechanical properties of the four welds. These two charts are typical of the qualification results using 1.20 titanium wires.

Using the same weld parameters, a 10-ft long cylinder "mock-up" weld was made and tested by the same methods. Panels were also welded into a 260-inch diameter aging test cylinder to evaluate and to qualify the production furnace. These welded panels were tested in the same general manner as the weld qualification panels and the cylinder mock-up weld. Table VIII gives the weld parameters for the panels for the furnace test. Complete results of furnace qualification are presented in the thermal treatment section of this report. The weld parameters for the 260-inch mock-up weld were as developed for the qualification welds.

Figure 13 shows a comparison of the fracture toughness of the qualification welds (Figure 12) and the mock-up and thermal test welds.

It is evident from this work that the fracture toughness of the mock-up welds and the panels from the furnace study are not as good as the fracture toughness of the weld qualification panels.

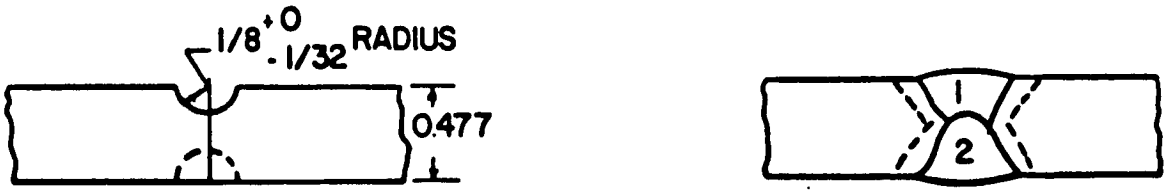
This drop in weld fracture toughness led to additional development work in subarc welding of maraging steel.

(1) Titanium in Weld Bead vs Fracture Toughness

The strength of the welds in the above studies was higher than parent plate due to the higher titanium content of the weld bead. Test failures occurred in the weld head-affected zone and not in the weld bead. Therefore, an investigation was made of the effect of lowering the weld bead titanium content on fracture toughness. Since only a comparison of toughness was desired, pre-cracked Charpy bars were used to obtain W/A values. Figure 14 is a plot of the titanium content of three weld beads vs fracture toughness. The strengths of the respective welds are also included. It is to be noted that dropping the titanium content of the bead to approximately half of the original weld qualification bead, an increase in fracture toughness was obtained with little decrease in failure strength.

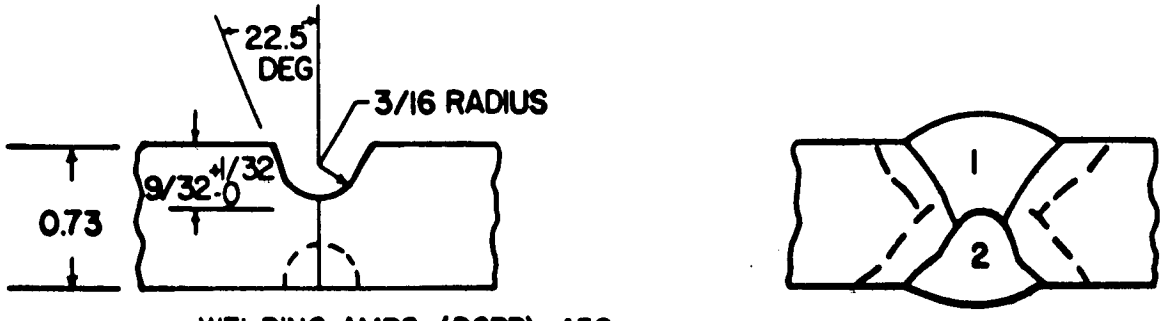
The investigation indicated that the most benefit in fracture toughness would be gained by lowering the titanium content of the bead. Therefore, the wire chemistry was changed to a nominal titanium content of 0.60 percent. The change generally produced bead chemistries in the 0.35 to 0.40 titanium range. In addition, a new flux was incorporated, Linde 105 Special (No Sil-No Mn) in an effort to further reduce the silicon content of the weld bead. This flux was more fluid and made it difficult to maintain weld bead contour.

0.477-IN. WELD QUALIFICATION PARAMETERS



WELDING AMPS (DCRP) - 400
ARC VOLTS - 35
TRAVEL SPEED - 13 IN/MIN
WIRE STICK-OUT - 1- 1/4 IN
PREHEAT TEMP - AMBIENT
INTERPASS TEMP - 250 F (MAX)
FILLER WIRE - NO. 08264
BASE MATERIAL - HEAT 53085
HEAT INPUT - 64,500 JOULES / IN.

0.730-IN. WELD QUALIFICATION PARAMETERS



WELDING AMPS (DCRP) - 450
ARC VOLTS - 31
TRAVEL SPEED - 7-1/4 IN./MIN
WIRE STICK-OUT - 1-1/4 IN.
PREHEAT TEMP - AMBIENT
INTERPASS TEMP - 250 F (MAX)
FILLER WIRE - NO. 08071, 3/32-IN. DIA
BASE MATERIAL - HEAT 53158
HEAT INPUT - 115,000 JOULES/IN.

NOTE: ALL SPECIMEN DIMENSIONS ARE IN INCHES

Figure 11 - Joint Configurations for 0.477-In. and 0.73-In. Submerged Arc Weld Specimens

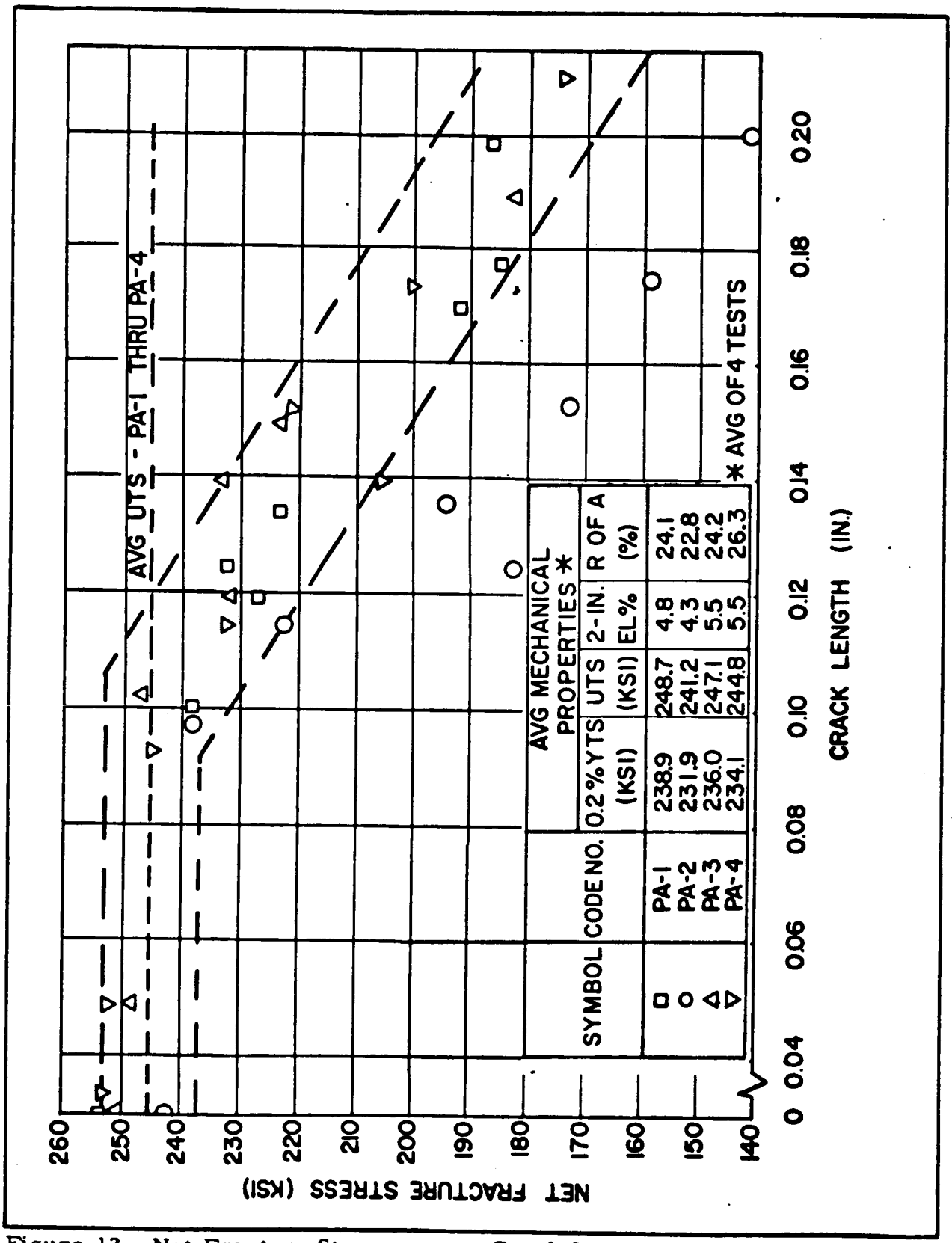
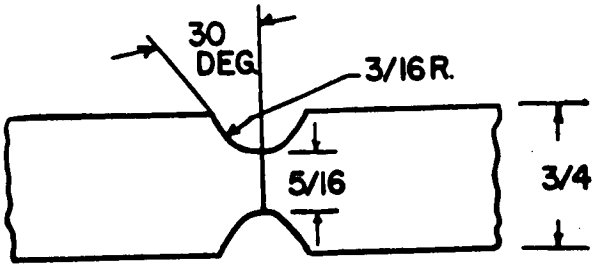


Figure 12 - Net Fracture Stress versus Crack Length of 0.73-In. Qualification Submerged Arc Welds (Code No. PA-1 through PA-4)

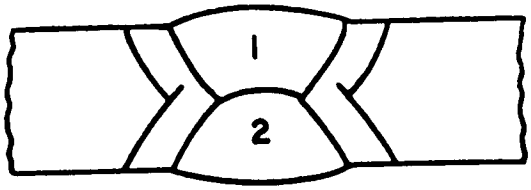
TABLE VIII

JOINT DESIGN AND TYPICAL WELDING DATA
FOR WELDING THE CARBON-STEEL SEGMENT TEST PANELS

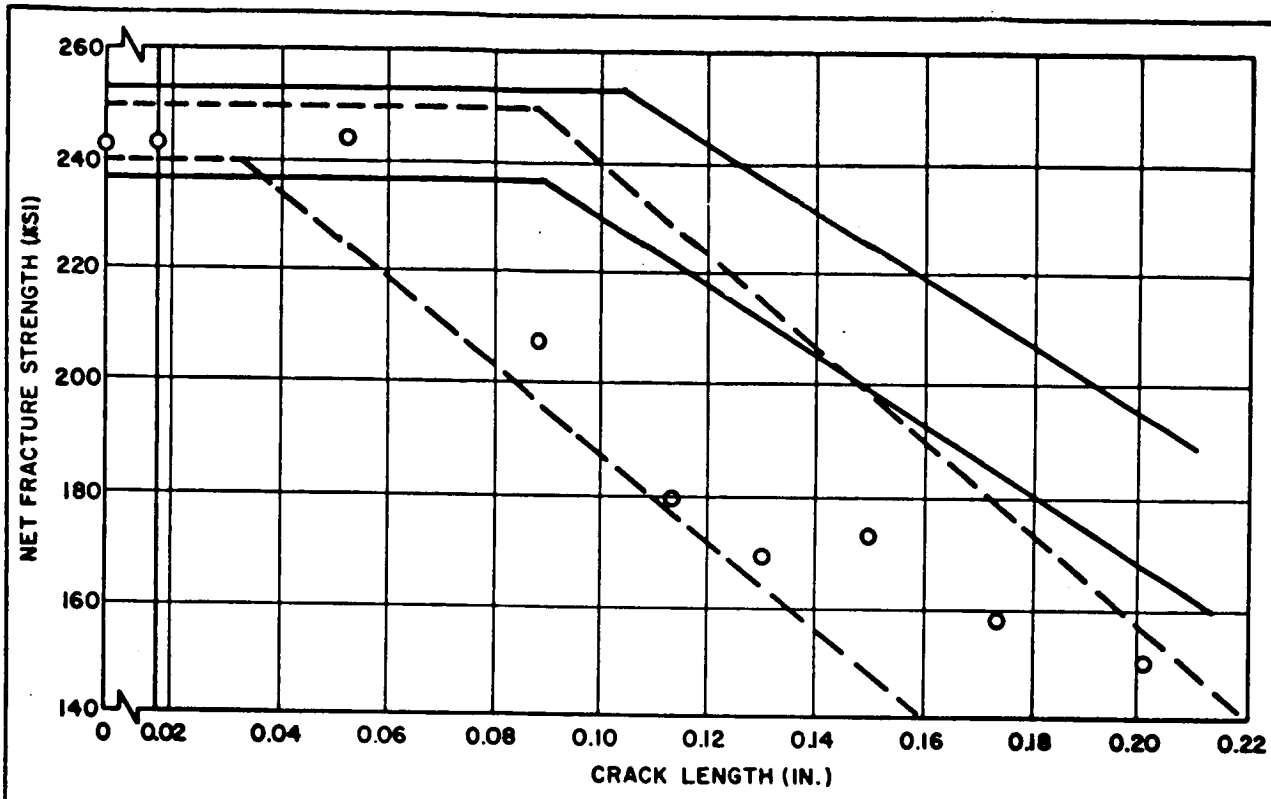
JOINT CONFIGURATION



BEAD SEQUENCE



Base material -	Maraging steel, Heat 14359, conforming to Thiokol specification SB-SP-174
Welding electrode -	Armetco wire, 1/8-in. diameter, heat 08071, conforming to Newport News specification RMC-22
Welding flux (Linde Co) -	Unionmelt grade 105, conforming to Newport News specification RMC-22
Welding process	Submerged arc
Welding power supply -	Two paralleled P and H constant voltage welders (direct current, reversible polarity)
Preheat temperature -	None
Interpass temperature -	250 F maximum
Heat input -	100,000 joules/inch
Welding current -	520 amps
Welding voltage -	27.5 volts
Travel speed -	8.5 inches per minute



SYMBOL	CODE
o	WELDS FROM 260-IN. CYLINDER MOCKUP
———	RANGE OF QUALIFICATION WELDS
- - - - -	RANGE OF FURNACE PANEL WELDS

TYPE WELD	MECHANICAL PROPERTIES			
	0.2 % YTS (KSI)	UTS (KSI)	EL (%)	R OF A (%)
FURNACE PANEL (AVG OF 3 TESTS)	236.0	243.3	5.3	24.3
	233.3	240.1	5.3	24.9
	239.4	244.9	4.7	24.8
	237.5	244.4	5.0	24.7
	238.0	244.8	9.3	40.1
	236.5	243.8	6.7	28.3
260-IN. MOCKUP (AVG OF 4 TESTS)	228.9	234.0	5.0	31.6

Figure 13 - Comparative Fracture Toughness Values for 3/4-in.-Thick Panel and Mockup Welds

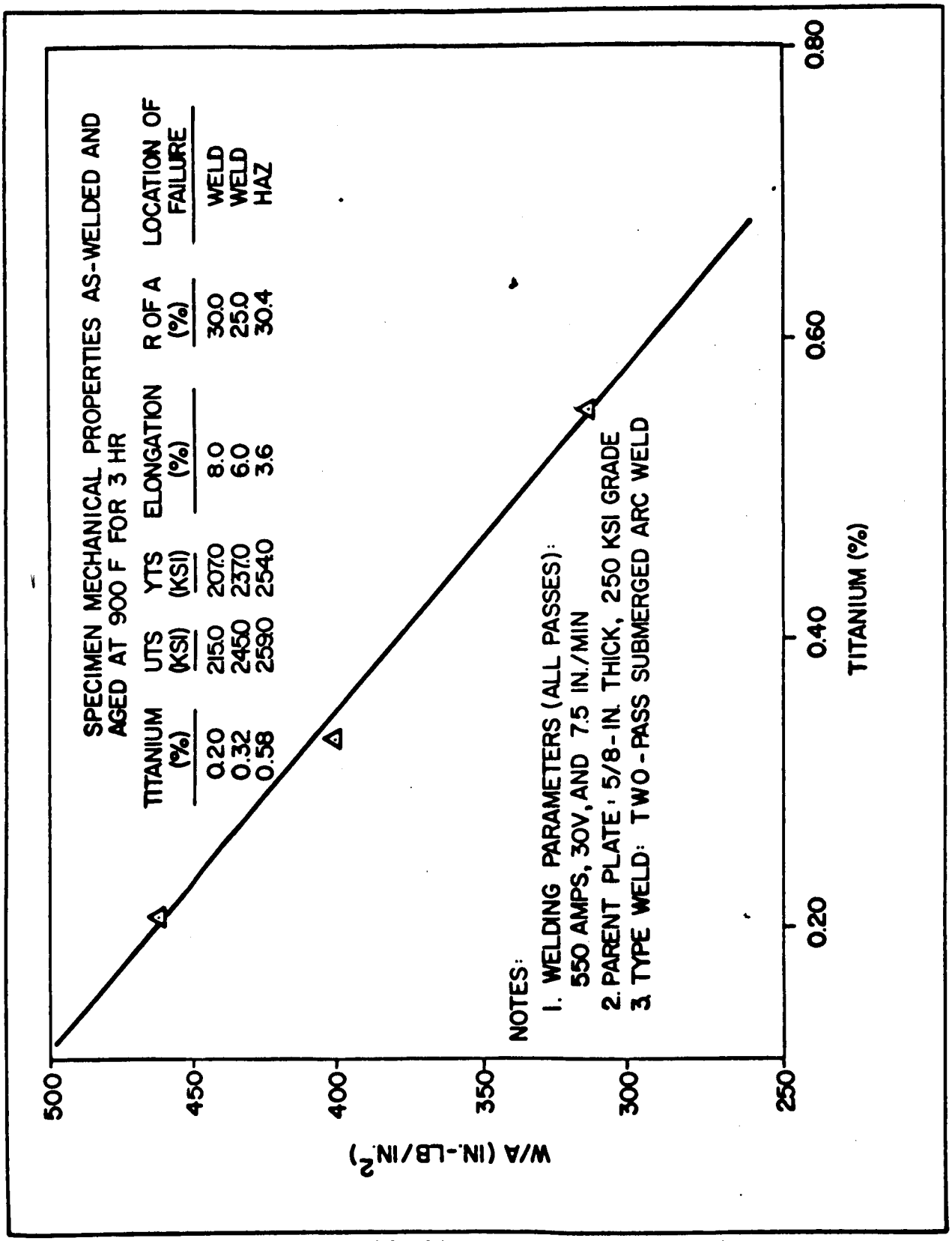


Figure 14 - Titanium Content of Weld versus Fracture Toughness

(2) Weld Cracking

One of the major problems encountered in submerged-arc welding was cracking of the welds. This cracking was of three distinct types:

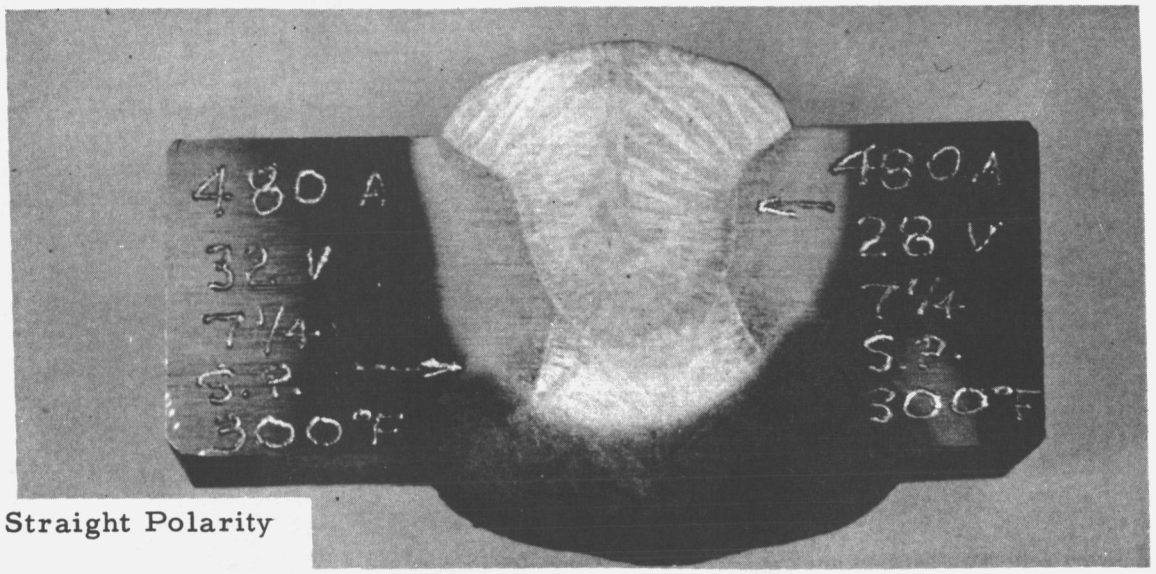
1. Cross cracking. This is a restraint or stress type cracking that, in many cases, is caused by hydrogen embrittlement. This type of cracking was most prevalent in the heavy-section welds. The solution to this problem was to use pre- and post-heat and revert the part after the first weld pass. The pre- and post-heat were used for control of hydrogen rather than as a stress relief. Reversion after the first weld pass accomplished the following: (1) Eliminated stresses in the aged zone of the heat-affected zone by transforming the entire weldment to metastable austenite; (2) prevented differential thermal shrinkage when the second pass was made; and (3) prevented aging of the first pass by the welding heat of the second pass. All three of these factors aided in reducing cracking of the first weld pass from the second weld pass heat input by eliminating locked-in stresses and limiting the level of superimposed stress from the heat-affected zone of the second weld pass.

2. Thermal shock cracking. This type of cracking was primarily associated with TIG weld repairs, therefore, it is covered in a following section of this report.

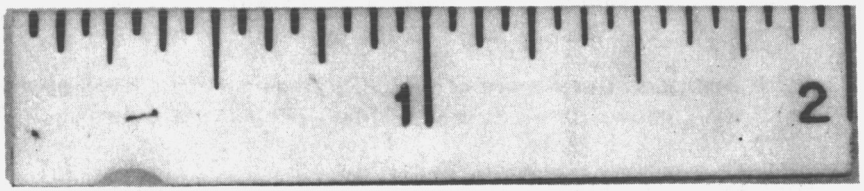
3. Centerline cracking. This type of crack is most often the results of stress caused by improper bead configuration if the cracks are hot or ingotism types. If, on the other hand, the cracks are cold cracks, occurring after solidification and cooldown, they could have resulted from several causes, such as faulty joint configuration, wrong chemistry of filler wire, and improper tooling configuration. The centerline cracks encountered were all of the hot or ingotism type. Examination of the weld bead configuration revealed an out-of-balance condition existed between the bead width and depth. This condition was eliminated by changes made to the weld parameters, i.e., reverse to straight polarity; Linde 105 Special (no Si-No Mn) flux to Linde 105; decrease in arc voltage and an increase in welding amps. A comparison of the typical bead configurations obtained from the old and new parameters is shown in Figure 15. These changes to the bead configuration resulted in reduction of the centerline cracking problem.

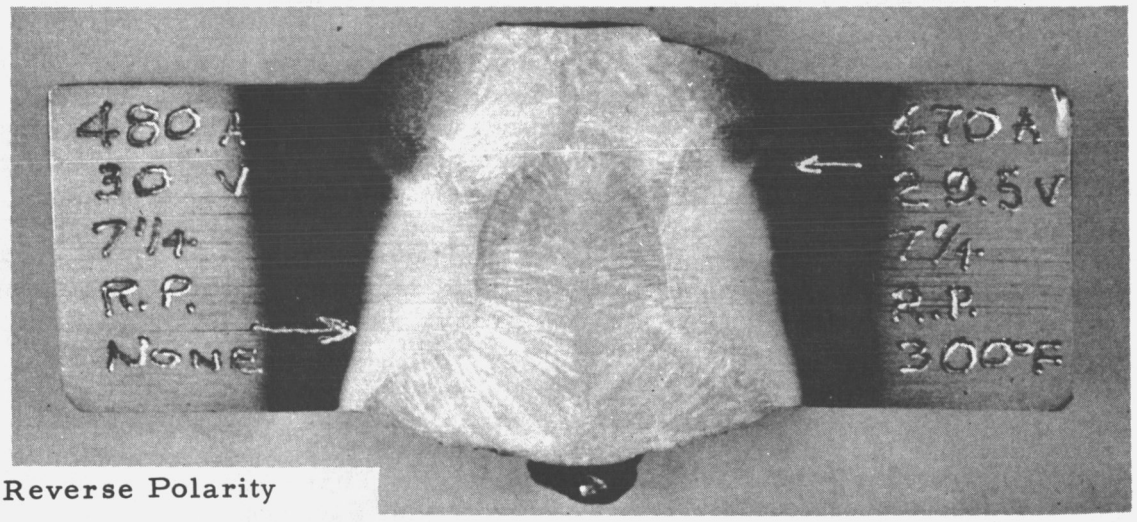
(3) Change in Welding Parameters

The changes made to the welding parameters required a requalification of the procedure. Therefore, welds were made in the two basic material thicknesses using the parameters, as given in Table IX. At the same time, the difference in physical properties obtained between round and flat tensile specimens were studied. The configuration of the test bars used is shown in Figure 16. The average results of both types of test for both plate thicknesses are shown in Figure 17. Note that the aging time temperature had



Straight Polarity



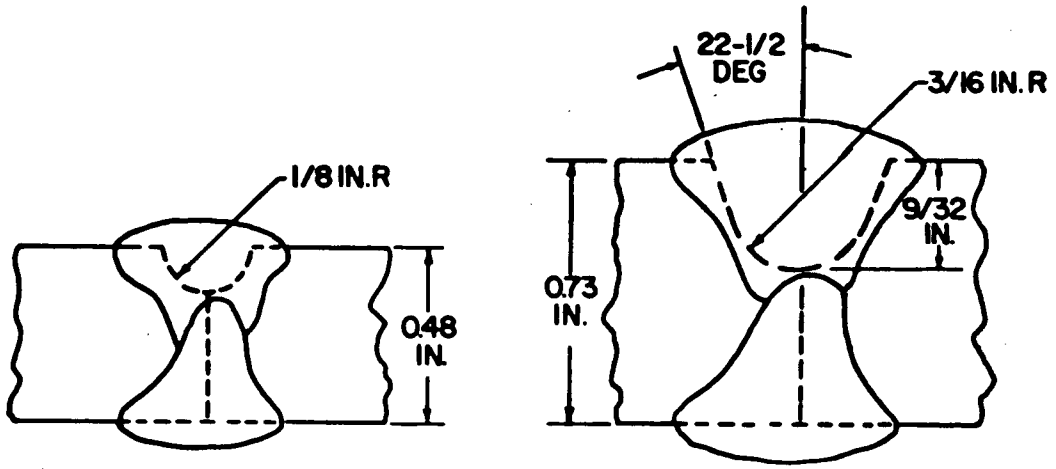


Reverse Polarity

Figure 15 - Comparison of Weld Bead Configuration Using Straight Polarity and Reverse Polarity Techniques

TABLE IX

IMPROVED WELD PARAMETER DATA FOR TWO-PASS SUBMERGED-ARC WELDS PARAMETRIC INVESTIGATION

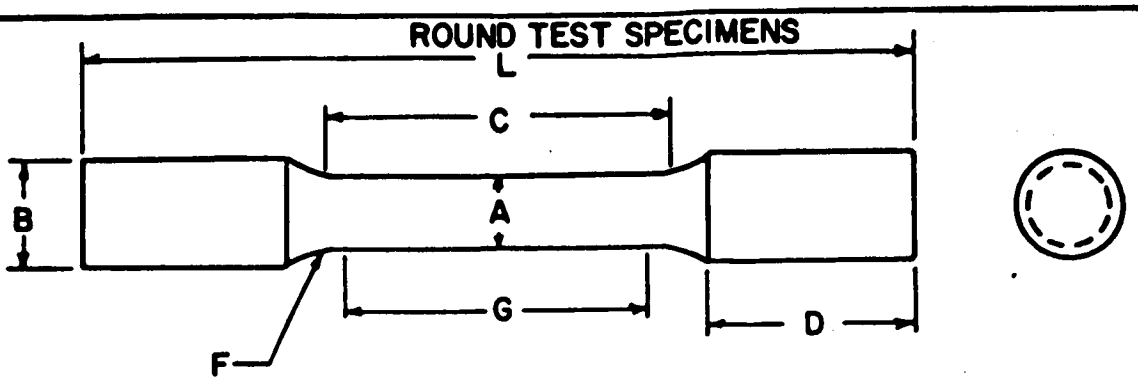


Materials and Parameters	1/2-In. Thick Plate	3/4-In. Thick Plate
Base material	U. S. Steel, heat no. X53013	U. S. Steel, heat no. X53158
Welding process	Submerged arc	Submerged arc
Welding electrode	Armetco heat no. 09391	Armetco heat no. 09391
Welding flux	Linde grade 105	Linde grade 105
Welding power input	Direct current, straight polarity	Direct current, straight polarity
Preheat temperature	300 F	300 F
Postheat temperature	300 F for 1/2-hr	300 F for 1/2-hr
Heat input	203,000 joules/weld inch	373 K-joules/weld inch
Welding current	420 to 430 amps	470 to 500 amps
Welding voltage	34 volts	28-1/2 to 31 volts
Travel speed	13.5 to 15 in./min	7.5 in./min

NOTE: 1. Weld side no. 2 was prepared by carbon-arc gouging and grinding to the joint configuration of side no. 1

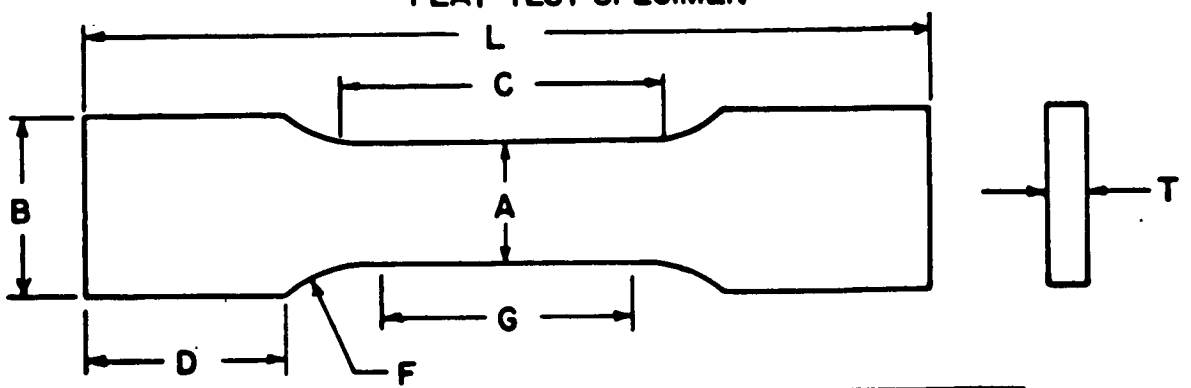
2. The flux was changed back to the standard Linde 105, as little or no improvement was obtained in silicon content with the special flux. Also, the fluidity of the special flux caused problems in bead contour (reinforcement) control.

ROUND TEST SPECIMENS



DIMENSIONS	BAR TYPE DIMENSIONS (IN.)			
	R1	R2	R3	R5
A	0.505 ± 0.010	0.357 ± 0.007	0.252 ± 0.005	0.113 ± 0.002
B	3/4	1/2	3/8	1/4
C	2-1/4	1-3/4	1-1/4	5/8
D	1	5/8	5/8	3/8
F	3/8	0.25	0.18	0.09
G	2.0 ± 0.005	1.4 ± 0.005	1.0 ± 0.005	0.45 ± 0.005
L	5-1/2	3-1/2	3	1-5/8

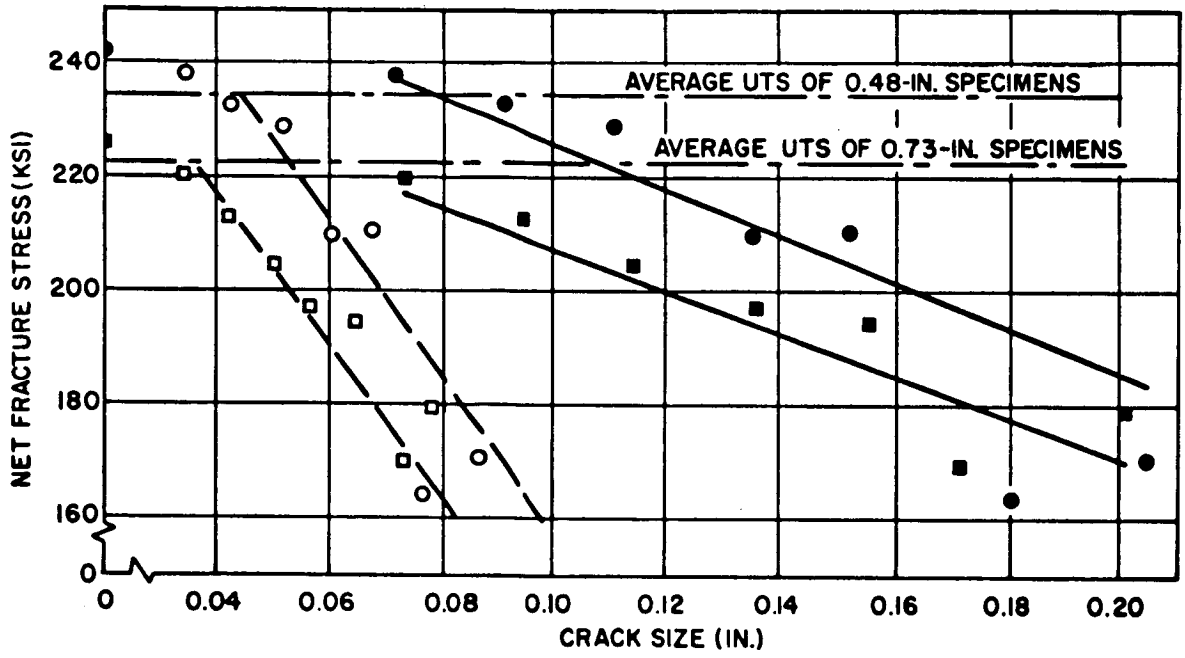
FLAT TEST SPECIMEN



DIMENSIONS	BAR TYPE DIMENSIONS (IN.)	
	F1	F2*
A	1-1/2 +1/8 -1/4	1
B	2	1-1/2
C	9 (MIN)	2-1/4 (MIN)
D	3 (APPROX)	--
F	1	1/2
G	8 ± 0.01	2 +0.125 -0
L	15	8
T	3/16 TO 2	PARENT PLATE

* MODIFIED DIMENSIONS

Figure 16 - Round and Flat Test Specimen Configurations



SYMBOL	CODE NO.	THICK-NESS(IN.)	AGING TREATMENT	WELD METAL COMP (%)			
				Ti	Mn	Si	Al
●	D99G05	0.48	4 HR AT 835 ± 10 F	0.33	0.14	0.06	0.06
■	D99G06	0.73	RMC-68 CYCLE	0.32	0.14	0.07	0.07
WELD WIRE	HEAT 09391	0.093	--	0.65	0.08	0.02	0.08

SPECIMEN TYPE	MECHANICAL PROPERTIES			
	0.2 % YTS (KSI)	UTS (KSI)	EL (%)	R OF A (%)
1/2-IN. ROUND BAR	231.8	234.3	4.3	28.3
1/2-IN. FLAT BAR	237.6	244.9	3.8	10.5
3/4-IN. ROUND BAR	215.6	222.5	3.2	17.5
3/4-IN. FLAT BAR	222.4	233.6	3.7	14.6

NOTE: CLOSED SYMBOL DENOTES CRACK LENGTH; OPEN SYMBOL, CRACK DEPTH

Figure 17 - Crack Size Versus Net Fracture Stress in Aged 0.48- and 0.73-in. Thick Submerged Arc Welds

been changed to the four-hour cycle at 835 F. Figures 18 and 19 show macro photographs of cross-sections of 1/2- and 3/4-inch welds made by using improved parameters.

Further investigation was accomplished using lower titanium in the weld bead than was used for the welds reported above to further improve fracture toughness. This work was not completed in time for use in 260-SL-1 case welding. However, the lower titanium wire was used for 260-SL-2 case welds. The results, strength and fracture toughness, are shown in Figure 20.

(4) Welding Procedures

(a) Weld Preparation

The flat cylinder plates were machined on the outside surface for both longitudinal and one circumferential seams. The dome gores were machined on the outside surface for the longitudinal welds after forming. The dome, attach flanges, Y-rings, and remaining cylinder circumferential weld preparations were machined on a boring mill on outside surface only. The inside surface weld preparation for all submerged-arc welds was done after making the outside surface weld pass by air-arc gouging and hand grinding.

(b) Weld Pass Sequence

In most cases the outside surface weld pass was made first. This procedure was used as an assist in controlling weld deformation. Two longitudinal welds were made using the reverse procedure, which resulted in a much more pronounced out-of-contour condition at the weld than was encountered when the outside surface weld pass was made first.

(c) Weld Conditioning

All welds were plateau ground then polished flush with the adjoining plate. This practice permitted ultrasonic examination of the weld bead and heat-affected zone and reduced the difficulty in X-ray interpretation encountered when the weld reinforcement in left intact.

b. Tungsten Inert Gas Welding (TIG)

The TIG welding method differs from the submerged-arc welding method in that an inert gas shields the weld puddle from oxidation rather than welding under a layer of flux. Another difference is that the arc-forming tungsten electrode is nonconsumable and the filler wire is fed into the molten weld puddle.

(1) Automatic TIG Welding

Automatic TIG welding was selected for the revised skirt-to-Y-ring joint, Figure 21) for several reasons: (1) limited access to the backside of the weld; (2) inability to control drop-through of a submerged-arc weld; and (3) excessive distortion from a one-sided submerged-arc weld. The welding procedure selected was a manual nonfiller wire, 100-percent fusion pass using argon as a backside purge. Backside purge was accomplished by sealing the opening between the skirt and dome with clear plastic and maintaining a constant flow of argon. Five automatic TIG passes were used to fill the double

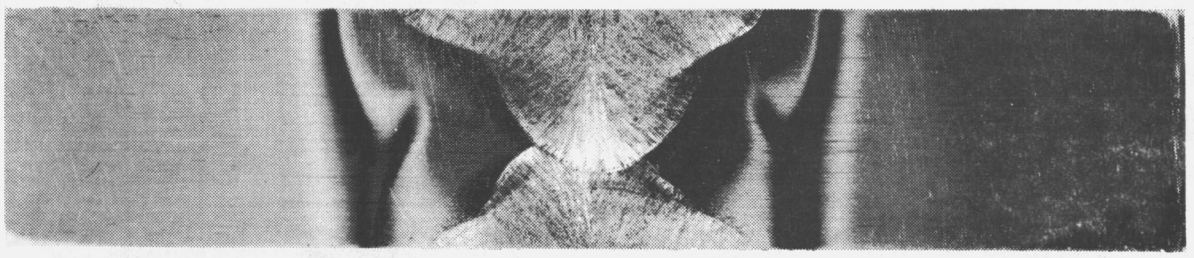


Figure 18 - Transverse Section of 1/2-In. Thick, Two-Pass Submerged Arc Weld Using Improved Weld Parameters (2X)

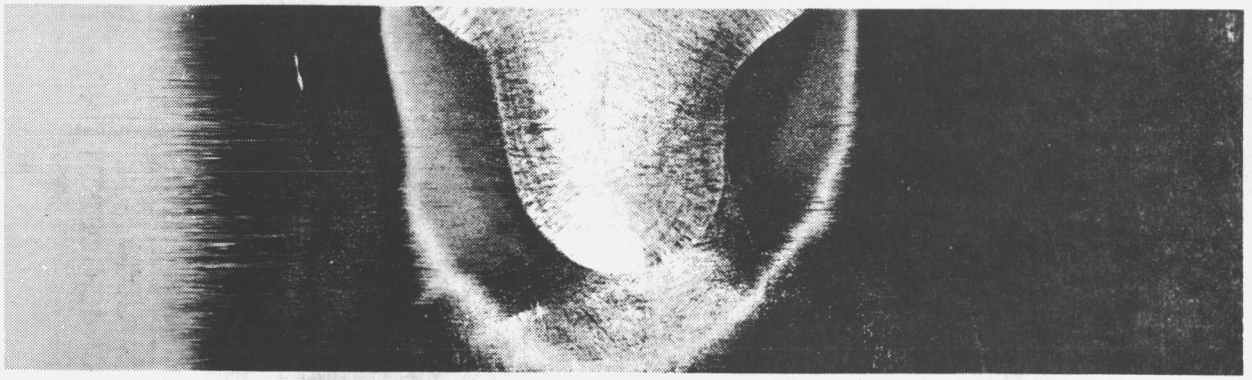


Figure 19 - Transverse Section of 3/4-In. Thick, Two-Pass Submerged Arc Weld Using Improved Weld Parameters (2X)

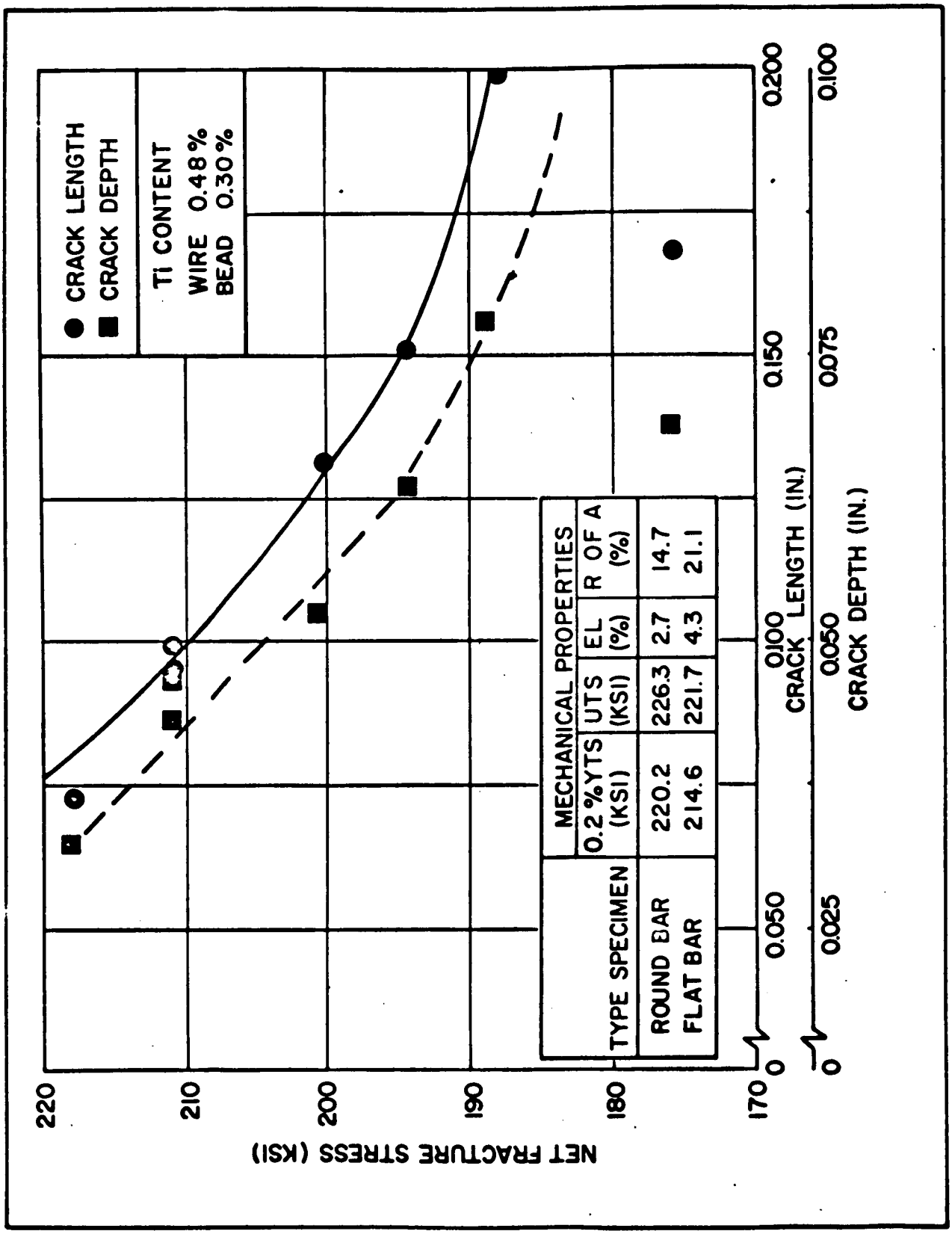
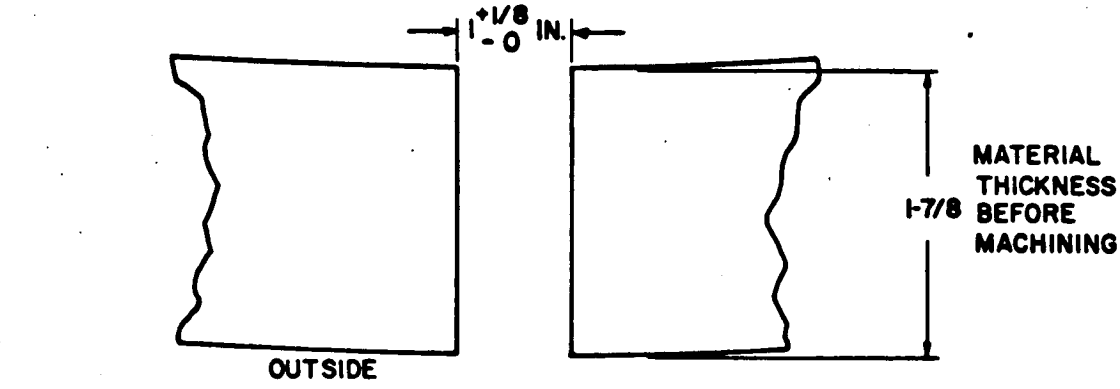
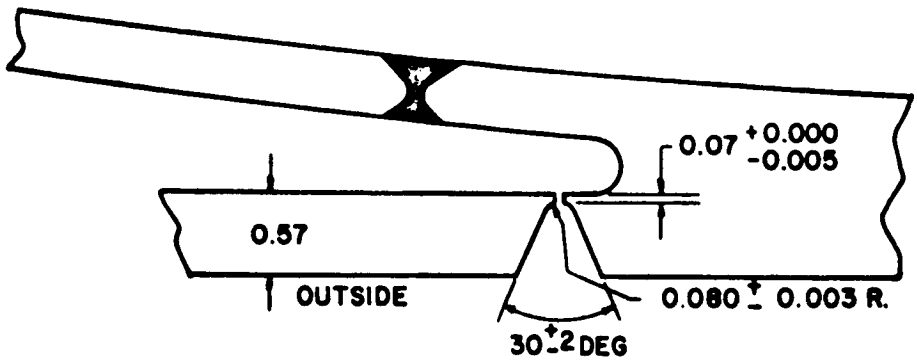


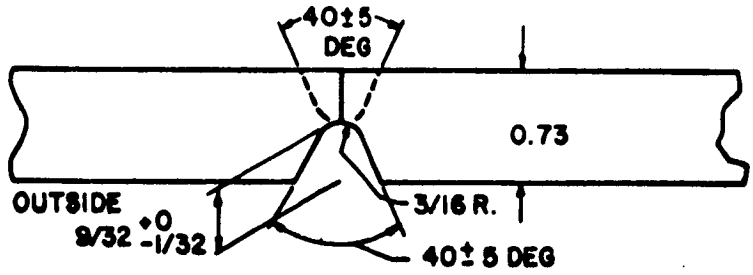
Figure 20 - Crack Size versus Net Fracture Stress in Submerged Arc Welds Made Using Low-Titanium Weld Wire



Y-RING JOINT CONFIGURATION - VERTICAL-SUBMERGED-ARC WELD



SKIRT-TO-Y-RING JOINT CONFIGURATION - MULTIPASS TIG WELD



CYLINDER-TO-CYLINDER CONFIGURATION - TYPICAL TWO-PASS SUBMERGED ARC WELD

Figure 21 - Typical Weld Joint Configurations for 260-SL Cases

U-joint. This type of welding was employed with the 156-inch diameter cases; therefore, the basic parameters were available. The development effort consists mainly of developing control of drop-through, correlation between radiography of a weld with an unground bead reinforcement, and micro and macro examination of the weld quality. Radiographic studies were necessary in order to establish the conditions which would appear on the X-ray as back-side lack of fusion when, in reality, it was a condition caused by the weld reinforcement. The effect of the drop-through on ultrasonic inspection was also determined. After establishing the feasibility of making and inspecting this type of weld, a weld qualification test panel was made by the welder who would make the production weld. The parameters used and the results obtained are given in Table X and Figure 22. The results indicated that the properties and quality of the weld were satisfactory.

(2) Repair by TIG Welding

TIG weld repair was performed in two areas: repair of parent plate and repair of welds. The repair of parent plate was an infrequent occurrence. It consisted mainly of repairing isolated pits and handling gouges. All repairs to 260-SL-1 parent plate were qualified by a repair mock-up made prior to repair of the plate. A typical example of this type of qualification is as follows: A defect 1-1/4-inch long by 3/4-inch wide by 0.073-inch deep was simulated and repaired using standard manual TIG welding procedures. The sample was aged at 900 F for three hours and a flat bar tensile specimen obtained and pulled. Four parent material unwelded control specimens were also pulled. The results obtained were as follows:

	0.2% Yield Tensile Stress (ksi)	Ult. Tensile Stress (ksi)	Elongation (%)	Reduction of Area (%)
Repair	254.0	258.4	9.0	28.4
Control	262.0	269.0	11.0	32.9

The efficiency, 97 percent on yield strength and 96.2 on ultimate tensile strength, are well above the weld design efficiency.

TIG weld repair of submerged-arc welds was more prevalent and caused more difficulty than repair of parent plate. The parameters used for TIG weld repair of case submerged-arc welds were derived from the TIG weld repair procedures used on the hydrotest adapter. For this reason no repair qualification was required prior to start of case weld repairs. It is to be noted that initially MIG (manual, fine wire) repair had been used on the hydrotest adapter. The results were poor, due to excessive porosity in the repair area. Therefore, this method of repair was discontinued during hydrotest adapter fabrication.

Initial repairs on the 260-SL-1 case resulted in cracking within the repaired area. The cracking appears to have initiated at the age-hardened section of the weld at the repair weld heat-affected zone, as shown in Figure 23. The cracking was multidirectional in nature and of the thermal shock type. An attempt was made to resolve the problem by controlling pre-heat at 350 F, reducing weld wire titanium content from 0.6 percent to 0.4 percent, and changing welding

TABLE X

WELD PARAMETERS OF TIG QUALIFICATION WELD

WELD MATERIAL AND CONDITIONS

Welding process - TIG (tungsten inert gas)

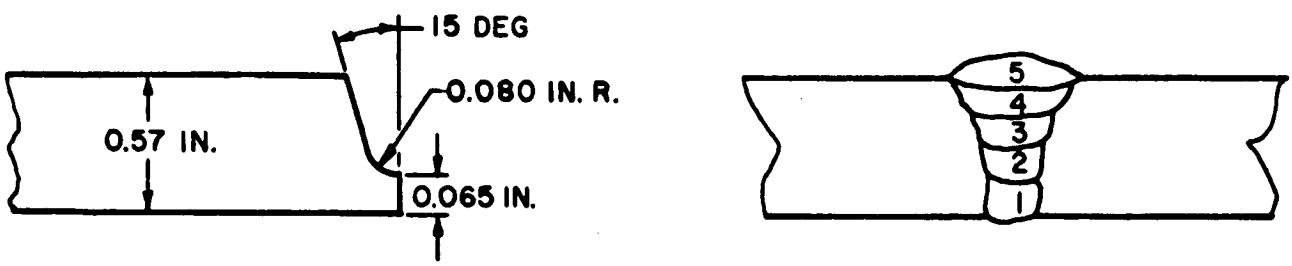
Filler metal - 3/32-in. diameter 18-percent nickel maraging steel

Preheat temperature - ambient

Interpass temperature - 250 F max

Weld preparation - clean joints with acetone

JOINT DESIGN AND BEAD SEQUENCE



WELD SETTINGS

Pass No.	Amperes	Volts	Travel Speed (in./min.)	Wire Feed (in./min.)	Argon Gas Flow (cu ft/hr)	
					Torch	Purge
1	340	12	5 1/4	12	35	10
2	310	13	4 5/8	12	55	35
3	370	15	4 1/2	22	55	35
4	400	14	4 1/2	22 1/2	55	35
5	400	14	4	22 1/2	55	35

NOTES: 1. A 1/8-in. tungsten electrode was used for pass 1, and a 3/16-in. tungsten electrode was used for passes 2 - 5

2. Base material was from heat X53158, slab 224412

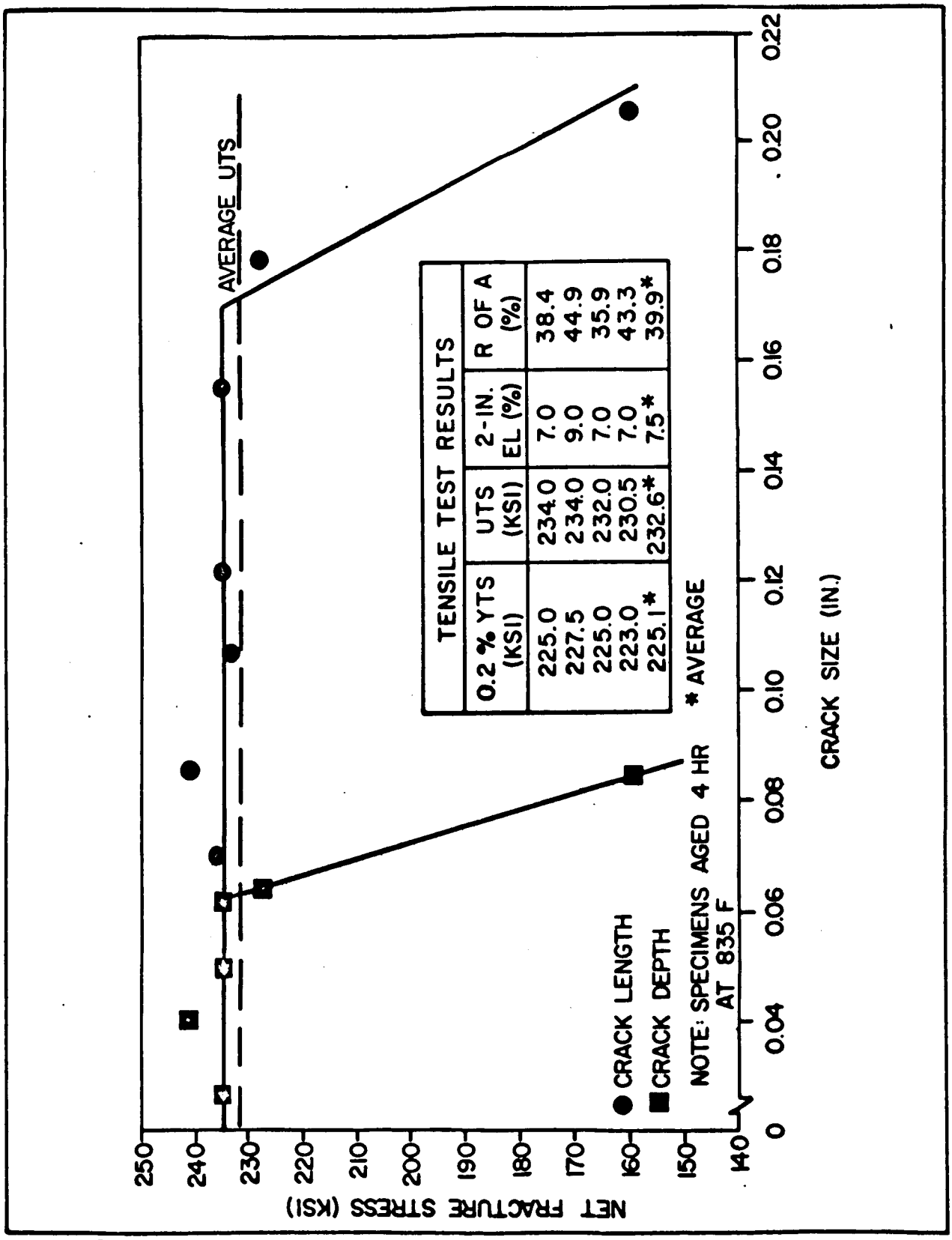


Figure 22 – Fracture Toughness Evaluation of Multipass TIG Qualification Weld

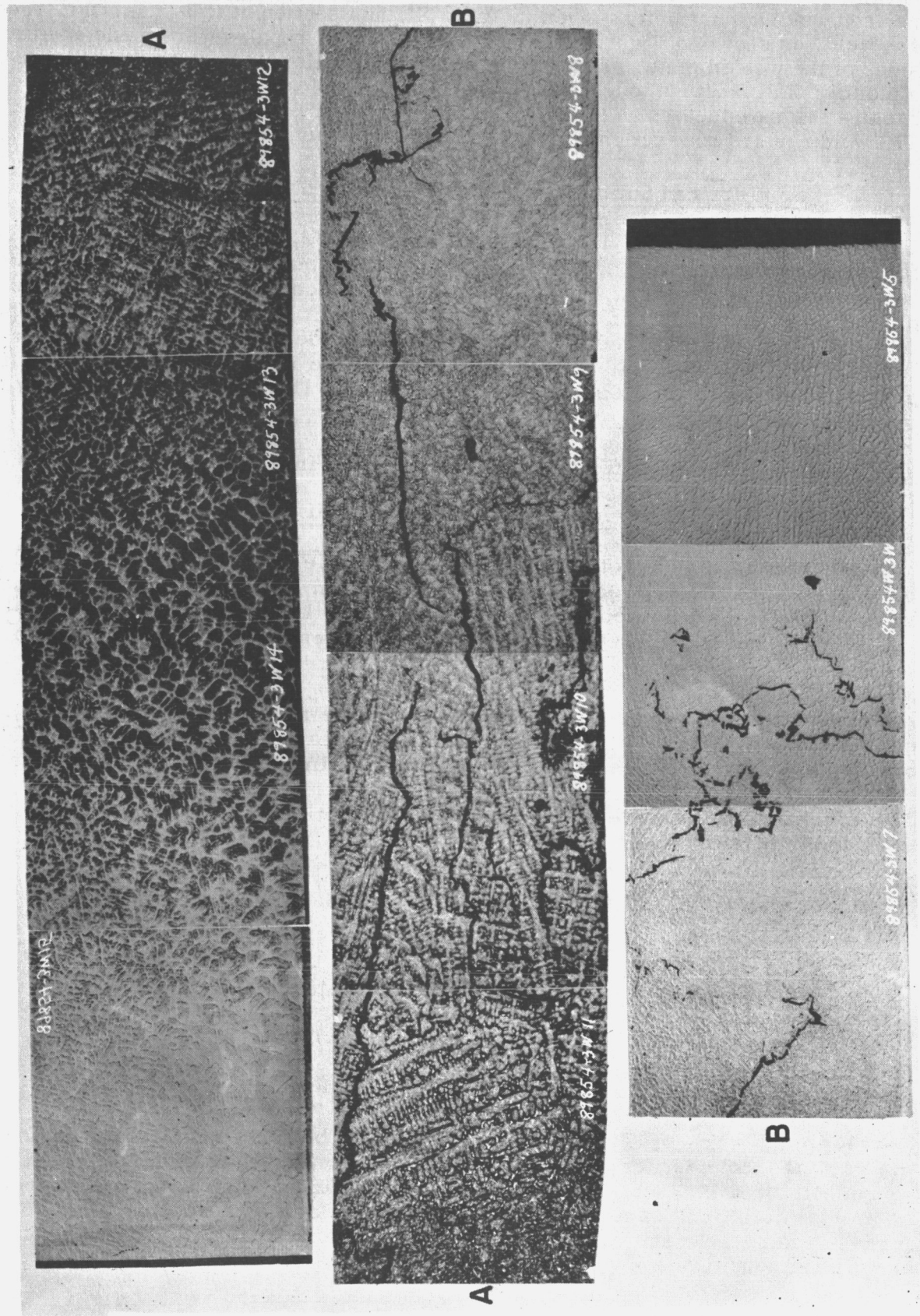


Figure 23 - Weld Crack Located in the Longitudinal Microspecimen.
(Mag: 100X and Etchant: Kroll's Reagent)

parameters. These changes required re-qualification. Repairs were made using the revised welding parameters given in Table XI, in a section of two-pass submerged-arc weld, as shown in Figures 24 and 25. In all, four repairs were made on alternate sides of the welded plate. Table XI presents the tensile test results, and Figure 26, a plot of (NFS) fracture toughness. These results indicate that multipass TIG weld repairs are satisfactory as far as strength and fracture toughness are concerned. TIG weld repairs however may induce cracking in the submerged-arc weld.

c. Vertical Submerged-Arc Welding (VSA)

The VSA weld process, a variation of the submerged-arc process, was used for welding the Y-ring longitudinal joints. The butt joint, shown in Figure 21, is positioned vertically, and weld forms (water cooled copper dams) are placed on either side and bottom of the weld joint. Granular flux is poured into the formed area, and a consumable electrode (weld wire) is submerged in the flux. After an arc is begun, the electrode is raised through the flux proportionately to the deposition of weld wire. The tooling required for this process was developed by the case fabricator.

The results of the qualification tests are shown in Table XII and Figure 27.

d. Production-Aged Weld Properties of 260-SL-1 Case

The mechanical and fracture toughness properties obtained from welded test bars aged with the respective components are in Table XIII. The nominal aging cycle for all components was 835 F for 3 1/2 to 4 hours. The K_{IC} values have been calculated from partial thickness crack tension test specimens.

Approximately 42 percent of the test values are not suitable for valid K_{IC} calculations as the gross fracture stress is greater than the uniaxial yield or the net fracture stress is greater than 1.1 times the gross fracture stress.

The four conditions necessary for valid calculation of K_{IC} from partial thickness tension tests are:

1. Stress gross (σ_G) < yield (σ_{YS})
2. σ_{NET} (net fracture stress) $< 1.1\ \sigma_G$
3. Crack depth < 1/2 specimen thickness
4. Crack length < 1/3 specimen width

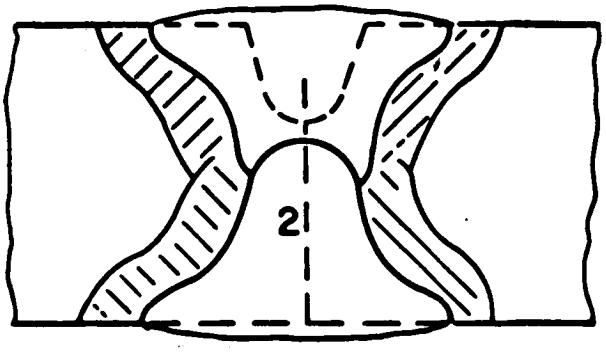
The tests in question do not satisfy conditions 1 and 2.

Development work by Thiokol has established that K_{IC} results obtained from the partial thickness crack tension tests are of the same order of magnitude as results obtained from slow bend tests and single edge notch tests providing sample, equipment, and calculations are correct. The scatter band obtained from partial thickness crack results is no greater than the scatter band associated with the slow bend or single edge notch test.

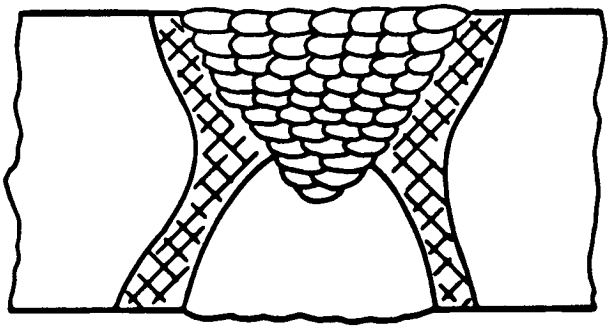
TABLE XI

BEAD SEQUENCE AND WELDING DATA OF MULTIPASS TIG WELD REPAIR INVESTIGATION

SUBMERGED ARC WELD CONFIGURATION



TYPICAL TIG WELD REPAIR



Weld Materials and Parameters	
Welding process	Tungsten arc, inert gas (TIG)
Welding power supply	Westinghouse; type RA; direct current, straight polarity
Inert gas	Pure argon, 40 cu ft/hr
Filler metal	Armetco, heat no. 09231, 1/16-in. dia
Electrode and cup size	3/32-in. dia tungsten no. 7 cup with gas lens
Preheat temperature	300 F
Interpass temperature	300 F
Welding current	150 amps
Welding voltage	15 to 16 volts

TENSILE CHARACTERISTICS OF TIG REPAIRS

Specimen No.	0.2 % Yield Tensile Stress (ksi)	Ult. Tensile Stress (ksi)	Elongation (%)	Reduction of Area (%)
1	204.0	218.0	7.0	35.4
2	215.0	228.0	4.0	24.1
3	216.0	228.0	2.0	29.4
4	210.2	223.5	5.0	34.4
Avg	211.2	224.4	4.5	30.8

NOTE: Specimens were aged at 835 F for 4 hours.

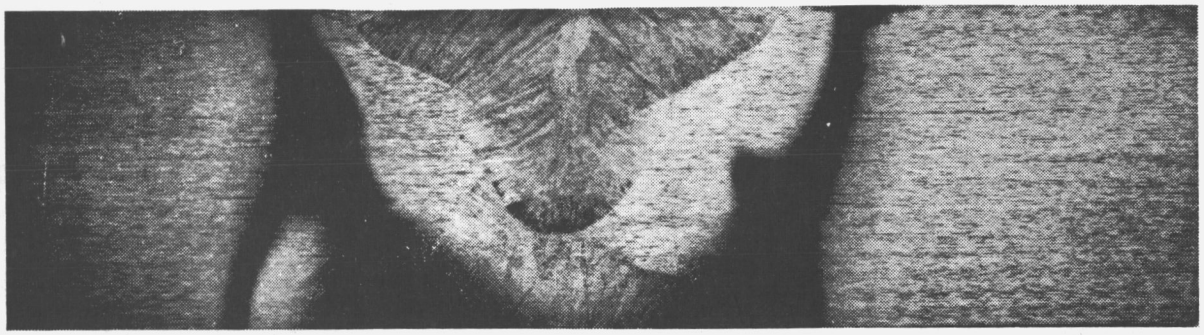


Figure 24 - Transverse Section of 3/4-In. Thick, Two-Pass Submerged Arc Weld (2X)

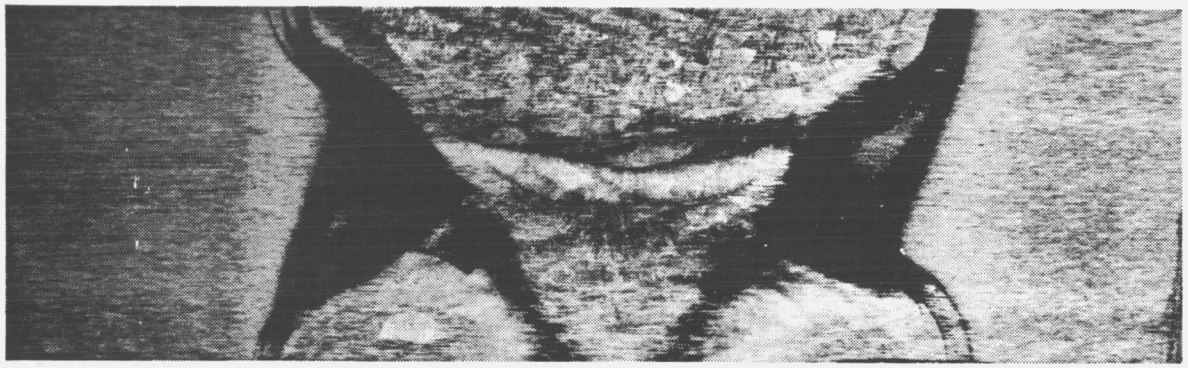


Figure 25 - Transverse Section of 3/4-In. Thick, Two-Pass Submerged Arc Weld Repaired Using Multipass TIG Weld Method (2X)

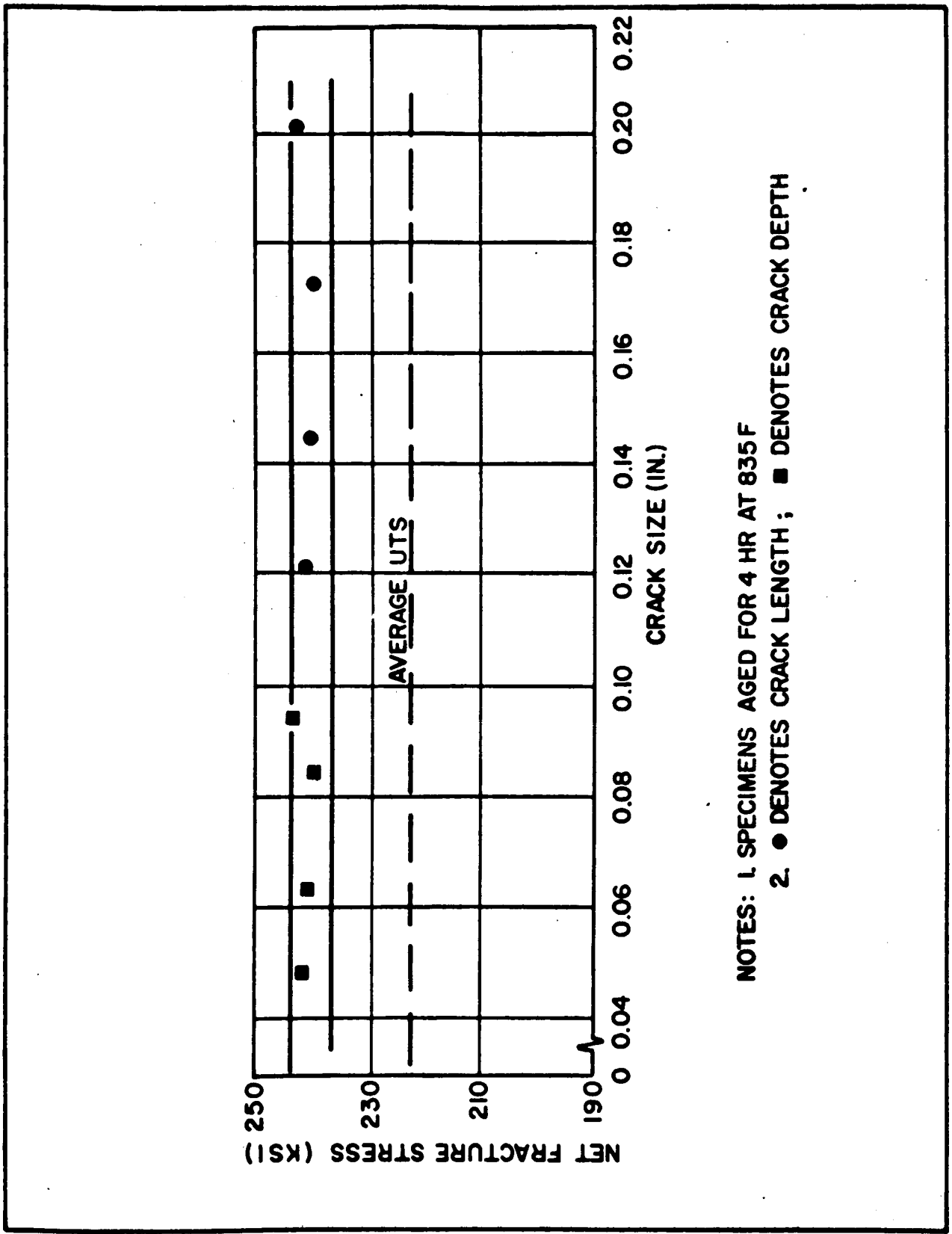


Figure 26 - Crack Size versus Net Fracture Stress of Specimens Taken from Heat-Affected Zone of TIG Repair Weld

TABLE XII

WELD PARAMETERS OF VERTICAL-SUBMERGED-ARC QUALIFICATION WELD

WELD MATERIAL AND CONDITIONS

Welding process - vertical submerged arc

Filler metal - Armetco heat 08066

Type flux - 60-percent calcium flouride and 40-percent flux 105

Flux condition - baked 1 hr at 600 F

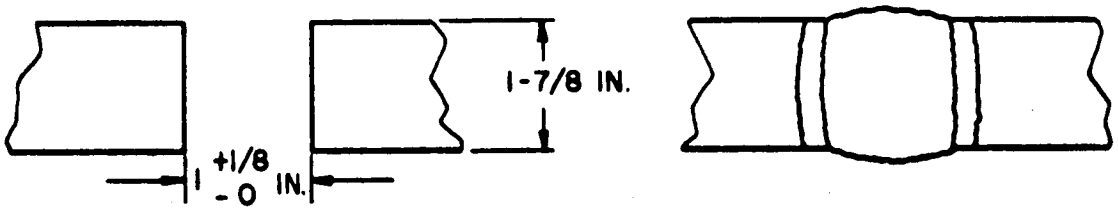
Weld preparation - clean joint with acetone

Preheat temperature - 250 F

Interpass temperature - 250 F max

Plate thickness - 1-7/8 in.

JOINT DESIGN AND BEAD CONFIGURATION



WELD SETTINGS

Amperes	Volts	Travel Speed (in./min.)	Wire Projection (in.)
500	38	22	2.5

NOTE: Base material was from heat 53201, plate 1C

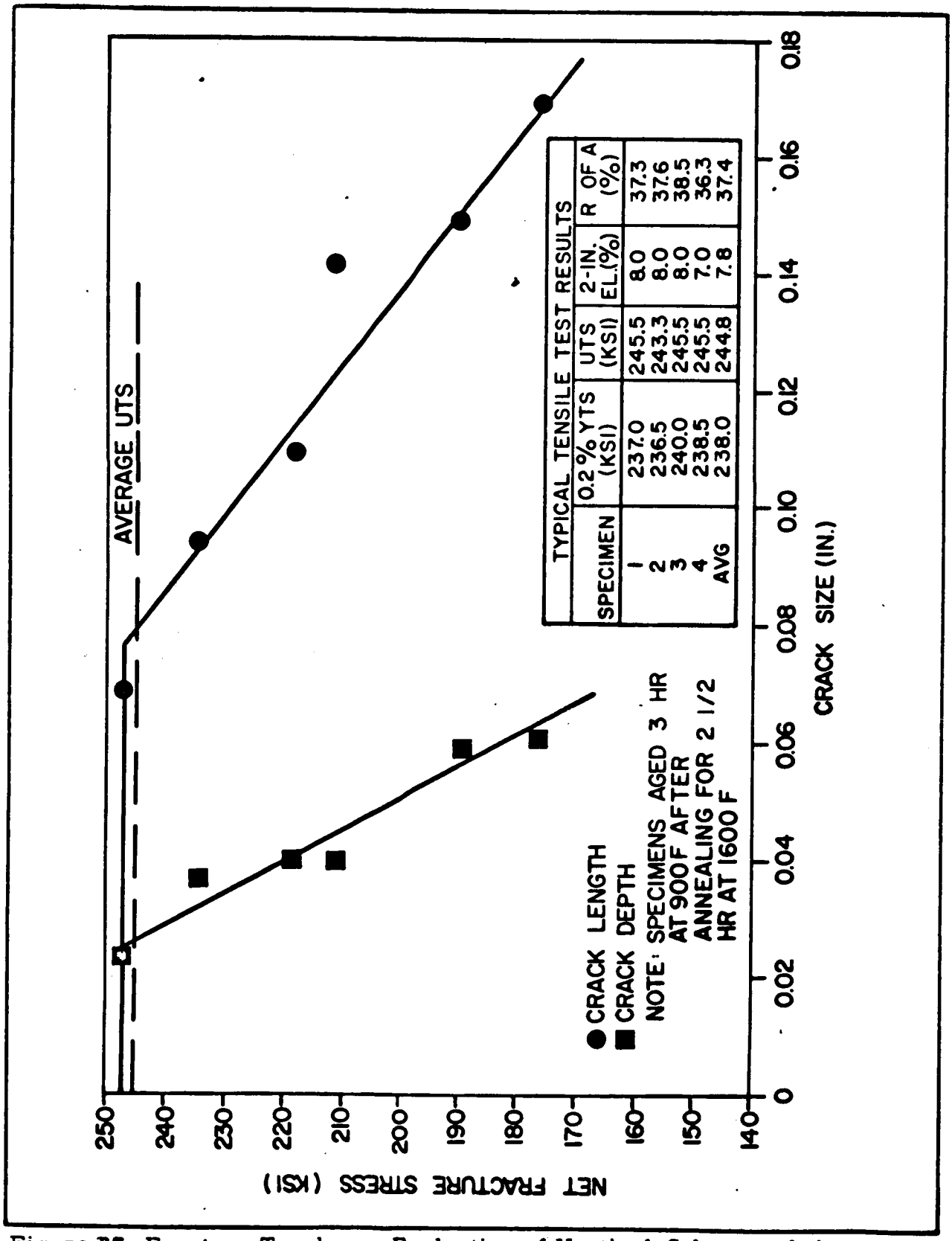


Figure 27- Fracture Toughness Evaluation of Vertical-Submerged-Arc Qualification Weld

TABLE XIII

MECHANICAL AND FRACTURE TOUGHNESS OF 260-SL-1 WELDS PRODUCTION AGED

Weld No.	Yield Tensile Strength (ksi)	Ult. Tensile Strength (ksi)	Gage Elongation (%)	Reduction of Area (%)	Crack Length (in.)	Crack Depth (in.)	Gross Fracture Stress (ksi)	Net Fracture Stress (ksi)	K_{IC} (ksi in.)
Forward Subassembly									
W2-1	228.2	236.4	5.0	16.2	0.100	0.048	208.3	214.0	60.1
W1-101	No test								
W1-102	253.3	246.5	3.0	8.7					
W1-103	225.3	228.6	6.0	23.8					
W1-104	224.1	228.6	6.0	31.7	No fracture test scheduled				
W1-105	No test								
W1-106	225.6	229.5	7.0	30.9					
W1-107	220.5	224.3	8.0	36.6					
W1-108	238.8	247.8	6.0	36.8					
W4-1	219.9	223.5	8.0	39.0	0.100	0.048	230.1	236.5	g
W6-1	229.9	233.0	9.0	40.2	0.150	0.046	212.1	219.0	73.2
W5-101	201.5[a]	206.0	10.0	61.3	0.098	0.040	223.1	227.2	g
W5-102	219.0	224.5	9.0	50.2	0.104	0.046	203.4	207.8	59.9
W3-101	220.0	226.0	8.0	47.8	0.100	0.048	231.2	235.3	g
W3-101	234.0	245.0	9.0	41.6	0.102	0.048	233.6	237.8	68.9
W3-102	233.0	240.0	4.0	25.4	0.103	0.049	178.1	181.4	51.5
W3-102	234.0	241.5	5.0	41.9	0.112	0.040	213.7	217.2	64.7
W3-103	234.0	239.0	8.0	46.9	0.097	0.047	206.4	209.8	58.6
W3-103	224.5	230.0	8.0	46.9	Bar cracked in two places				
W3-104	232.0	243.0	11.0	51.1	0.104	0.050	239.9	244.6	g
W3-104	229.0	238.5	6.0	30.5	0.098	0.042	220.6	224.0	63.3
W8-1	192.0[b]	202.5	6.0	35.9	0.092	0.025	226.3	228.3	g
W7-101	211.0	217.0	9.0	47.3	0.100	0.042	214.5	218.2	g
W7-102	219.0	223.0	c	45.3	0.104	0.042	217.5	218.3	64.5
Center Subassembly									
W7-201	223.0	231.0	9.0	53.6	0.100 0.111	e 0.045	228.0 207.0	228.0 210.8	g N.C.
W7-202	230.5	224.0	6.0	37.1	0.098 0.100	0.045 0.037	197.0 213.3	200.1 216.2	56.0
W8-2	230.0	235.0	8.0	40.2	0.108	0.045	204.3	207.9	61.0
W8-2	228.0	232.0	7.0	40.2	0.102	0.037	210.0	212.9	N.C.
W7-203	No test (Both bars used pre-aging)				0.103 0.100	0.046 0.034	203.9 214.4	207.5 217.1	59.6 N.C.
W7-204	213.0	222.0	1.0[d]	43.7	0.105 0.100	e e	226.4 222.1	226.4 222.1	g g
Forward to Center Subassembly (Local Age)									
W9-12	---	224.0	4.0	29.4	0.100	0.043	206.5	209.8	N.C.
Aft Subassembly									
W7-301	No test								
W7-302	No test								
W8-3	234.0	237.0	3.0[c]	27.8	0.100	0.025	235.6	237.8	g
W3-301	237	242.0	9.0	44.6	0.098	f			
W3-301	237.5	242.0	5.0	45.5	Edge cracks				
W3-302	231.0	237.0	5.0	29.5	0.104	0.025	230.4	232.6	63.7
W3-302	234.0	240.0	9.0	44.0	0.092	f			
W3-303	243.0	251.0	8.0	49.2	0.098	f			
W3-303	237.0	247.0	8.0	46.3	0.097	0.033	239.0	241.9	g

TABLE XIII (Cont'd)

MECHANICAL AND FRACTURE TOUGHNESS OF 260-SL-1 WELDS PRODUCTION AGED

Weld No.	Yield Tensile Strength (ksi)	Ult. Tensile Strength (ksi)	Gage Elongation (%)	Reduction of Area (%)	Crack Length (in.)	Crack Depth (in.)	Gross Fracture Stress (ksi)	Net Fracture Stress (ksi)	K_{IC} (ksi in.)
W3-304	225.0	230.0	9.0	47.8	0.097	0.048	225.5	229.3	64.4
W3-305	237.5	249.4	8.0	45.2	0.098	0.045	232.6	236.6	66.9
W3-305	234.5	244.0	8.0	43.1	No second fracture test bar				
W3-306	234.0	245.0	10.0	46.3	0.101	0.046	209.4	213.2	60.7
W3-306	231.0	246.0	9.0	43.4	No second fracture test bar				
W4-3	231.2	239.5	6.0	26.8	Cracked in wrong place				
W10-301	229.0	238.5	5.0	18.1	Cracked in wrong place				
W10-302	229.0	240.0	5.0	18.1	0.098	0.032	233.3	236.0	g
W10-303	228.0	238.0	8.0	38.8	Edge crack				
W10-304	234.0	245.0	5.0	23.4	Edge crack				
W10-305	235.5	245.5	5.0	22.0	0.075	0.015	231.2	232.1	52.1
W10-306	230.0	240.0	5.0	77.7	Did not break through crack				
W10-307	225.0	234.0	7.0	33.1	Edge crack				
W10-308	222.0	232.0	10.0	47.2	Cracked in wrong place				
W5-301	231.0	236.0	c	20.2	0.104	0.050	212.8	217.6	62.7
W5-302	233.5	237.5	7.0	44.6	0.103	0.024	232.8	235.3	63.9
W2-3	208.7	213.5	7.0	37.0	0.108	f	218.8	218.8	g
W10-3	No test								
W1-301	229.9	239.2	2.0	8.0	No fracture tests scheduled				
W1-302	233.1	242.4	8.0	27.0					
W1-303	222.2	226.4	8.0	32.6					
W1-304	209.5	221.4	6.0	20.1					
W1-305	235.7	243.8	9.0	28.7					
W1-306	216.0	223.5	10.0	37.3					
W1-307	216.5	222.7	8.0	36.3					
W1-308	223.9	231.7	8.0	37.1					
W6-3	238.5	246.0	9.0	41.9	0.104	0.025	241.1	243.9	g

a Specimen was under gage

b Test result indicates bar was faulty

c Specimen broke outside gage length

d Specimen broke near gage mark, invalidating gage measurement

e Specimen broke in heat-affected zone

f Specimen did not break at imposed crack

g K_{IC} invalid as defined in text

N. C. Not calculated

5. Thermal Processing

a. Annealing

The temperature of solution annealing was specified to be within 1500 to 1650 F. A range was specified to allow compensation for the effects of the titanium content range (high titanium content - high strength, low titanium content - low strength) permitted by specification without varying the aging temperature. Figure 28 is a plot of the effect of varying the anneal temperature while maintaining a constant age temperature. It will be noted that there is approximately a 15,000 psi strength difference between the 1500 F and 1650 F anneal temperatures.

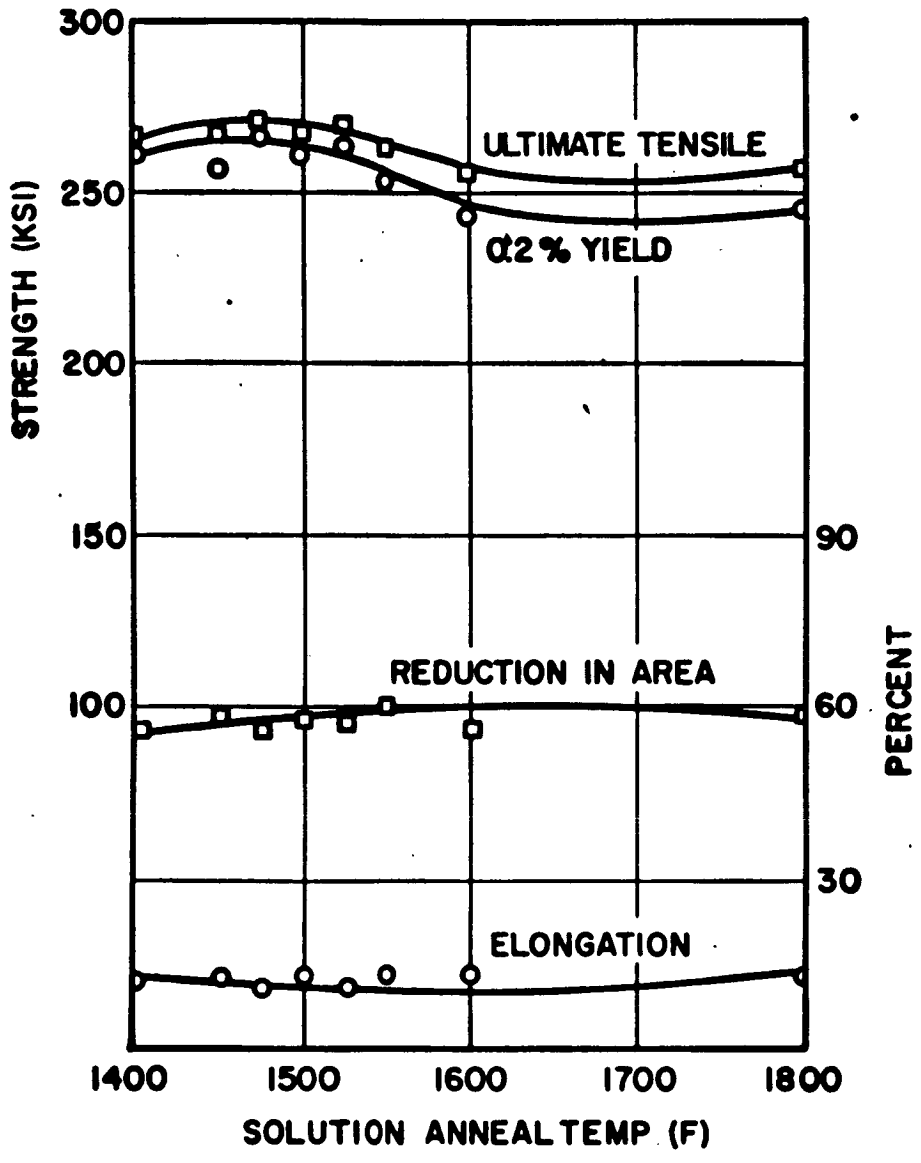
b. Reversion and Re-Solution Annealing

The basic metallurgy of the phases and transformations involved in maraging steel are austenite, nickel-iron martensite, precipitation hardened martensite and metastable austenite. The last phase, metastable austenite, is obtained through the process called reversion. This phase does not form in any appreciable amount in cooling from the austenitic phase at the solution annealing temperature of approximately 1500 F. However, on heating the martensitic material in the range 1200 to 1300 F, the transformation to a metastable austenite is very rapid. On cooling to room temperature, the material instead of transforming at approximately 500 F to martensite remains austenitic . This phase can only be changed by heating above the austenitizing temperature of approximately 1350 F and cooling to room temperature which causes the material to transform to martensite again.

The practice of transforming martensite to metastable austenite was used as an aid to property improvement by grain re-orientation and in preventing weld cracking by suppression of phase changes which caused high stress due to differential shrinkage. By far the major application was in preventing weld cracking. As deposited weld metal on cooling to room temperature is martensitic. Imposing differential heat on this structure by the second weld pass results in solution annealing, reversion, and aging. Each of these conditions has a different shrinkage value; therefore, high stresses are set-up which can result in cracking. If the first pass is reverted, the only change that can result from the heat of the second pass is solution annealing. Reverted material does not age, and the amount of additional material available for reversion is very small. Therefore, the magnitude of imposed stress is lower.

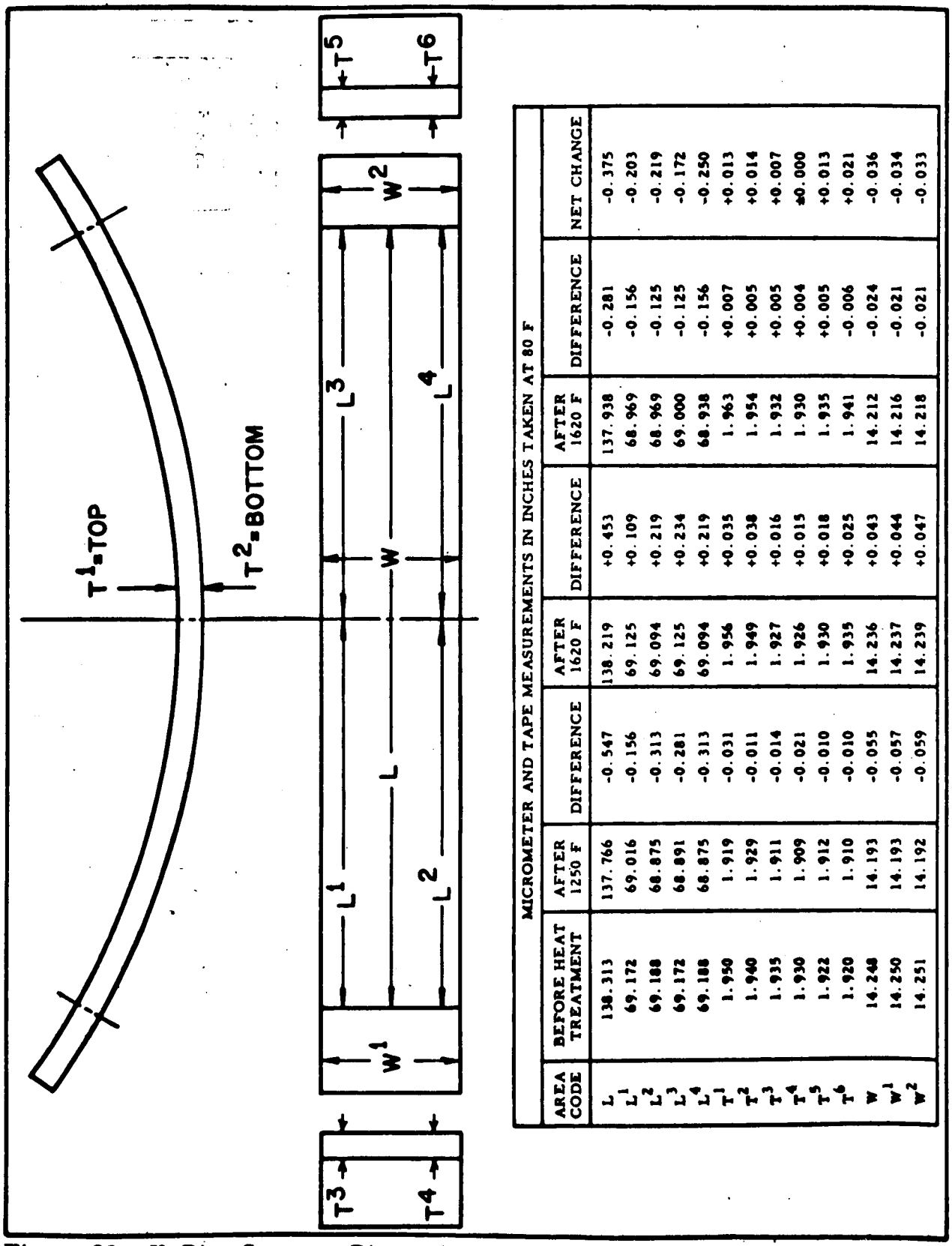
As stated above, there is shrinkage which occurs in the reversion process. In order to determine what effect this shrinkage would have on dimensional control, two pieces of material were subjected to reversion at 1250 F and double annealed at 1620 F. Measurements were taken before and after thermal treatment and the results shown in Figures 29 and 30. These results show that the specimens grew in the thickness plane and shrank in dimensions both parallel and transverse to the rolling direction. This work was further confirmed by a similar series of tests by the nozzle fabricator. Diameter allowances were made in all thick section components to be reverted to allow for shrinkage.

c. Aging



NOTE: SPECIMENS WERE SOLUTION ANNEALED FOR 30 MIN AT INDICATED TEMP, AIR COOLED, AND AGED 3 HR AT 900 F.

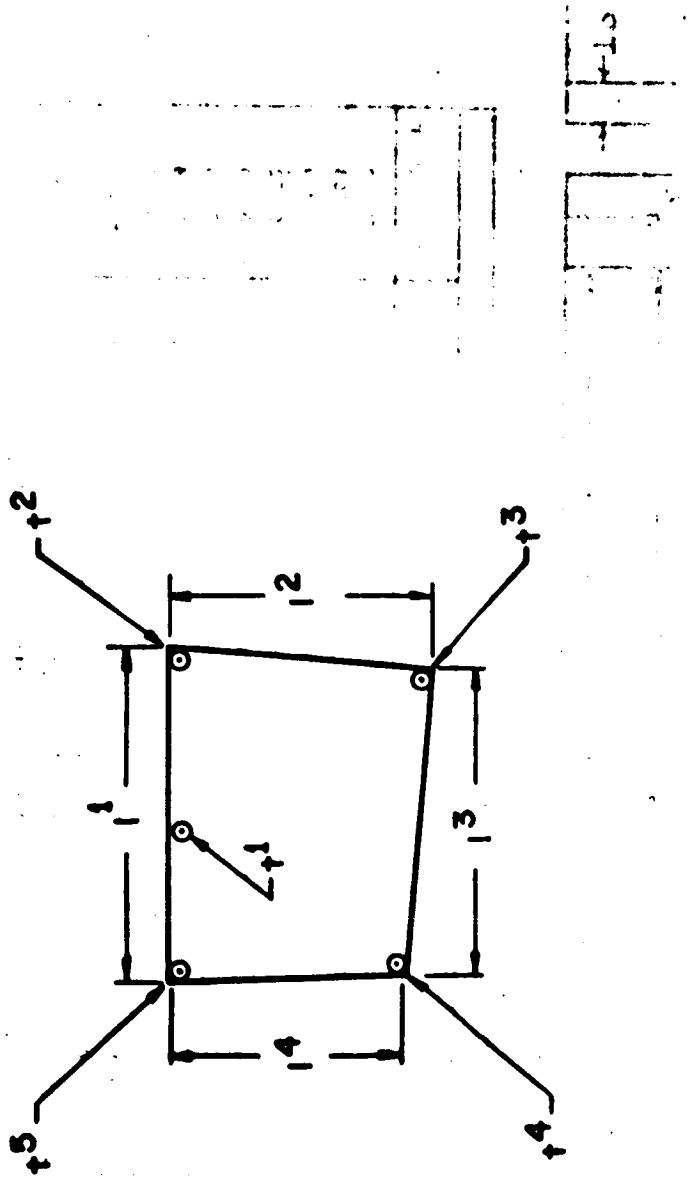
Figure 28 - Effect of Solution Annealing Temperature on Aged Tensile Properties of 18-Percent Nickel Maraging Steel (250-ksi Grade)



MICROMETER AND TAPE MEASUREMENTS IN INCHES TAKEN AT 80 F

AREA CODE	BEFORE HEAT TREATMENT	AFTER 1250 F	DIFFERENCE	AFTER 1620 F	DIFFERENCE	AFTER 1620 F	DIFFERENCE	NET CHANGE
L	138.313	137.766	-0.547	138.219	+0.453	137.938	-0.281	-0.375
L^1	69.172	69.016	-0.156	69.125	+0.109	68.969	-0.156	-0.203
L^2	69.188	68.875	-0.313	69.094	+0.219	68.969	-0.125	-0.219
L^3	69.172	68.891	-0.281	69.125	+0.234	69.000	-0.125	-0.172
L^4	69.188	68.875	-0.313	69.094	+0.219	68.938	-0.156	-0.250
T^1	1.950	1.919	-0.031	1.956	+0.035	1.963	+0.007	+0.013
T^2	1.940	1.929	-0.011	1.949	+0.038	1.954	+0.005	+0.014
T^3	1.935	1.911	-0.014	1.927	+0.016	1.932	+0.005	+0.007
T^4	1.930	1.909	-0.021	1.926	+0.015	1.930	+0.004	±0.000
T^5	1.922	1.912	-0.010	1.930	+0.018	1.935	+0.005	+0.013
T^6	1.920	1.910	-0.010	1.935	+0.025	1.941	-0.006	+0.021
W	14.248	14.193	-0.055	14.236	+0.043	14.212	-0.024	-0.036
W^1	14.250	14.193	-0.057	14.237	+0.044	14.216	-0.021	-0.034
W^2	14.251	14.192	-0.059	14.239	+0.047	14.218	-0.021	-0.033

Figure 29 - Y-Ring Segment Dimensions Taken during Component Shrinkage Evaluation



MICROMETER MEASUREMENTS IN INCHES TAKEN AT 80 F

AREA CODE	BEFORE HEAT TREATMENT	AFTER 1250 F	DIFFERENCE	AFTER 1620 F	DIFFERENCE	AFTER 1620 F	DIFFERENCE	NET CHANGE
l_1^1	30.218	30.079	-0.039	30.187	+0.108	30.150	-0.037	-0.068
l_2^2	27.903	27.776	-0.154	27.870	+0.094	27.830	-0.040	-0.073
l_3^3	26.166	26.048	-0.118	26.135	+0.087	26.107	-0.028	-0.059
l_4^4	25.597	25.479	-0.118	25.568	+0.099	25.535	-0.033	-0.062
t_1^1	1.918	1.909	-0.009	1.922	+0.013	1.928	+0.006	+0.010
t_2^2	1.930	1.920	-0.010	1.936	+0.016	1.940	+0.004	+0.010
t_3^3	1.943	1.932	-0.011	1.950	+0.018	1.955	+0.005	+0.012
t_4^4	1.940	1.930	-0.010	1.946	+0.016	1.951	+0.005	+0.011
t^5	1.926	1.916	-0.010	1.931	+0.015	1.936	+0.005	+0.010

Figure 30 - Scrap Plate Dimensions Taken During Component Shrinkage Evaluation

Most of the work on establishing aging response of maraging steel had been conducted in electric furnaces. Insofar as the furnace to be used for the case was oil-fired kerosene, it was necessary to determine if any special controls would be needed. In addition, various possible charging and heating practices were studied. The results, tabulated in Table XIV, of the laboratory effort were confirmed in the production furnace (reported in Technical Notes RPL-TDR-64-7 and 64-58). The results of these studies led to the following conclusions:

1. The use of a properly designed oil-fired furnace is satisfactory for aging of 18-percent nickel maraging steel, providing sulphur content of the fuel is controlled.

2. Oil-fired furnace combustion products do not appear to induce any damaging effects on the mechanical or metallurgical properties of maraging steel.

3. Test results confirmed the planned use of the large, oil-fired furnace for aging segments. Tests have shown that the furnace is capable, without modification, of attaining the necessary thermal uniformity and control response in the required temperature range.

4. A thermal cycle for the oil-fired furnace was delineated and recorded. This cycle was compatible with attainment of the (as then defined) optimum material properties in 230 ksi maraging steel.

5. The thermal cycle established was adequate for aging the two-pass submerged-arc weldments. The properties from these welds satisfied the requirements for welds established at that time. The products of combustion from the oil-fired furnace had no apparent damaging effect on these weldments.

The 900 F aging temperature originally specified leads to an over-strength condition that is responsible for reduced fracture toughness of welded material. A lower temperature, 835 F, was selected from development work accomplished outside the 623A program effort. Figure 31 is a plot of fracture toughness (W/A) and yield strength versus aging temperature.

d. Local Aging

As stated in the fabrication section of this report, local aging of two circumferential welds in each 260 case is required. The 156-inch cases had locally aged welds also; therefore, feasibility of accomplishing this was well established. Different type heaters and controls were planned for the 260-inch case welds than had been used for the 156-inch case welds. Therefore, welds were made in aged material and locally aged with the proposed quartz lamps system to qualify the process. Tensile results are included with a plot of fracture toughness in Figure 32. Strength and fracture toughness are normal or above normal; therefore, this process is satisfactory for local aging maraging steel welds.

TABLE XIV

ELECTRIC VERSUS KEROSENE FURNACE TENSILE SPECIMEN TEST RESULTS

Specimen Conditioning	Type Furnace	Average Mechanical Properties			
		0.2 % Offset YTS (psi)	UTS (psi)	2-in. Area Elongation (%)	Area Reduction (%)
Charge at 900 F, age 3 hr, air cool	Electric	247,500	251,500	8	35.4
Charge at 900 F, age 3 hr, air cool	Kerosene	247,750	252,000	10	40.5
Charge cold, heat 100 F/hr to 900 F, age 2 hr, air cool	Electric	237,750	242,000	10	37.9
Charge cold, heat 100 F/hr to 900 F, age 2 hr, air cool	Electric	246,250	251,750	8.5	43.7
Charge cold, heat 100 F/hr to 900 F, age 3 hr, air cool	Electric	248,000	252,250	7.5	37
Charge cold, heat 100 F/hr to 900 F, age 1 hr, cool 100 F/hr to 500 F, air cool	Electric	254,000	257,500	9.0	42
Charge cold, heat 100 F/hr to 900 F, age 2 hr, cool 100 F/hr to 500 F, air cool	Electric	254,750	258,250	8	39.2
Charge cold, heat 100 F/hr to 900 F, age 3 hr, cool 100 F/hr to 500 F, air cool	Electric	261,750	266,300	7.5	36.9
Charge cold, heat 100 F/hr to 900 F, age 3 hr, cool 100 F/hr to 500 F, air cool	Kerosene	256,500	261,000	9.0	39.6

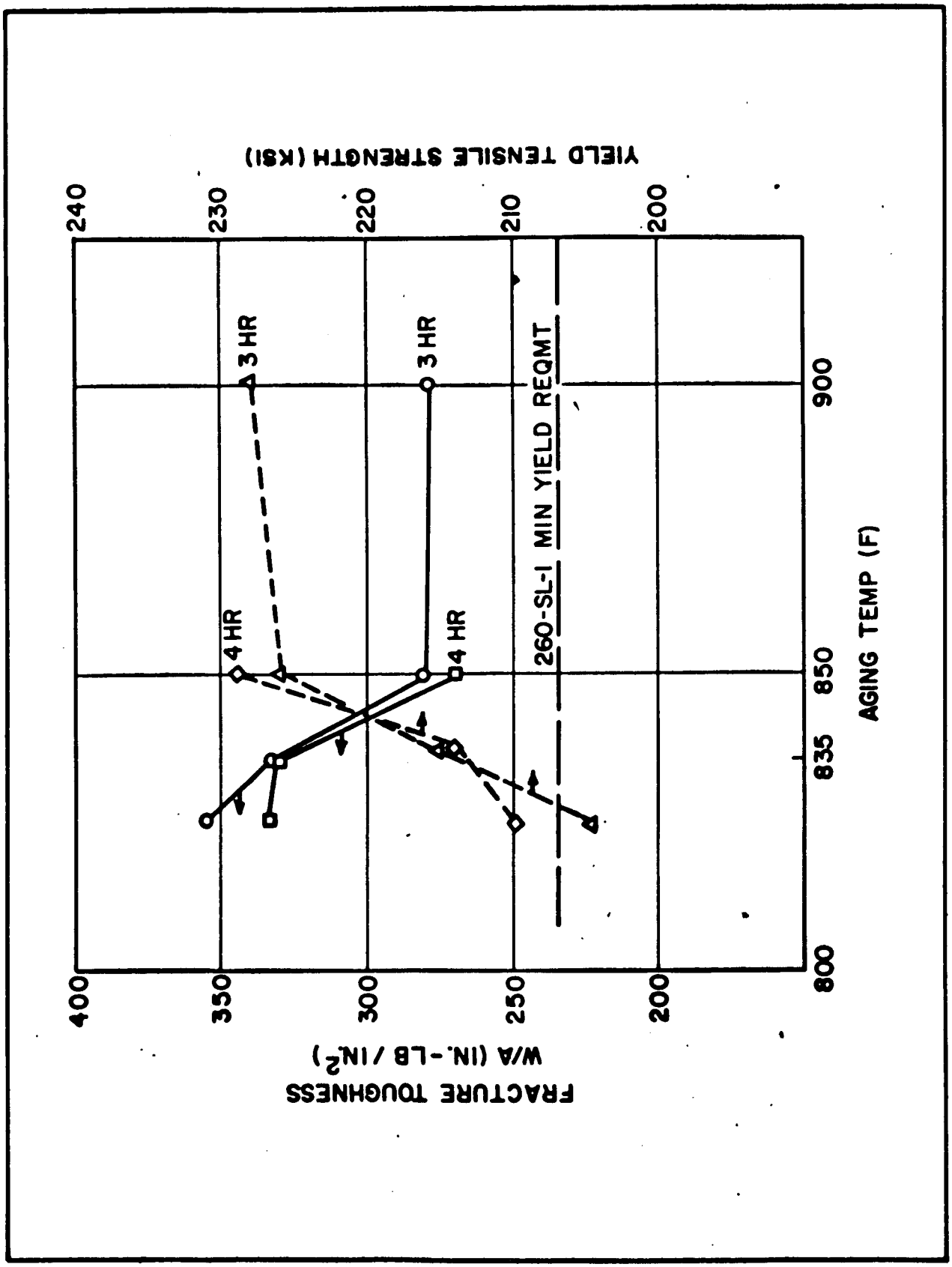


Figure 31 - Weld Fracture Toughness and Yield Strength versus Aging Temp

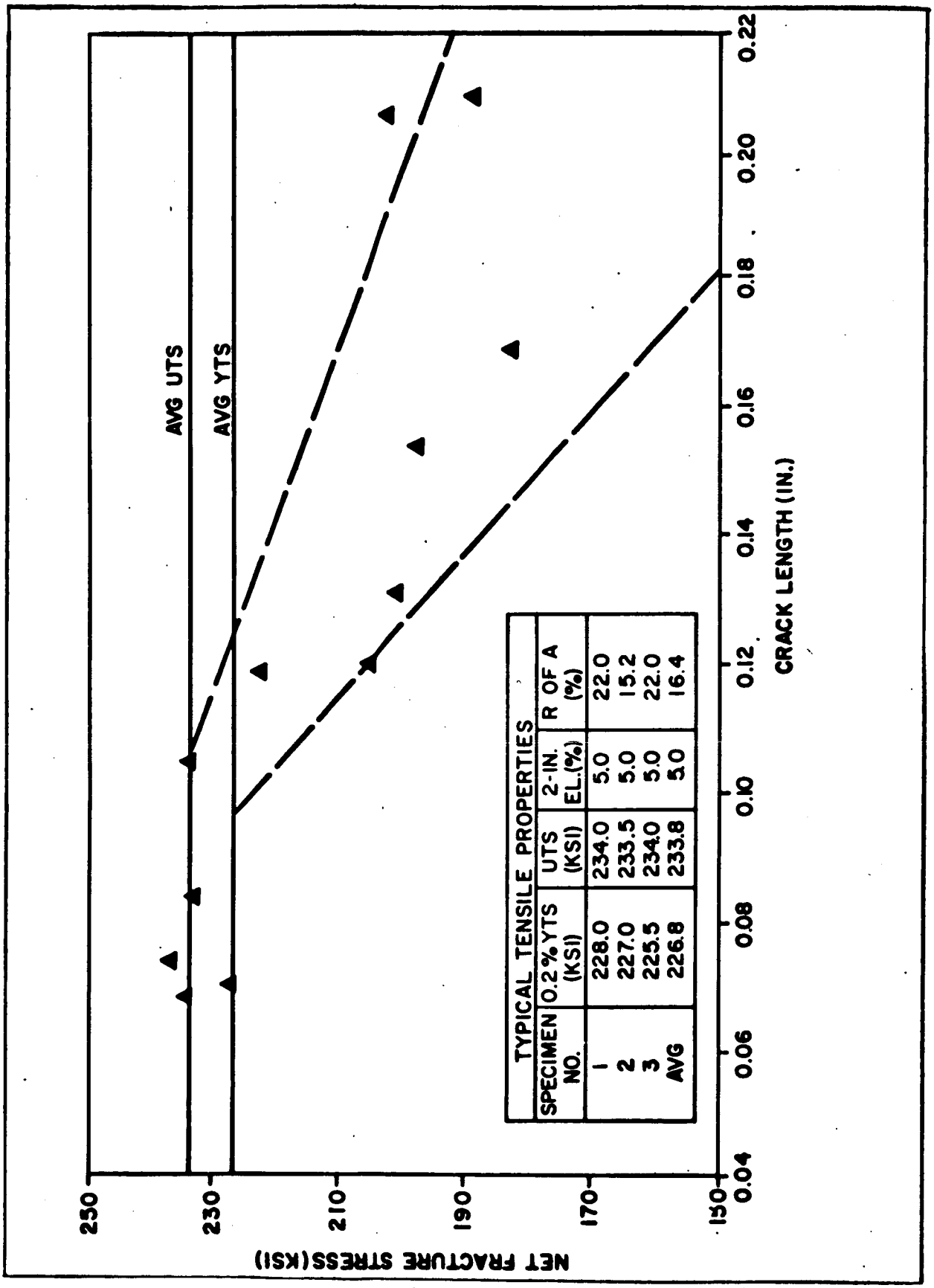


Figure 32 - Fracture Toughness of Locally Aged Welded Panels

6. Machining, Drilling, and Tapping

Machining was performed on case components in the aged as well as the unaged condition. All final machining was done with the material in the aged condition. Drilling and tapping were done with the material in the aged condition with the exception of the skirt holes. Figures 33 and 34 illustrate these operations.

a. Machining

The following parameters were used for machining in the aged condition:

Roughing cuts

Chip load	0.180 in.
Feed	0.015 in.
Speed	60 SFM (surface feet per minute)

Finish machining

Chip load	0.010 to 0.015 in.
Feed	0.015 in.
Speed	60 SFM

A K-6 carbide tool with approximately a 7-deg positive rake was used.

b. Drilling and Tapping

Aged maraging steel is best drilled with cobalt drills. Drill life is low, however, dimensional control is good. Due to the fact that the material softens as it is tapped it does not fill tapping die threads completely. Tapping can be done either by machine or hand. However, due to the gumminess of the material, there is a great tendency to "bell" when hand tapping.

The following parameters are recommended for drilling and tapping:

Drilling (11/16-in. dia. hole)

Speed	52 RPM
Feed	0.009 in.
Coolant	Soluble oil and water

Tapping

Speed	12 RPM
Coolant	White lead

These parameters were developed using high-speed tools in a radial drill press.

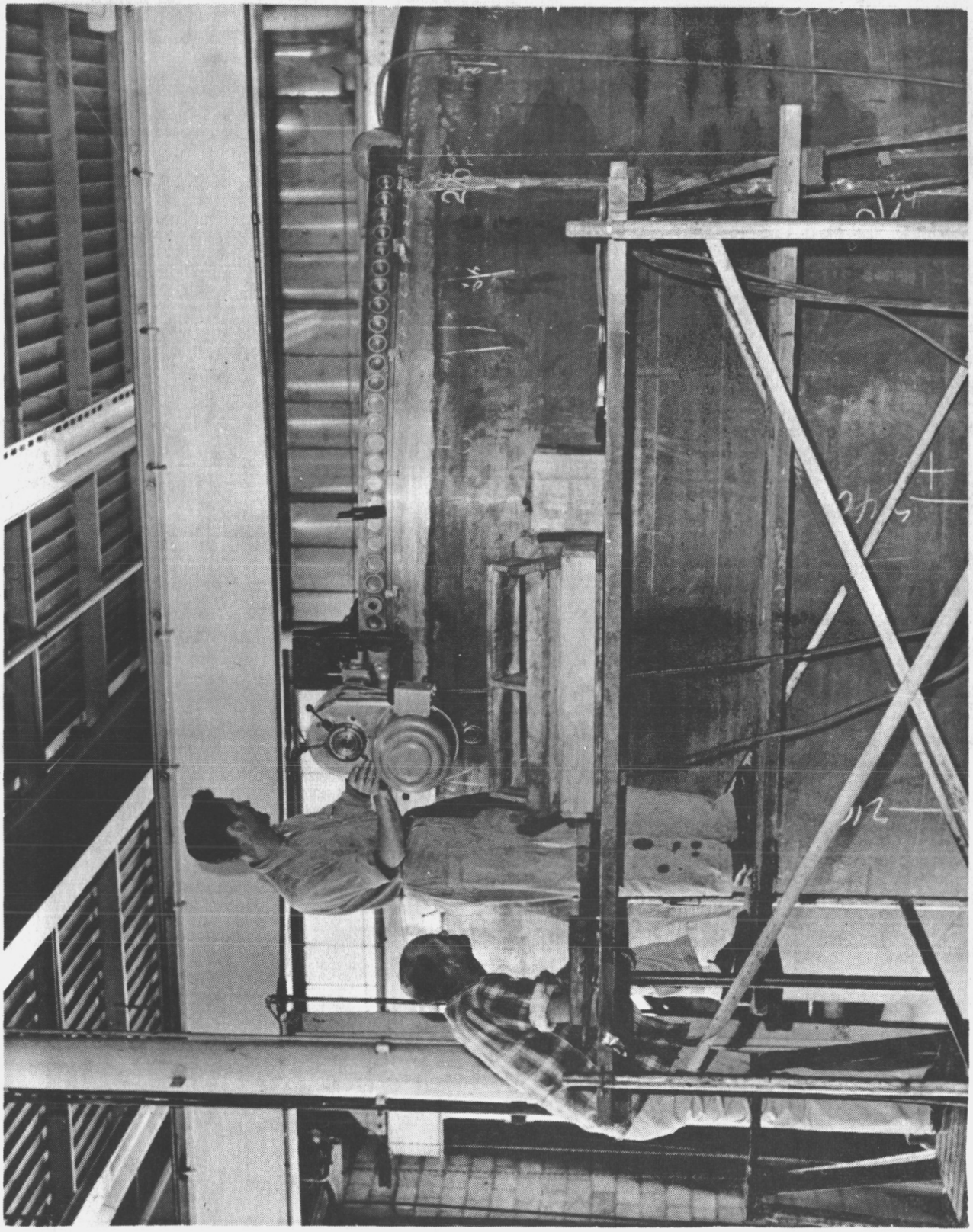


Figure 33 - Drilling 156-2C-1 Case Joint Ring

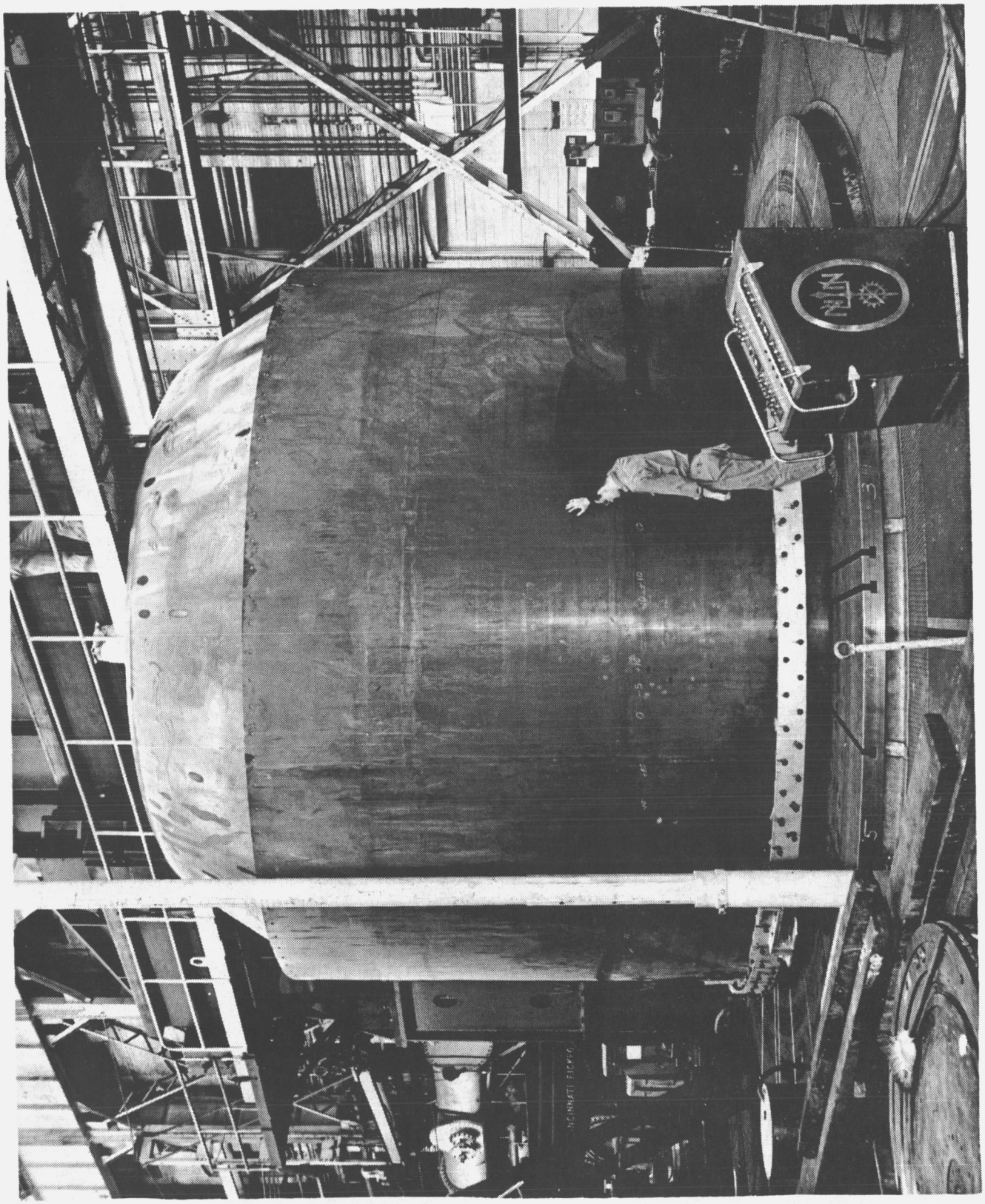


Figure 34 - Machining 260-SL-1 Case Aft Attach Flange in Aged Condition

V. NONDESTRUCTIVE TESTING

Inspection and quality control were continuing functions prior to, during, and after fabrication processing. In particular, inspection operations were concentrated at the following listed points in the fabrication and assembly process: (1) material receiving, layout, and preparation, (2) prior to skirt installation, (3) prior to aging of the forward, center, aft, and forward closure subassemblies, and (4) after final assembly prior to hydrotest. Deviations or discrepancies from drawing and/or specification were submitted for material review.

A. PROCUREMENT INSPECTION

Material was purchased to specifications and subjected to testing, inspection, and certification by the steel manufacturer. Material review was conducted when deviations from specification occurred.

1. Plate

Positive identification was established immediately upon receipt of all materials. Receiving inspection and testing were performed in accordance with specification provisions. Except for early phases of the program, all plate was ground after rolling at the mill and prior to use in the fabrication process. Ultrasonic inspection was performed by the compressional and shear wave methods over 100 percent of the plate surfaces. Shear wave inspection was performed in both the longitudinal and transverse directions. Dye penetrant inspection was accomplished in accordance with specifications over 100 percent of plate surface area. A number of plates were rejected for use in motor case fabrication as a result of dye penetrant and ultrasonic inspections.

Local grinding operations were required in other plate areas to remove defects prior to fabrication use. Metallurgical and mechanical properties testing were accomplished by the steel producer and more extensive testing was performed by the case fabricator and Thiokol. A small percentage of material was rejected due to inadequate properties as defined by material specifications. Deviations from specification in plate and forging material are listed in Table XV. All discrepancies were processed through approved material review procedures and were analyzed from the aspect of form, fit, and function. All material except that previously reported above was subsequently used in the fabrication of the case.

2. Forgings

A ring forging was used for the aft attach flange on both 260-SL-1 and 260-SL-2 cases and for the large flange of the forward closure assembly on the 260-SL-2 case. The inspection and testing required on forgings were very similar to requirements as set forth for plate material. The notable exception in inspection requirements relating to forgings as compared with plate material was the more stringent requirement applicable to laminar defects. Problems encountered with forgings used in fabrication were minor.

3. Processing Material

Welding wire, flux, welding gases, bolts, O-rings, preservatives, and coatings were procured to drawings and/or specifications. No particular problems occurred. Deviations in weld wire chemistry, listed in Table XVI, were minor in nature and were used following Material Review Committee action.

4. Critical Tooling

Efforts in inspection and control were concentrated on tooling which would affect form, fit, or function of motor case components. Precautions were taken to assure proper tooling configuration prior to forming and to assure the maintenance of the configuration throughout the span of time during the forming and fabrication process. The results obtained from utilization of the tooling confirmed that the extra precaution and effort expended were worth-while. Problems encountered with forming were few and of minor proportions.

B. FABRICATION AND PROCESS QUALITY CONTROL

Material inspection requirements (critical flaw sizes) were derived from engineering studies performed on the material selected for case fabrication use. Considerable development work was involved in establishing methods to carry out required inspection. This development was centered mainly in the area of ultrasonics. Criteria for inspection of material and welds are summarized below:

1. General Defects

The material in the final product shall be free of detrimental defects such as laps, seams, pipes, slivers, scale, porosity, or cracks.

2. Surface Acceptance Criteria

All plate material was initially inspected to a flaw-free criterion. Defects were removed in all instances where bleeding occurred utilizing type II penetrants in accordance with MIL-I-6866 (ASG) dated 19 June 1953. After the material was initially accepted and at a later date in the fabrication process, acceptance standards were changed as follows:

Reject for indications of -

Cracks	- regardless of length
Laps	- regardless of length
Linear fissures	- regardless of length
Other linear voids	- regardless of length

Rounded defects greater than 0.045 in. diameter

Linearly disposed rounded defects up to 0.045 in. diameter, four or more in a line and separated from each other by less than 0.0625 in.

3. Laminar Defects

a. Plates

Defects equal to or exceeding the area of 3/4 in. diameter flat bottom hole constituted cause for rejection. Early in the program it became obvious

TABLE XV

MATERIAL DISCREPANCIES DURING 260-SL-1 CASE FABRICATION

Heat	Plate, Forging, or Area Identification	Reason for Material Review
X53085	193029A	Overthickness
X53088	195996A	Minor variations in chemical and/or mechanical properties
X53088	195996B	
X53085	193025B	
X53085	193029A	
X53085	193029B	
X53085	193026A	
X53085	193026B	
X53088	195997	
X53085	193027	
X53085	193031	
X53088	196003	
X53088	195999	
X53085	193025B	Overthickness
X53085	193026A	Overthickness
X53088	193029A	Low R of A values
X53088	195997	Undergage areas
X53085	193029B	Low R of A values
X53085	193025B	Low R of A and high YTS values
X53085	193026A	Low R of A and high YTS values
X53085	193026B	Low R of A and High YTS values
X53085	193027	High aluminum and sulphur content, and high YTS values
X53085	193031	Depression in plate
X53085	193029B	Laminar defects in HAZ
X53088	196003	Low YTS values
X53085	193029B	Laminar defect in HAZ
X53085	193031	Surface pits
X53013	156897A	Surface pits
X53085	193026B	Surface discontinuity
X53013	156897A	High YTS values
X53085	193029A	High YTS values
X53085	193029A	Low R of A values
X53085	193026A	High YTS values
X53085	19302A	Low R of A and high YTS values
X53085	193026B	Undergage area
X53085	193025B	Low R of A and high YTS values
X53085	193025B	Low R of A values
X53085	193026B	High YTS values
X53085	193026B	Low R of A and high YTS values
X53085	193029B	Low R of A and high YTS values
X53088	195996A	Low yield and YTS values
X53471	41701	Undergage areas
X53471	41704	Undergage areas
X53088	195999	Undergage areas
X53088	196003	Undergage areas

TABLE XV (Cont'd)

MATERIAL DISCREPANCIES DURING 260-SL-1 CASE FABRICATION

Heat	Plate, Forging, or Area Identification	Reason for Material Review
X53085	193031	High YTS values
X53085	193031	Undergage areas
53541	3A	Low R of A and elongation values
X53471	41704	Low YTS values
X53085	193029B	Undergage areas
AA☆	S/N2	Low YTS and UTS values
53541	2A	High YTS values
53541	2A	Low R of A and elongation and high YTS (thru thickness) values
53540	3A	High YTS values
53540	3A	Low R of A and elongation (thru thickness) values
53541	2A	Low R of A and elongation and high YTS (thru thickness) values
X53540	4B	Low R of A and elongation, and low YTS and UTS (thru thickness)values
	Fwd cyl assy welds W7-101 and S7-102	Undergage areas
	Center cyl assy 41703 and 41704 "B" specimens	One specimen above maximum YTS; one specimen below minimum YTS and UTS values
X53088	196003	Undergage area because of ultrasonic defect removal
	Center cyl assy parts 701, 702, 801, and 802	Undergage areas
	Fwd subassy welds	Undergage areas prior to aging
	Aft subassy weld W8-3	Ultrasonic (laminar) indications in HAZ
	Fwd closure part 603	Undergage areas after receipt and forming
	Fwd subassy "D" (weld) specimens	Specimen deviations - low YTS, UTS, R of A, and elongation
	Aft Subassy weld W6-3	Ultrasonic (laminar) indications in weld and HAZ

☆Forging

TABLE XV (cont'd)

MATERIAL DISCREPANCIES DURING 260-SL-1 CASE FABRICATION

Heat	Plate, Forging, or Area Identification	Reason for Material Review
	Aft subassy welds	Undergage areas prior to aging
	Center cyl assy aged "D" specimens	Low elongation result and one NFS specimen with improper results
	Fwd subassy aged "B" specimens	Low YTS. UTS, and R of A; and one NFS specimen with improper results
	Motor case assy	Sixteen specimens unavailable for processing
	Motor case assy weld W9-12	One ultrasonic (laminar) indication in weld
	Aft subassy aged "B" specimens	Low YTS and UTS, and one NFS specimen with improper results
	Center cyl assy aged "D' specimens	Two NFS specimens with improper results
	Aft subassy aged "D" specimens	Four of 34 specimens had deviations relating to YTS, UTS, elongation, and R of A. Twelve of 24 NFS specimens broke out of notch with proper results
	Fwd subassy aged "D" specimens	Four of 22 specimens with deviations relating to YTS, UTS, elongation, and R of A. One of 16 NFS specimens broke outside of notch with improper results
	Motor case assy weld W9-23	Undergage areas in weld and/or HAZ
	Aft subassy part 905	Undergage area in plate
X53471	Fwd cyl assy plate 41701	Undergage area in plate
	Fwd closure assy weld W2-401	Undergage area in weld and/or HAZ

TABLE XV (cont'd)

MATERIAL DISCREPANCIES DURING 260-SL-1 CASE FABRICATION

Heat	Plate, Forging, or Area Identification	Reason for Material Review
	Motor case assy W9-23 "D" specimen aging	YTS results unobtainable on one specimen of "simulation" pre-aging cycle
	Fwd closure assy "D" specimens	Low UTS and improper results on one NFS specimen because of breaking outside notch
	Motor case assy weld W9-23	Undergage areas
	Motor case assy weld W9-23	Ultrasonic (laminar) indications in weld and HAZ
	Fwd closure cap aged "B" specimens	Low UTS, elongation, and R of A values
	Fwd closure assy part 602 aged "B" specimens	Low UTS, elongation, and T of A values
	Aft attach flange transition assy weld S10-308	One post-aged repair not re-aged
	Aft subassy aged "D" specimens (evaluation)	Low elongation and R of A values; and incomplete NFS test results on specimens utilized before aging for evaluation
	Motor case assy weld W9-23 aged "D" specimens (evaluation	YTS results unobtainable on one specimen utilized before aging for evaluation
	Motor case assy welds W1-307, W2-3, and W8-2	Undergage areas
	Motor case assy welds W1-104, W1-307, W2-3, and W8-2	Weld repairs required after aging

TABLE XV (cont'd)

MATERIAL DISCREPANCIES DURING 260-SL-1 CASE FABRICATION

NOTES:

1. Discrepancies include material receipt, fabrication, and processing.
2. HAZ denotes weld heat-affected zone; UTS denotes ultimate tensile strength; YTS denotes yield tensile strength; and R of A denotes percent reduction of gage area in tensile specimens.

TABLE XVI

WELD WIRE DISCREPANCIES FOR 260-SL-1 CASE

Wire No.	Reason for Material Review
X08882	Low molybdenum, high oxygen content
X07249	Low molybdenum and titanium content
X08388	Low molybdenum content
X08097	Low molybdenum content
X09231	High oxygen and hydrogen content
X09395	High oxygen, low molybdenum content
X08817	High molybednum content
X09301	High hydrogen content
X09411	High nitrogen content
X09397	High oxygen, nitrogen, and hydrogen; low molybdenum content

that this defect size, which was arbitrarily established, was not consistent with the quality desired. Defects of this size would probably cause problems later and were larger than required by mill capability. This criterion was changed to an area equal to or exceeding a 3/8-in. diameter flat bottom hole and was used without causing rejection of plate.

b. Forgings

Defects equal to or exceeding the area of 5/64-in. diameter (0..00479 sq. in.) flat bottom hole constituted cause for rejection.

4. Nonlaminar Defects

a. Plates and Forgings

Defects exceeding an area greater than 0. 008 sq. in. constituted cause for rejection.

b. Weld Acceptance Criteria

Radiographic acceptance criteria for motor case welds are delineated in Standard I of MIL-R-11468 dated 24 September 1958.

5. Radiographic Equipment and Procedure

The primary tools utilized for material and weld inspection were liquid penetrants, radiographic, and ultrasonic equipment.

The radiation source utilized for material thickness up to 2 inches was a 275 kv Triplett and Barton X-ray machine - A type AA film in sheets 7 in. by 17 in. The areas being X-rayed were marked in 12-inch lengths and each film overlapped the preceding film by 5 inches. The film was processed in automatic equipment, in accordance with the manufacturer's recommendations.

At the start of the program, a source-to-film distance of 54 inches was established. Although this resulted in a 2 percent sensitivity, as determined by standard penetrameters, attempts were made to improve the resolutions by varying the focal distance and exposure time. As a result, a source-to-film distance of 36 inches was established with an exposure time of 3-1/2 minutes.

Radiographs presented for interpretation were required to be free of blemishes or film defects that might mask or be confused with defects in the material being examined. If any doubt existed as to the true nature of the condition on the film, additional radiographs of the same location were made until satisfactory definition was obtained. Radiography was performed generally in accordance with MIL-STD-453 and Thiokol engineering specification SB-SP-176, "Radiographic Inspection of Materials."

According to current standards throughout industry, a 2-percent sensitivity is generally accepted as readily available based on the use of standard penetrameters. These standards and problems associated therewith are discussed in the following exerpts from NDT Handbook, Society of Nondestructive Testing.

"Section 20.36

PENETRAMETERS

As a check on the adequacy of the radiographic technique, it is customary to place a standard test piece, called a penetrameter, on the source side of the specimen. The penetrameter is a simple geometric shape made of a material radiographically similar to the specimen itself, and usually contains some simple structure, such as holes. Its thickness is a definite proportion (say, 2 percent) of the specimen thickness. The radiographic technique may be considered satisfactory if the penetrameter and its structures show clearly in the radiograph. If the radiographic procedure has been able to demonstrate a 2 percent difference in specimen thickness, i.e., to show the structure of a 2 percent penetrameter, the penetrameter sensitivity is said to be 2 percent or better. Ordinarily, 2 percent penetrameter sensitivity is considered satisfactory, but for some purposes a lower percentage is desired, while in other classes of work a greater percentage may be acceptable."

"Section 20.38

PENETRAMETER INTERPRETATION

It should be remembered that even if a certain hole in a penetrameter is visible in a radiograph, a cavity of the same diameter and thickness may be invisible. The penetrameter holes, having sharp boundaries, give an abrupt though small change in metal thickness, while a natural cavity with more or less rounded sides gives a gradual change. Therefore, the image of the hole will be sharper and more easily seen in the radiograph than will the image of the cavity. Similarly, a fine crack may be of considerable extent, but if the X-rays happen to pass from tube to film normal to the plane of the crack, its image on the film may be invisible because of the very gradual transition in photographic technique and not as a measure of the sizes of cavity which can be shown."

It is apparent that, even with a 2-percent sensitivity, defects of greater than 2 percent of the thickness may not be detected depending on orientation of the defect or thickness normal to the X-rays.

Because of this apparent deficiency in the use of radiographic technique alone, it was decided to supplement this nondestructive testing method by also using ultrasonic techniques. The use of ultrasonic methods to supplement the radiographic method was intended to preclude the possibility of any critical defect going undetected.

6. Ultrasonic Equipment and Procedures

The type of equipment used throughout the ultrasonic inspection was Branson Sonorays, Models 5, 50A, and 50B. For inspection of plate materials, a semiautomatic scanning system was used which included the Branson Sonoray Model 50B and Sonogate Type C with an audible alarm system provided by the contractor. Transducers were from 1/2 to 1 in. in diameter transmitting and receiving units and 3/8 in. to 3/4 in. diameter dual crystal units operated at 2.25 mc. Transducers were of a suitable size, angle, and frequency to produce a clear indication from a 0.004 sq. in. area notch. The most frequently used crystal size was 1/2 in. diameter at an angle of 50 degrees and

a frequency of 2 to 3 mc. Procedures were in accordance with MIL-STD-271A and Thiokol Chemical Corporation engineering specification SB-SP-4. Qualified operators demonstrated the ability to calibrate and operate equipment to the test examiners in addition to being thoroughly familiar with inspection requirements and acceptance standards. Calibration samples were of the same type of material used in fabrication and were used prior to and during the inspection sequence, as required, to assure proper equipment operation and detection capability.

Compressional wave inspection for laminar defects was performed over 100 percent of the plate surface. Shear wave inspection for nonlaminar defects was performed over 100 percent of the plate surface in both the longitudinal and transverse directions. After part layout, heat-affected zone inspection was carried out to the 5/64 in. flat bottom hole criteria (compressional wave inspection) After completion of welding, the weld and heat-affected zones were inspected for both laminar and nonlaminar defects, as described above. This area consisted of the weld and all the area within 1 inch of each side of the weld. Further details of procedures used can be found in RMC-43 and appendices.

7. Discussion

As stated earlier and as evidenced by supporting data and documentation in the Motor Log Book, inspection and quality control was a continuing effort throughout the fabrication process. Inspection reviews and/or audits were performed at selected points in process flow to assure maintenance of quality to that point and to prevent difficulties during further processing operations. An example of typical fabrication and inspection process flow is shown in Figure 35.

One problem encountered was related to weld inspection and involved the inability of ultrasonic inspection equipment to distinguish reliably the defect areas from coarse dendritic grain structure which generally occurred in the center of the weld. In effect, the grain structure could possibly serve to mask out a defect present in this zone. A dual crystal device was developed and utilized for the specific purpose of improving the inspection in this particular area. An investigation of new developments in crystals to aid in alleviation of the above problem was also accomplished. However, a completely satisfactory technique was not found

Extensive NDT inspection was utilized for the inspection of welds and heat-affected zones prior to aging. All intended heat-affected zone areas in plate material were inspected ultrasonically to a more stringent requirement than other plate areas prior to and after welding. Radiographic, ultrasonic, and dye penetrant methods were utilized for inspection of all welds including adjacent heat-affected zones. Areas of repair required the same inspections as were performed on the original weld. In addition, in-process inspections were performed to ensure defect removal prior to repair. Quality audits were performed to gain assurance that all welds had been fully inspected in accordance with drawings and specifications prior to introduction of subassemblies into the furnace for aging. A final audit was conducted prior to hydrotest operations. Audit efforts also covered all other areas of drawing and specification requirements to determine if discrepancies had gone unnoticed or had been disposed of properly. Local aging equipment utilized for heat treatment of assembly welds performed the intended task well and close control over desired temperatures was accomplished.

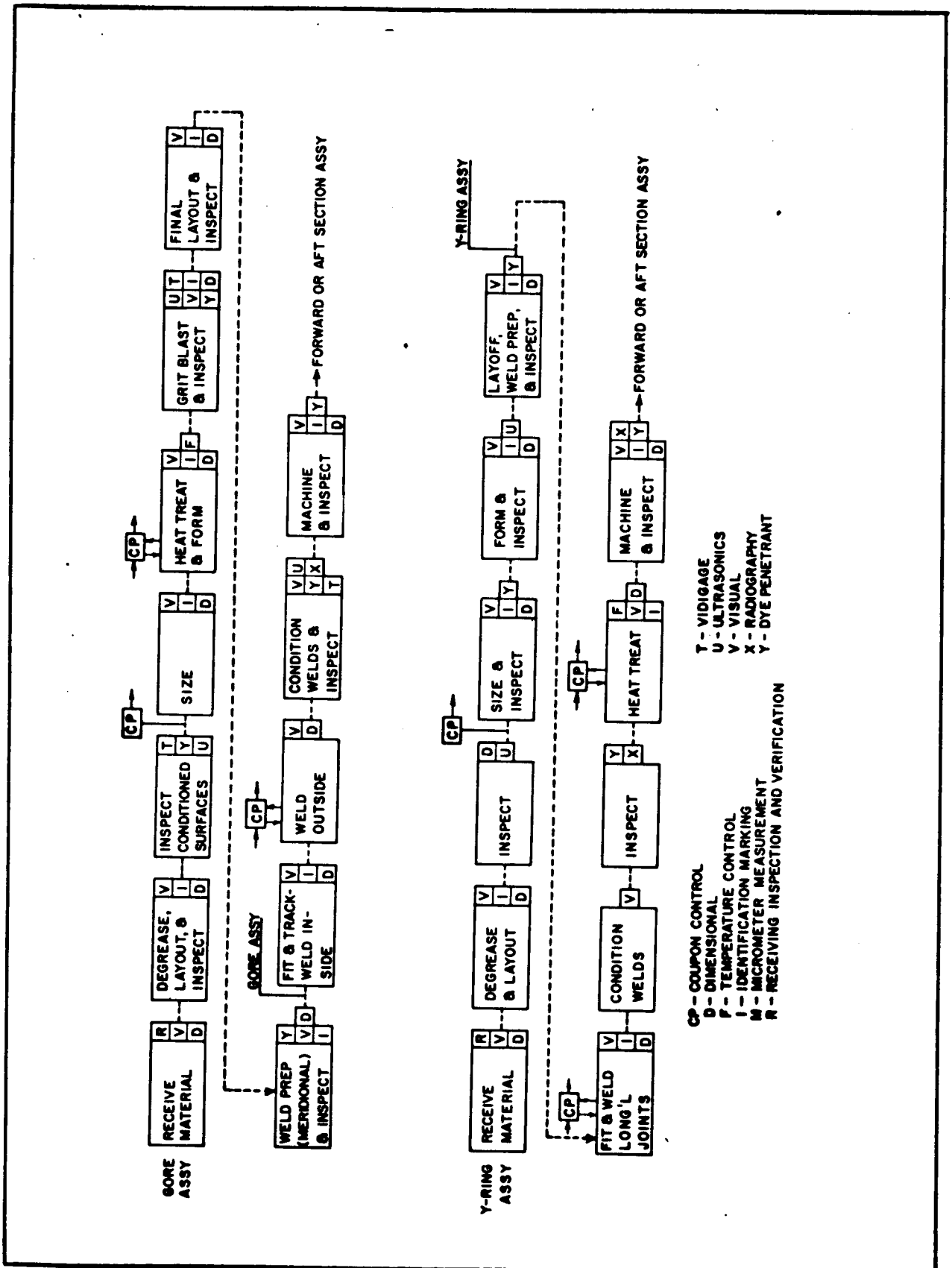


Figure 35 - Diagram of Typical Fabrication and Inspection Flow

Inspection of case subassembly welds after aging was limited. It consisted of inspection of the forward closure to forward gore assembly weld using methods in accordance with specifications relating to dye penetrant, ultrasonic, and radiographic inspection and radiographic inspection of aft attach flange transition assembly joints. The latter inspection was accomplished because of concern over possible effects of flexure which occurred during fixturing of the aged subassembly for drilling operations. First planning called for drilling of holes in the aft attach flange utilizing horizontal boring mill equipment. In the process of fixture installation for drilling, considerable movement took place which had not been foreseen. Due to this circumstance plus the fact that the welds in the above-mentioned area were less ductile than desired, it was decided that the re-inspection of welds was necessary. This inspection revealed no deleterious effect of aging on the assembly welds. Drilling was eventually performed with the assembly in the vertical position due to unsatisfactory fitup of the drill jig in the horizontal position.

The original NDT plan for the 260-SL-1 case included inspection after aging and again after hydrotest. As the program progressed, defects became less prevalent and the need for repairs decreased. An evaluation of all available data indicated that NDT subsequent to aging was not necessary. It appeared that all defects had been located and properly repaired and that considerable time and costs could be saved. As a result, ultrasonic and radiographic inspection of the weld areas after aging was eliminated from the program. It is still uncertain whether or not additional inspections would have indicated rejectable defects in the areas where defects have been subsequently located as a result of the hydrotest failure. Coating of the case inside surface with epoxy paint (KOROPON) was accomplished on each of the three subassemblies, following aging operations. A considerable number of precautionary measures were instituted to assure noncontamination of surfaces preceding the start of processing. These measures included careful cleaning of surfaces with solvent, a laboratory check on cleanliness of containers for cleaning agents, hoses, air lines, and nitrogen lines. Surgically clean white gloves were provided for personnel involved in making wipe tests and the application of tape to suspect defect areas.

After grit blasting some surface defects appeared. These were covered with tape for subsequent repair after coating so that the clean surface would not be contaminated. After coating and curing, the taped areas were exposed, inspected, and unacceptable discontinuities were removed by sanding.

Preparations for hydrotest included an extensive amount of system check-out and verification. Check-out included calibration and certification of gages, valves, switches, strain gages, and instrumentation. Support structure and auxiliary equipment were checked for ample clearances and the ability to function properly for the purpose intended. Dry runs were conducted utilizing operating personnel to satisfy proper and acceptable system operation.

Dimensional inspections were performed on individual case components, subassemblies, and the final assembly. Dimensional review was conducted throughout processing and particularly at the points prior to aging of the three subassemblies and on the final assembly prior to hydrotest. Any discrepancies that arose are listed in Table XVII. The listed discrepancies were processed in accordance with approved material review procedures.

After re-inspection of the forward closure assembly, it was determined that the reported inward bulges did not exist. All other discrepancies were analyzed to determine effect on form, fit, and function with the resulting action to use as is.

TABLE XVII

DIMENSIONAL DISCREPANCIES FOUND IN 260-SL-1 CASE

Case Component	Drawing Requirement	Actual Condition
Aft attach flange	Allowance of 3 turns on 3/4-16-2B thread (580 holes)	Gage enters full depth in 2 holes
Aft attach flange	Allowance of 3 turns on 3/4-16-2B thread (580 holes)	5-1/2 max turns with gage in 11 holes
Aft attach flange	1.15-in. max tap drill depth 3/4-16-2B holes	3 holes overdepth (0.008, 0.018, and 0.222 in.
Aft attach flange	125 RMS surface finish	200 RMS max
Fwd subassy	No inward bulge	3 bulges (0.062-in. max)
Center subassy	0.180-in. max outward bulge	3 bulges (0.218-in. max)
Fwd closure assy	91.900-in. min length	91.702 in.
Fwd closure and cap	Bolt circle maintained concentricity within 0.020 in. (16 holes)	Six holes out-of-tolerance to 0.020-in. max
Fwd closure and cap	Allowance of 3 turns on 5/16-24-2B thread	No-go gage enters to depth of 9/32 in.
Fwd closure assy	No inward bulge	Re-inspection disproved presence of inward bulges
Fwd subassy	125 RMS surface finish	150 to 200 RMS max
Motor case assy	Skirt concentricity inspected at final assy	Full TIR inspection not accomplished. Previous subassembly inspection acceptable

VI. HYDROTEST

A. SUMMARY

The hydrostatic test of the 260-SL-1 case resulted in a case failure at a pressure of 542 psig or approximately 56 percent of hydrotest pressure.

All phases of the test were performed as scheduled up to the time of failure. Magnitudes of predicted and measured strains at 500 psig were in close agreement in most areas.

B. PURPOSE AND OBJECTIVES

The purpose of this test was to verify the design and manufacturing techniques for the 260-SL-1 motor case.

Primary test objectives were:

1. Verify the structural integrity of a monolithic case of roll-and-weld construction using a piston at the aft end of the case to simulate a thrust load applied to the forward skirt. The case was allowed to expand both radially and axially.

2. Determine post effects of hydrotest pressure on the case and other components by dimensional and visual inspection.

C. TEST CONFIGURATION

The test configuration consisted of components described in the following Space Booster Division drawings: 260-SL-1 Case (Space Booster Division Drawing IS 10001); Nozzle-to-Case Adapter (Drawing IS 11005); Hydrotest Nozzle Adapter (Drawing IS 18004); Hydrotest Piston (Drawing ST 10678). Case details are described elsewhere in this report, and the nozzle-to-case adapter in a companion report.

D. HYDROTEST TOOLING AND HANDLING EQUIPMENT

1. Hydrotest Adapter

The hydrotest adapter (Drawing IS 18004) was fabricated from 250-ksi grade maraging steel.

The hydrotest adapter consisted of a large, lower attach flange fabricated from five 72-deg segments; a conical membrane fabricated from four, 1-1/4-in. thick plate segments; and a smaller, upper flange forging. The upper

flange opening was 63.002 in. in diameter to accommodate the hydrotest piston.

Welding of the large forward flange segments was by the vertical submerged-arc technique. The remaining portions of the adapter were welded by the two-pass submerged-arc process.

The hydrotest adapter had been previously used to hydrostatic test the 156-2C-1 segmented case to a pressure of 960 psig.

2. Piston

A detailed description of the hydrotest piston is shown on tooling drawing ST 10678. Material used in the piston was cast steel per ASTM A 27-60-grade 65-35 with a yield strength of 33,000 psi. The casting was annealed prior to finish machining. The piston was 5 in. thick and 64 in. at the largest diameter. An O-ring groove was provided in the interface diameter of 62.990 in. to form a pressure seal between the piston and hydrotest adapter. One hole was provided in the piston for bleeding the air from the case.

3. Hydrotest Tower

The hydrotest tower was a steel structure similar to a four-legged stool, which provided support for the piston at the aft end of the case/nozzle adapter/hydrotest adapter assembly. Figure 36 shows the case located in the hydrotest tower. The primary structural element was a pair of double-web box girders which served as the immediate support for the piston. Uplift on the box girders was resisted by a simple truss on two opposite sides of the tower, which transmitted the load to the four-corner verticals. The upward load on the concrete foundation was resisted by a cylindrical steel element between the foundation and the case forward skirt.

4. Handling Equipment

The completed case, assembled with the forward and aft lifting rings, was transferred to a 100-ton capacity Talbert trailer for mandrel removal. After mandrel removal, the case was transferred by crane to a 200-ton capacity railroad car. Supports for the case were made up of nine pieces of 12 × 12 fir blocking at each end of the case. A layer of 1 × 6 soft pine was used between the case and blocking. The railroad car was then moved to the hydrotest tower. Upon arrival at the test tower, the case was positioned so that the aft lifting ring was under the centerline of the tower. Lifting blocks were connected to the aft lifting ring by means of a link. A crane was connected to the forward lifting ring. Both ends were raised simultaneously and the railroad car was removed. The forward end of the case was lowered onto a trunnion stand outfitted with multi-ton rollers. The aft end was hoisted into the tower with the lifting blocks and the forward end moved into the tower on the trunnion. When the case was in the vertical position, the trunnion was removed, the skirt support was assembled, and the case lowered onto the support.

At this point, the hydrotest piston was raised up in position against the box girders. The piping was connected and the case was ready for testing.

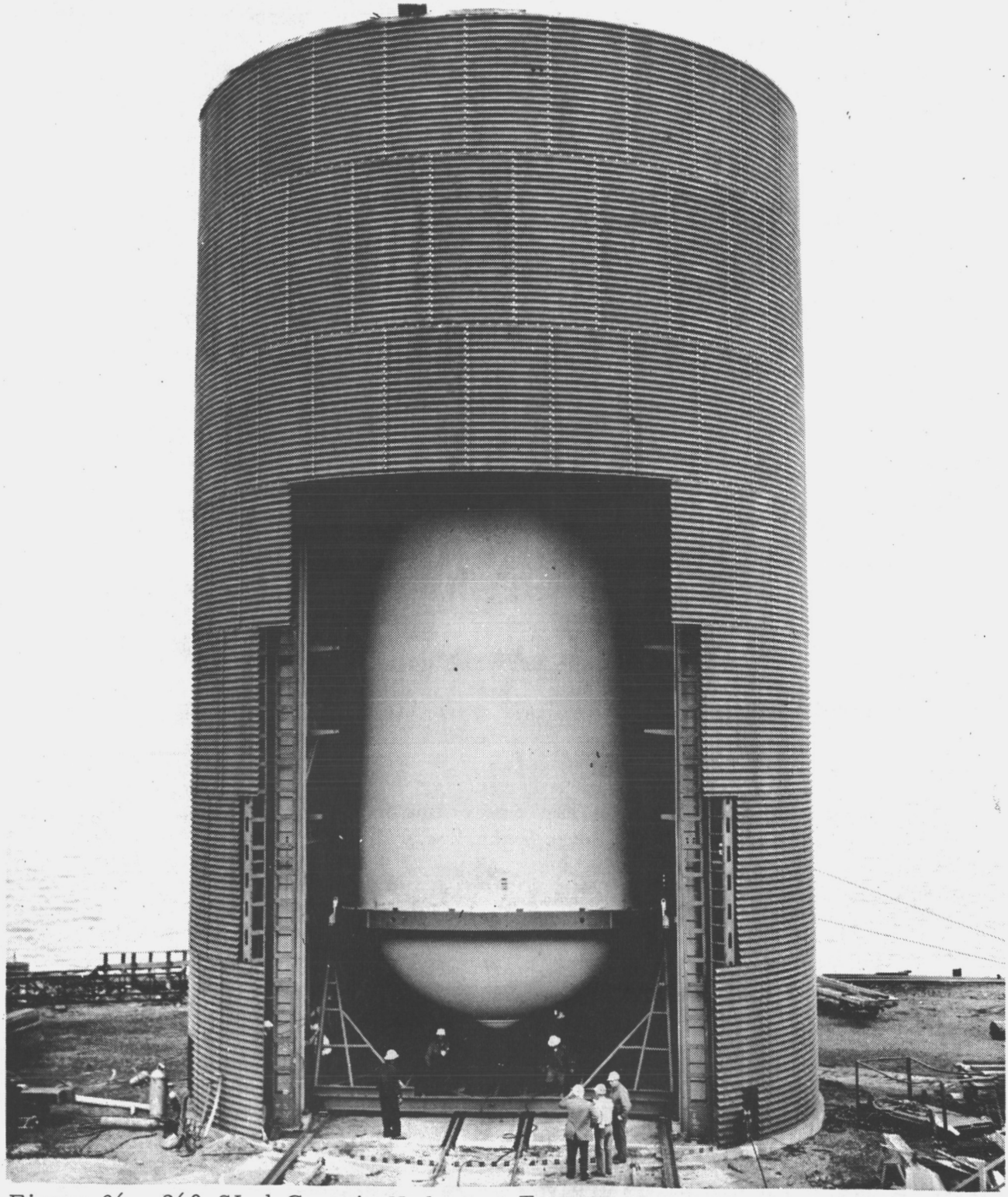


Figure 36 - 260-SL-1 Case in Hydrotest Tower

5. Pressurization System

The hydrotest pressurization system consisted of a duplex pump rated to deliver 54 gpm at 100 psi, an auxiliary pressure pump rated at 2.14 gpm at 10,800 psi, a chemical pump for injecting sodium dichromate, and the required valves, gages, pipe, and tubing. Two pressure relief valves were installed in the system set to relieve pressure at 970 psig. Two, three-in. vacuum breakers were installed on the vent side of the piping to prevent a vacuum in the case when draining the water. A schematic of the pressurization system is presented in Figure 37.

E. INSTRUMENTATION

1. Pressure Measurements

a. Equipment

Two systems were utilized to indicate and record pressure levels during the case hydrotest: A set of pressure gages for visual observation and a pressure transducer/recorder for automatic recording of pressure.

1. Two Bourdon tubes, (Manning, Maxwell, and Moore), with 8-1/2 in. dial, range - 0 to 1000 psig, further described below:

   a. One Ashcroft, type 1279 A, 10-lb graduations, 5 psi accuracy, located in test room

   b. One Ashcroft, type 1082 H, 5-lb graduations, 2.5 psi accuracy, located in pump room

2. One Ashcroft, 10-in. dial, 5-lb graduations, 0 - 1000 psi range, located in test room

Pressure connections for the gages were made in the piping at the head end of the case.

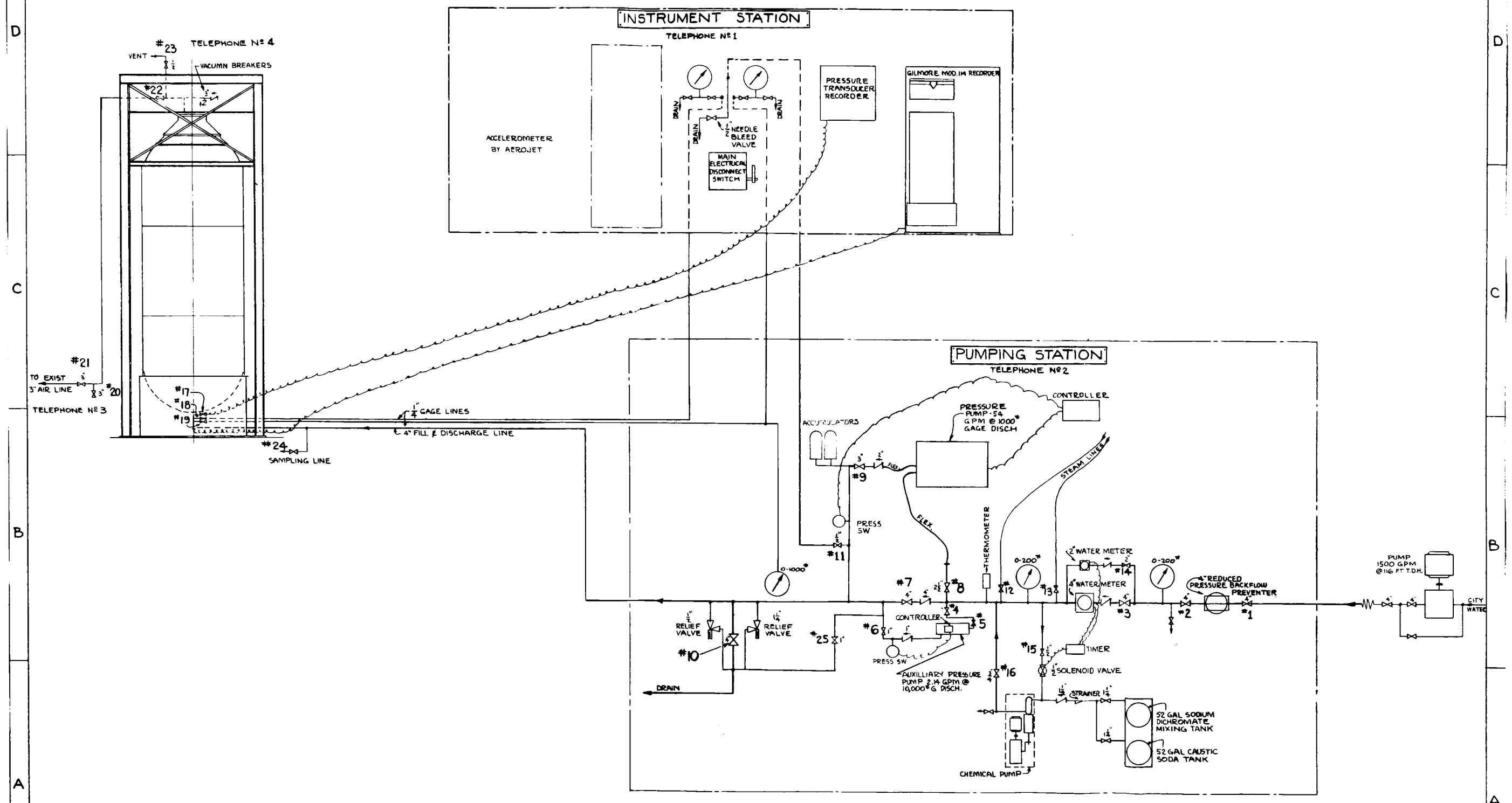
The automatic recording system consisted of one pressure transducer and one pressure recorder. The transducer was made by Dynisco, Model No. PT-31-5M, strain gage rated at 5000 psi maximum. A Leeds and Northrup, 1 mv, potentiometer recorder was used for recording the pressure.

b. System Accuracy

The primary gage used for the pressurization of the case was the 10-in. Ashcroft gage. It was estimated that the gage could be read within plus or minus 1/2 psi at the gage marks and within plus or minus 1 psi between marks.

The gage was calibrated to be correct at 950 psi against a standard which was certified accurate within 1/4 percent. The tester used for calibrating the gage was calibrated with standards traceable to the National Bureau of Standards, Washington, D. C. Thus, at 960, the pressure may be 960 ± 2.4 psi ± 0.5 psi. Case pressure could then vary between 957.1 minimum and 962.9 maximum.

SBR-89.865



260 INCH ROCKET MOTOR CASE HYDROSTATIC TEST PIPING DIAGRAM

FIGURE 2, RMC 44
REV. C

86-A

FIGURE 37
PAGE 86-B

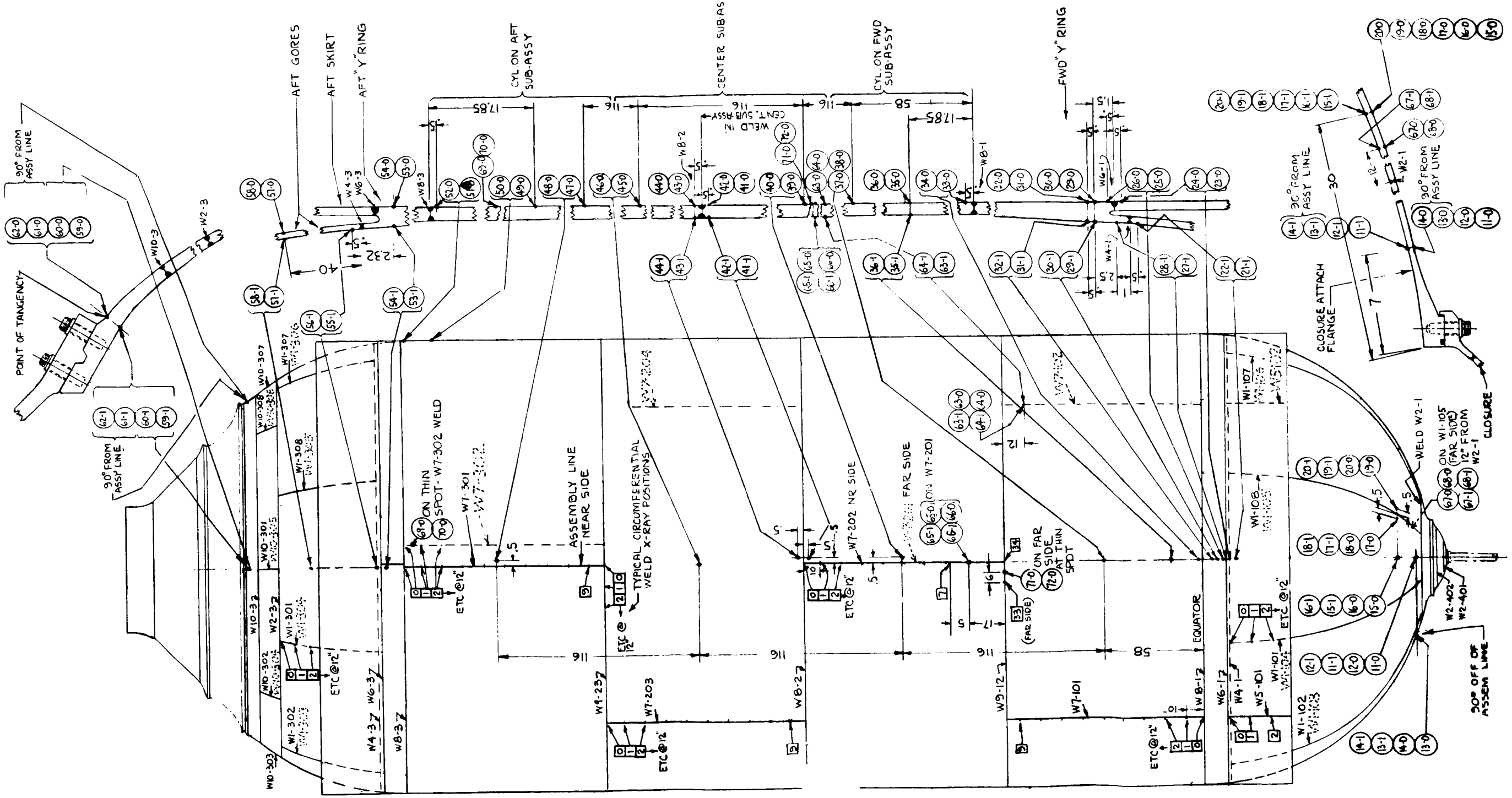


FIGURE 38
PAGE 87-B

89-A

The pressure transducer originally planned for use in the hydrotest was damaged just prior to initiation of the test. Another transducer of the same type was substituted. The transducer had not been calibrated, but pressures recorded were consistent with the primary gage (10-in. Ashcroft). A post-test calibration check of the transducer and recorder using a standard with a certified accuracy of 0.03 percent indicated a pressure of 905 psi at a standard pressure of 900 psi.

c. Location of Transducers and Recorders

Connections for the pressure gages were provided in the piping at the head end of the case. The pressure transducer was also located in the piping at the head end. Gages and recorder were located in the instrument station a safe distance away from the tower, as shown in Figure 37.

2. Strain Measurements

a. Equipment

Strain gages used to measure strains experienced by the case were Baldwin-Lima-Hamilton, 120 ohms, thermal compensating gages. Two types of gages were used: (1) FABX-25-1256 for biaxial measurement and (2) FABX-25-1256 for uniaxial measurement. The gages were bonded to the specified locations with Eastman 9-10 cement and waterproofed with Gage Kote No. 5.

The equipment used for recording strain versus load was a Gilmore Autographic Plotter, Model 114. The plotter was capable of recording and plotting 96 channels of data.

b. System Accuracy

The Gilmore strain gage plotter, Model 114, has a rated accuracy of ± 1 percent of full scale for each range. The Baldwin-Lima-Hamilton strain gages have a rated accuracy of ± 1 percent. It was estimated that the remaining portion of the system has an accuracy of ± 2 percent. Therefore, the system has a total estimated accuracy of ± 4 percent.

c. Location of Gages and Recorder

Ninety-six strain gages were utilized during the test. Forty of the gages were located on the inside of the case and the remaining fifty-six were located on the outside surface of the case. Final locations of the gages are shown in Figure 38. Twelve gages were located specifically to monitor three areas of contour deviations at different welds. The recording equipment was located in the instrumentation station, as shown in Figure 37.

3. Accelerometers

Twenty-four accelerometers were attached to the 260-SL-1 case as part of a case failure warning technique under development by Aerojet-General Corporation. This portion of the test was conducted by Aerojet under contract with NASA. The type of instruments and location of accelerometers were established by Aerojet. The results of the test are not included as part of this report.

F. TEST PROCEDURE

1. Test Procedure Documents

The 260-SL-1 case, instrumentation, and equipment were prepared and installed in accordance with the following documents prepared by Newport News Shipbuilding and Dry Dock Company for Thiokol:

1. RMC-60, Manufacturing Plan
2. RMC-44, Procedure for Hydrostatic Test for 260-Inch Motor Case

2. Deviations from Specified Procedure

The hydrostatic test procedure (RMC-44) was adhered to except for the following conditions:

1. The automatic chemical metering pump specified in paragraph 3.4 was replaced with a mechanical pump for injecting sodium dichromate into the filling water.

2. The procedures call for maintaining pH factor of 7.0 ± 0.5. Although not provided for in the procedure, caustic soda (sodium hydroxide) solution was used for this purpose.

3. The preliminary pressurization cycle specified in paragraph 5.2 and Figure 1 required a pressure level of 300 psig; however, the actual pressure was raised to 350 psig. This was done to separate marks on the strain gage recording for preliminary pressurization from those for final pressurization.

4. The procedure specified two 8-1/2-in. Ashcroft pressure gages for the test. A 10-in. Ashcroft gage with 5-lb graduations was also used and because of its known accuracy, was adopted as the primary reference for the control of pressure.

G. COMPARISON OF PREDICTED PERFORMANCE WITH ACTUAL DATA

1. Pressure

The hydrotest consisted of three pressurization cycles, defined in Hydrotest Procedure, RMC-44; leak test pressurization cycle, strain gage exercise cycle, and final pressurization cycle. Planned and actual pressure cycles are shown in Figure 39 for the last two cycles. The leak test cycle was performed on Saturday, April 10, 1965, and the last two cycles were conducted on Sunday, April 11, 1965.

2. Strain and Stress

Predicted strains at various pressure levels of the final pressurization cycle, along with predicted stress level at 960 psig, are presented in Figure 40. All predicted values are based on minimum or near minimum wall thicknesses

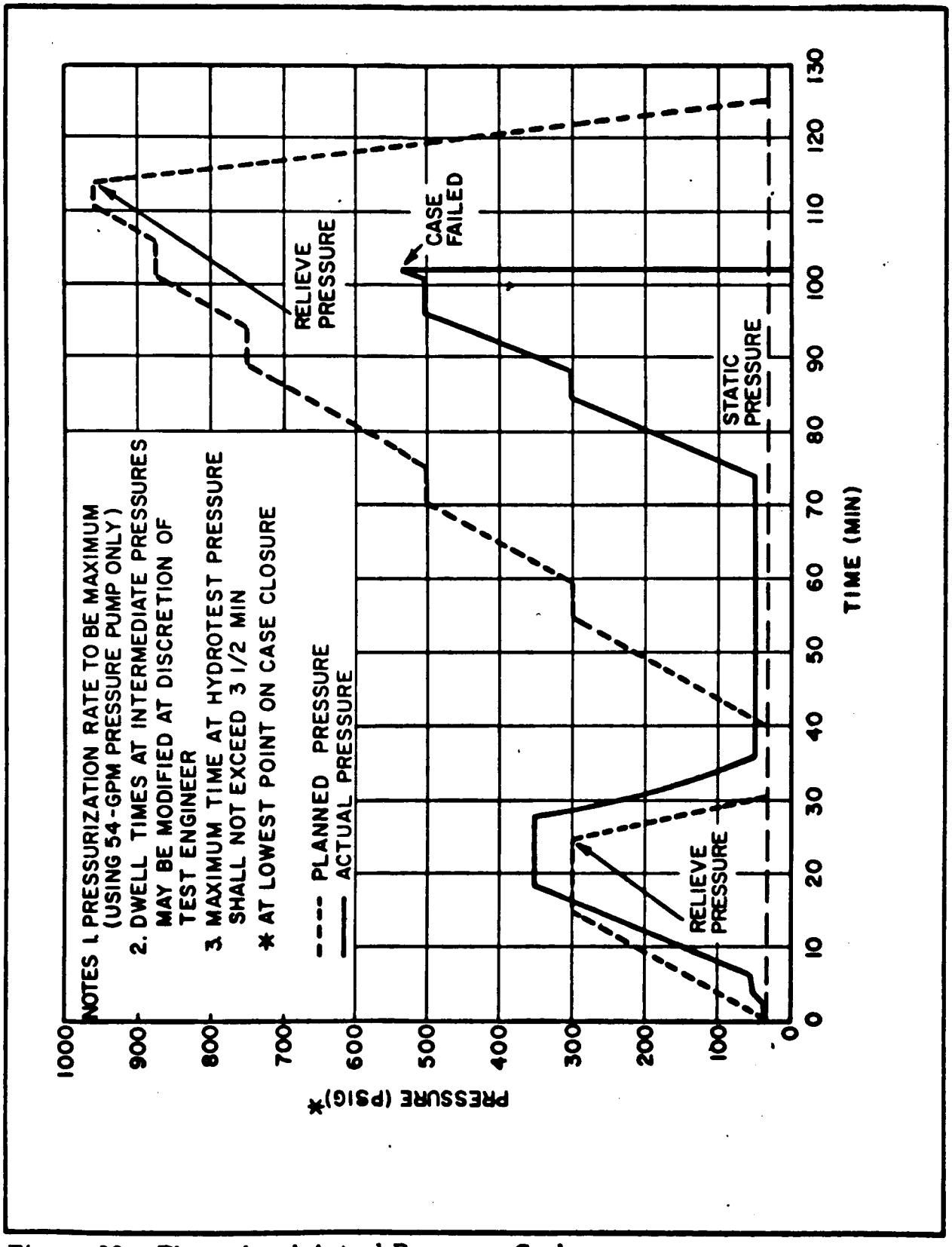
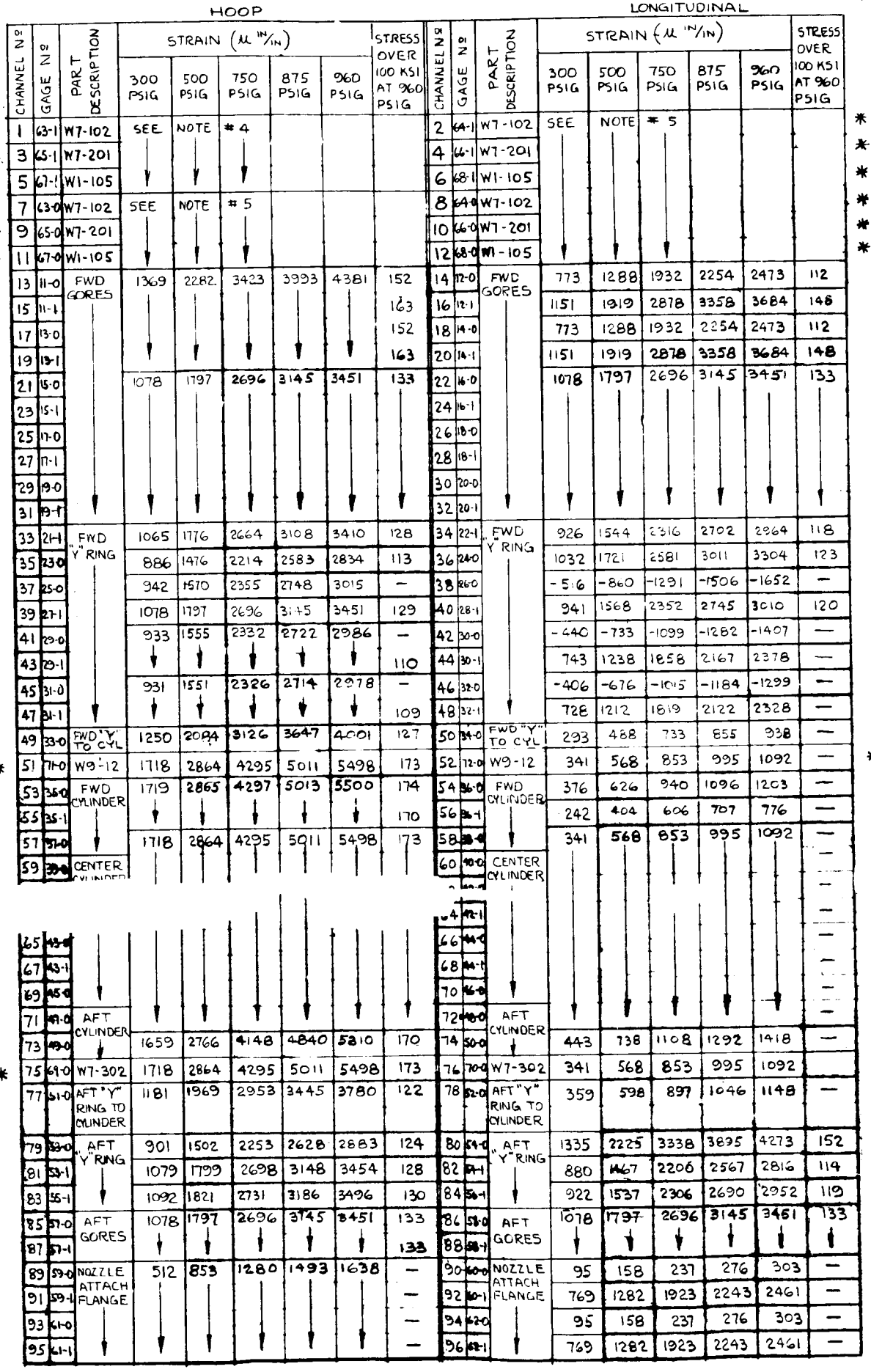


Figure 39 - Planned and Actual Pressure Cycles

GAGES NOT LISTED IN SEQUENCE MARKED THUS *



	HOOP								LONGITUDINAL							
	CHANNEL Nº	GAGE Nº	PART DESCRIPTION	STRAIN (μ IN/IN) 300 PSIG	500 PSIG	750 PSIG	875 PSIG	960 PSIG	STRESS OVER 100 KSI AT 960 PSIG	CHANNEL Nº	GAGE Nº	PART DESCRIPTION	STRAIN (μ IN/IN) 300 PSIG	500 PSIG	750 PSIG	875 PSIG	960 PSIG	STRESS OVER 100 KSI AT 960 PSIG
*	1	63-1	W7-102	SEE	NOTE	# 4				2	64-1	W7-102	SEE	NOTE	# 5				*
*	3	65-1	W7-201	↓	↓	↓				4	66-1	W7-201	↓	↓	↓				*
*	5	67-1	W1-105	↓	↓	↓				6	68-1	W1-105	↓	↓	↓				*
*	7	63-0	W7-102	SEE	NOTE	# 5				8	64-0	W7-102	↓	↓	↓				*
*	9	65-0	W7-201	↓	↓	↓				10	66-0	W7-201	↓	↓	↓				*
*	11	67-0	W1-105	↓	↓	↓				12	68-0	W1-105	↓	↓	↓				*
	13	11-0	FWD GORES	1369	2282	3423	3993	4381	152	14	12-0	FWD GORES	773	1288	1932	2254	2473	112	
	15	11-1	↓	↓	↓	↓	↓	↓	163	16	12-1	↓	1151	1919	2878	3358	3684	148	
	17	13-0	↓	↓	↓	↓	↓	↓	152	18	14-0	↓	773	1288	1932	2254	2473	112	
	19	13-1	↓	↓	↓	↓	↓	↓	163	20	14-1	↓	1151	1919	2878	3358	3684	148	
	21	15-0	↓	1078	1797	2696	3145	3451	133	22	16-0	↓	1078	1797	2696	3145	3451	133	
	23	15-1	↓	↓	↓	↓	↓	↓	↓	24	16-1	↓	↓	↓	↓	↓	↓	↓	
	25	17-0	↓	↓	↓	↓	↓	↓	↓	26	18-0	↓	↓	↓	↓	↓	↓	↓	
	27	17-1	↓	↓	↓	↓	↓	↓	↓	28	18-1	↓	↓	↓	↓	↓	↓	↓	
	29	19-0	↓	↓	↓	↓	↓	↓	↓	30	20-0	↓	↓	↓	↓	↓	↓	↓	
	31	19-1	↓	↓	↓	↓	↓	↓	↓	32	20-1	↓	↓	↓	↓	↓	↓	↓	
	33	21-1	FWD "Y" RING	1065	1776	2664	3108	3410	128	34	22-1	FWD "Y" RING	926	1544	2316	2702	2964	118	
	35	23-0	↓	886	1476	2214	2583	2834	113	36	24-0	↓	1032	1721	2581	3011	3304	123	
	37	25-0	↓	942	1570	2355	2748	3015	—	38	26-0	↓	-516	-860	-1291	-1506	-1652	—	
	39	27-1	↓	1078	1797	2696	3145	3451	129	40	28-1	↓	941	1568	2352	2745	3010	120	
	41	29-0	↓	933	1555	2332	2722	2986	—	42	30-0	↓	-440	-733	-1099	-1282	-1407	—	
	43	29-1	↓	↓	↓	↓	↓	↓	110	44	30-1	↓	743	1238	1858	2167	2378	—	
	45	31-0	↓	931	1551	2326	2714	2978	—	46	32-0	↓	-406	-676	-1015	-1184	-1299	—	
	47	31-1	↓	↓	↓	↓	↓	↓	109	48	32-1	↓	728	1212	1819	2122	2328	—	
	49	33-0	FWD "Y" TO CYL	1250	2084	3126	3647	4001	127	50	34-0	FWD "Y" TO CYL	293	488	733	855	938	—	
*	51	71-0	W9-12	1718	2864	4295	5011	5498	173	52	72-0	W9-12	341	568	853	995	1092	—	*
	53	35-0	FWD CYLINDER	1719	2865	4297	5013	5500	174	54	36-0	FWD CYLINDER	376	626	940	1096	1203	—	
	55	35-1	↓	↓	↓	↓	↓	↓	170	56	36-1	↓	242	404	606	707	776	—	
	57	37-0	↓	1718	2864	4295	5011	5498	173	58	38-0	↓	341	568	853	995	1092	—	
	59	39-0	CENTER CYLINDER	↓	↓	↓	↓	↓	↓	60	40-0	CENTER CYLINDER	↓	↓	↓	↓	↓	—	
	65	43-0	↓	↓	↓	↓	↓	↓	↓	64	42-1	↓	↓	↓	↓	↓	↓	—	
	67	43-1	↓	↓	↓	↓	↓	↓	↓	66	44-0	↓	↓	↓	↓	↓	↓	—	
	69	45-0	↓	↓	↓	↓	↓	↓	↓	68	44-1	↓	↓	↓	↓	↓	↓	—	
	71	49-0	AFT CYLINDER	↓	↓	↓	↓	↓	↓	70	46-0	↓	↓	↓	↓	↓	↓	—	
	73	49-0	↓	1659	2766	4148	4840	5310	170	72	48-0	AFT CYLINDER	443	738	1108	1292	1418	—	
*	75	69-0	W7-302	1718	2864	4295	5011	5498	173	74	50-0	↓	341	568	853	995	1092		*
	77	51-0	AFT "Y" RING TO CYLINDER	1181	1969	2953	3445	3780	122	76	70-0	W7-302	359	598	897	1046	1148	—	
	79	53-0	AFT "Y" RING	901	1502	2253	2628	2883	124	78	52-0	AFT "Y" RING TO CYLINDER	1335	2225	3338	3895	4273	152	
	81	53-1	↓	1079	1799	2698	3148	3454	128	80	54-0	↓	880	1467	2206	2567	2816	114	
	83	55-1	↓	1092	1821	2731	3186	3496	130	82	54-1	↓	922	1537	2306	2690	2952	119	
	85	57-0	AFT GORES	1078	1797	2696	3145	3451	133	84	56-1	↓	1078	1797	2696	3145	3451	133	
	87	57-1	↓	↓	↓	↓	↓	↓	133	86	58-0	AFT GORES	↓	↓	↓	↓	↓	↓	
	89	59-0	NOZZLE ATTACH FLANGE	512	853	1280	1493	1638	—	88	58-1	↓	95	158	237	276	303	—	
	91	59-1	↓	↓	↓	↓	↓	↓	—	90	60-0	NOZZLE ATTACH FLANGE	769	1282	1923	2243	2461	—	
	93	61-0	↓	↓	↓	↓	↓	↓	—	92	60-1	↓	95	158	237	276	303	—	
	95	61-1	↓	↓	↓	↓	↓	↓	—	94	62-0	↓	769	1282	1923	2243	2461	—	
										96	62-1	↓							

FIGURE 40
PAGE 91

SBR-89.865

even though, in many areas, the fabricated item was at maximum or near maximum thickness. Table XVIII shows measured strains and stress at 500 psig. It should be noted that since all strain gages were zeroed with the case full of water and vented at the top, all observed strains are net values, referred to a net pressure 30 psi less than gage pressure. Accordingly, Table XVIII shows both recorded values at 500 psig and values proportioned upward to reflect the actual pressure at respective gages.

Stresses may be obtained from strain values with the following formula:

$$\sigma_x = 29.67\ (10^6)\ (\epsilon_x + 0.3\ \epsilon_y)\ \text{psi}$$

where ϵ_x and ϵ_y are strains with units of micro inches/inch. Implicit in this formula is a value of modulus of elasticity of the steel of 27×10^6 psi, and a value of Poisson's ratio of 0.30.

Comparisons of measured and predicted stress at 500 psig are illustrated for key areas. In these figures, hoop and meridional directions are designated θ and ϕ, respectively; and the symbol σ represents stress. Subscripts o and i designate outside and inside surfaces, respectively.

a. Forward Dome

Figure 41 shows the stresses in the forward dome. Hoop stresses on the inner and outer surfaces of the weld joint between the polar port and gores and meridional stresses on the outer surface at the same location were higher than the predicted stresses. The meridional stress becomes compressive on the inner surface.

Gages located on the gores at locations away from welds and adjacent to welds measured stresses lower than those predicted.

b. Forward Y-Ring

Measured stresses in the cylinder adjacent to and aft of the Y-ring were lower than predicted (Figure 42). Observed stresses in the Y-ring were generally lower than predicted; however, meridional stresses at three points were higher. Change of radius based on strain measurements at the thick end of the Y-ring was substantially lower than the prediction. Inside and outside hoop strains are nearly the same, indicating that the hoop direction contour was not changing locally.

c. Cylinder Membrane

Tabulated cylinder membrane stresses (Figure 43) indicate generally lower values than those predicted. Stress in or adjacent to cylinder hoop welds showed some deviation from predicted values based on pure membrane conditions. Bending of not great significance did exist at these welds due to mismatch. At longitudinal welds, where the greatest deviation from contour occurred, (locations 2 and 4), the highest stresses in the case were recorded.

d. Aft Y-Ring

TABLE XVIII

MEASURED STRAINS & STRESSES AT 500 PSIG

GAGE	LOCATION	RECORDED STRAIN AT 500 PSI DATA POINT	TOTAL STRAIN AT 500 PSI DATA POINT	STRESS AT 500 PSI DATA POINT	GAGE	RECORDED STRAIN AT 500 PSI DATA POINT	TOTAL STRAIN AT 500 PSI DATA POINT	STRESS AT 500 PSI DATA POINT
63-1	W7-102	3920	4095	125.2	64-1	390	407	48.6
65-1	W7-201	3650	3805	117.0	66-1	440	459	47.4
67-1	W1-105	2130	2261	80.3	68-1	1400	1486	64.2
63-0	W7-102	1150	1201	38.5	64-0	310	324	20.3
65-0	W7-201	1050	1095	35.4	66-0	320	334	19.6
67-0	W1-105	1350	1433	56.3	68-0	1450	1486	58.4
11-0	Fwd Gore	2490	2644	97.0	12-0	1970	2091	85.6
11-1	Fwd Gore	2600	2760	74.2	12-1	-810	-860	+1.0
13-0	Fwd Gore	2480	2633	96.0	14-0	1890	2007	82.9
13-1	Fwd Gore	2550	2707	75.3	14-1	-540	-573	+7.1
15-0	Fwd Gore	1510	1603	61.7	16-0	1490	1582	61.2
15-1	Fwd Gore	1330	1412	56.2	16-1	1510	1603	60.1
17-0	Fwd Gore	1300	1380	53.2	18-0	1300	1380	53.2
17-1	Fwd Gore	1550	1646	63.0	18-1	1490	1582	61.6
19-0	Fwd Gore	1340	1423	54.8	20-0	1330	1412	54.6
19-1	Fwd Gore	1560	1656	63.4	20-1	1510	1603	62.3
* 21-1	Fwd "Y" Ring	820	864	44.	* 22-1	2000	2110	70.1
* 23-0	Fwd "Y" Ring	800	843	29.8	* 24-0	510	537	23.5
* 25-0	Fwd "Y" Ring	820	864	31.7	* 26-0	650	684	28.0
* 27-1	Fwd "Y" Ring	800	843	46.4	* 28-1	1650	174.	59.1
* 29-1	Fwd "Y" Ring	850	896	21.4	30-0	-550	-579	-9.3
* 8-1	Fwd "Y" Ring	800	843	37.	30-1	1390	1465	51.0
* 31-0	Fwd "Y" Ring	840	885	21.3	32-0	-520	-548	-8.4
* 31-1	Fwd "Y" Ring	800	843	37.7	32-1	1350	1411	49.7
* 33-0	Fwd "Y" to Cyl	1500	1580	50.3	* 34-0	370	390	25.6
71-0	W9-12	2300	2400	71.0	72-0	0	0	21.4
35-0	Fwd Cyl	2400	2520	80.2	36-0	570	600	40.2
35-1	Fwd Cyl	2350	2470	76.3	36-1	320	336	31.9
37-0	Fwd Cyl	2490	2611	82.0	38-0	485	509	38.3
39-0	Cent. Cyl	2000	2080	66.3	40-0	490	510	33.6
41-0	Cent. Cyl	2210	2290	69.2	42-0	150	155	25.0
41-1	Cent. Cyl	2740	2840	92.1	42-1	860	891	51.7
43-0	Cent. Cyl	2270	2350	71.8	44-0	220	2280	27.8
43-1	Cent. Cyl	2620	2715	87.8	44-1	810	839	49.1
45-0	Cent. Cyl	2300	2368	74.2	46-0	430	443	34.2
47-0	Aft. Cyl	2020	2061	64.9	48-0	400	408	30.4
49-0	Aft. Cyl	2470	2517	79.2	50-0	500	509	37.6
69-0	W7-302	2300	2339	77.3	70-0	800	814	15.2
51-0	Aft "Y" Ring to Cyl	1610	1637	53.1	52-0	500	509	29.7
* 53-0	Aft "Y" Ring	800	814	21.0	* 54-0	-350	-356	-3.4
* 53-1	Aft "Y" Ring	850	864	57.8	* 54-1	1350	1373	48.4
* 55-1	Aft "Y" Ring	820	834	47.6	* 56-1	2520	2563	83.5
57-0	Aft Gore	1410	1428	51.3	58-0	1000	1013	42.7
57-1	Aft Gore	1600	1620	58.2	58-1	1350	1367	55.0
59-0	Noz Att Flg	750	758	22.9	60-0	+50	51	8.3
59-1	Noz Att Flg	690	697	27.1	60-	710	718	27.5
61-0	Noz Att Flg	720	728	21.7	62-0	+20	20	7.1
61-1	Noz Att Flg	660	667	31.6	62-1	1320	1334	45.5

(1) GAGES ZEROED WITH VESSEL FULL OF WATER

(2) PROPORTIONED UPWARD FOR WATER HEAD TO GAGE ELEVATION

VALUES INDICATED BY ASTERISK REPRESENT SUBSTANTIAL DEVIATION FROM PREDICTION

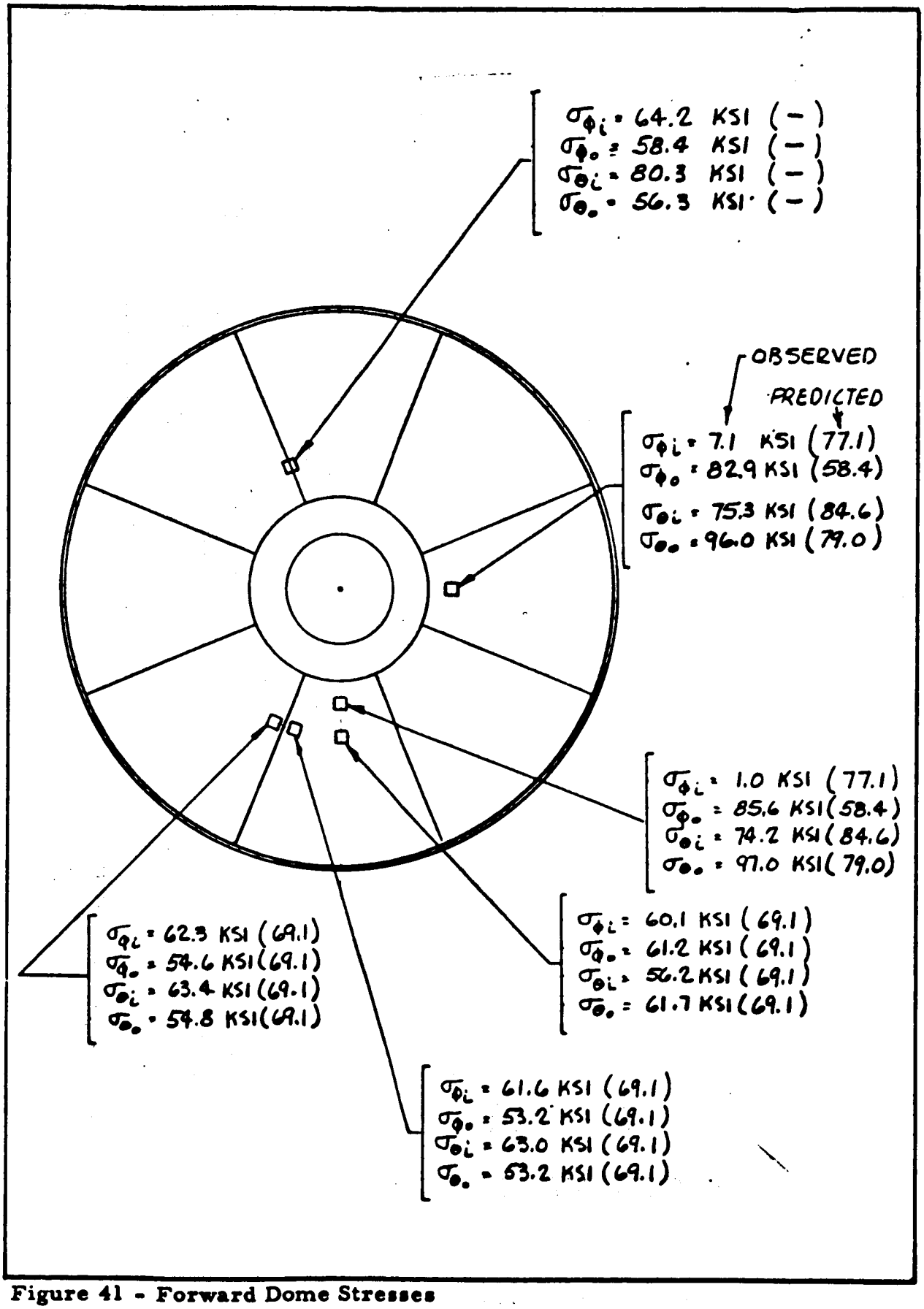


Figure 41 - Forward Dome Stresses

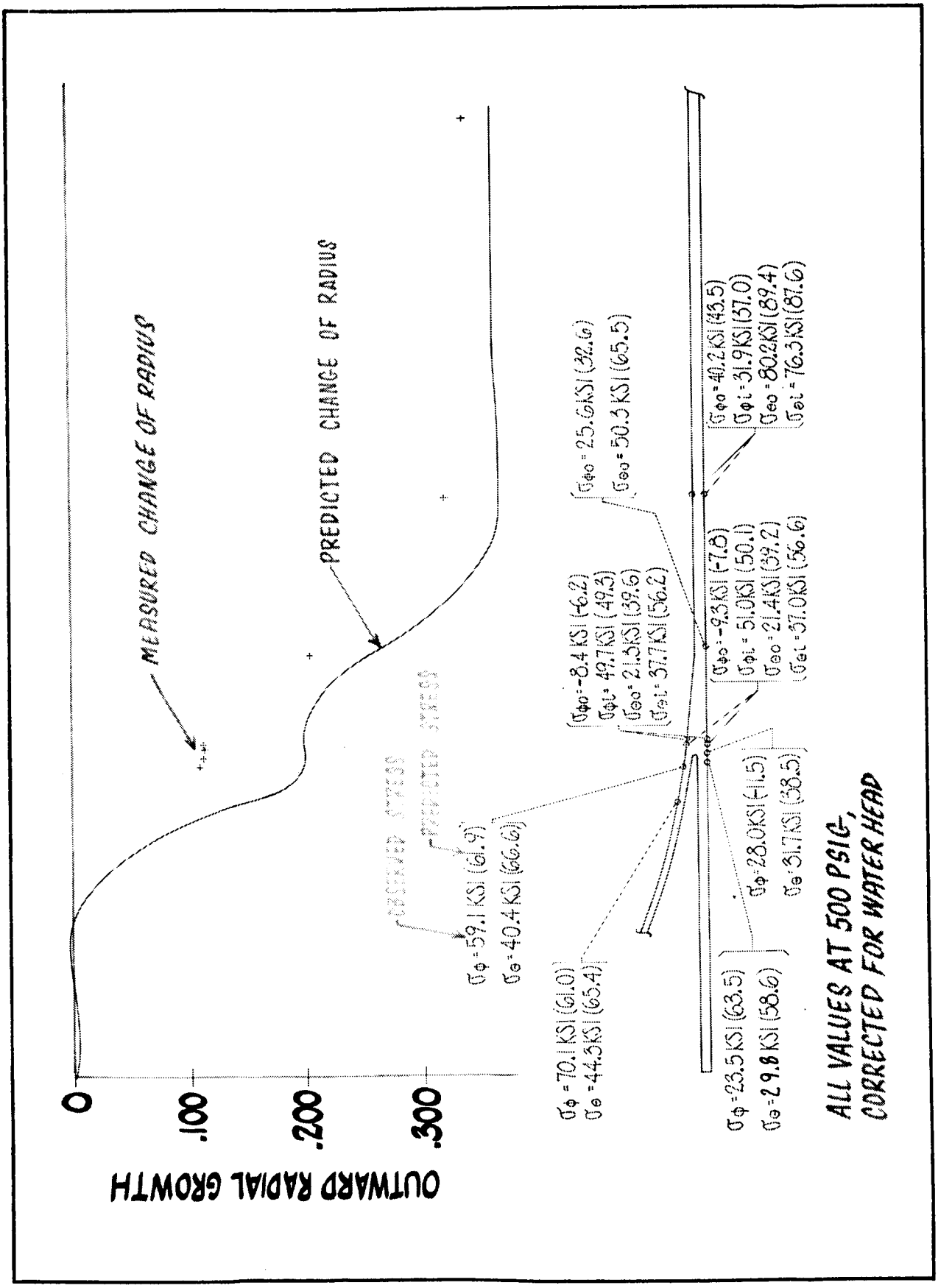
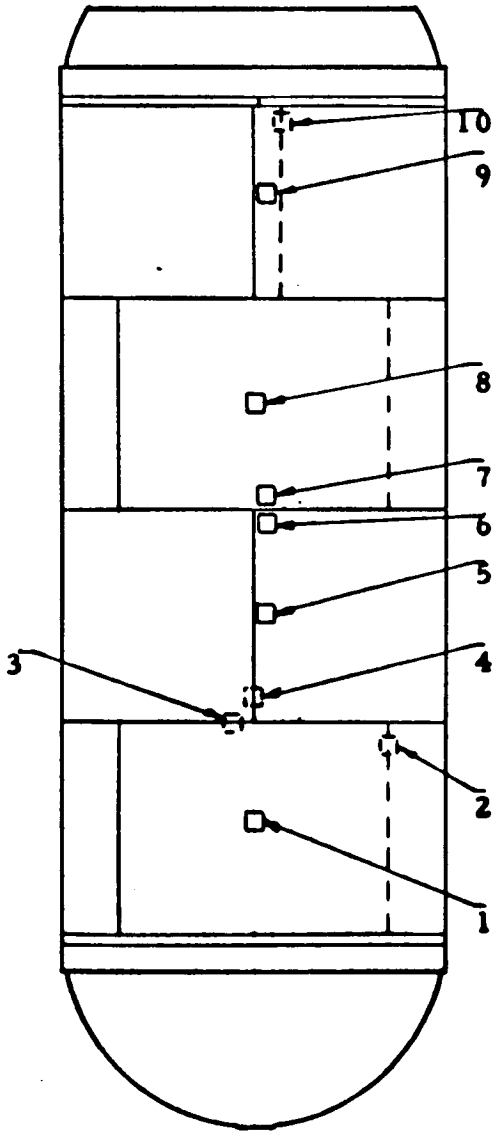


Figure 42 - Forward Y-Ring Stresses



Location		Predicted Stress, psi	Measured Stress, psi
1	σ_{ϕ_o}	41.8	38.3
	σ_{θ_o}	88.8	82.0
2	σ_{ϕ_i}	---	48.6
	σ_{ϕ_o}	---	20.3
	σ_{θ_i}	---	125.2
	σ_{θ_o}	---	38.5
3	σ_{ϕ_o}	---	21.4
	σ_{θ_o}	90.5	71.0
4	σ_{ϕ_i}	---	47.4
	σ_{ϕ_o}	---	19.6
	σ_{θ_i}	---	117.0
	σ_{θ_o}	---	35.4
5	σ_{ϕ_o}	41.4	33.6
	σ_{θ_o}	88.0	66.3
6	σ_{ϕ_i}	41.3	51.7
	σ_{ϕ_o}	41.3	25.0
	σ_{θ_i}	87.7	92.1
	σ_{θ_o}	87.7	69.2
7	σ_{ϕ_i}	41.3	49.1
	σ_{ϕ_o}	41.3	27.8
	σ_{θ_i}	87.7	87.8
	σ_{θ_o}	87.7	71.8
8	σ_{ϕ_o}	41.0	34.2
	σ_{θ_o}	87.2	74.2
9	σ_{ϕ_o}	40.7	30.4
	σ_{θ_o}	86.4	64.9
10	σ_{ϕ_o}	---	45.2
	σ_{θ_o}	86.1	77.3

Figure 43 - Cylinder Stresses

Measured stresses in the aft Y-ring and the areas adjacent to the Y-ring were lower than predicted except the inside meridional stress at the Y-ring/aft dome weld joint (Figure 44). Bending in the meridional direction at this point is approximately 26 percent higher than predicted.

e. Nozzle Attach Flange

Measured stresses in the aft dome region were close to predicted values (Figure 45). One inside gage forward of the nozzle attach flange indicated a meridional stress slightly higher than the predicted value.

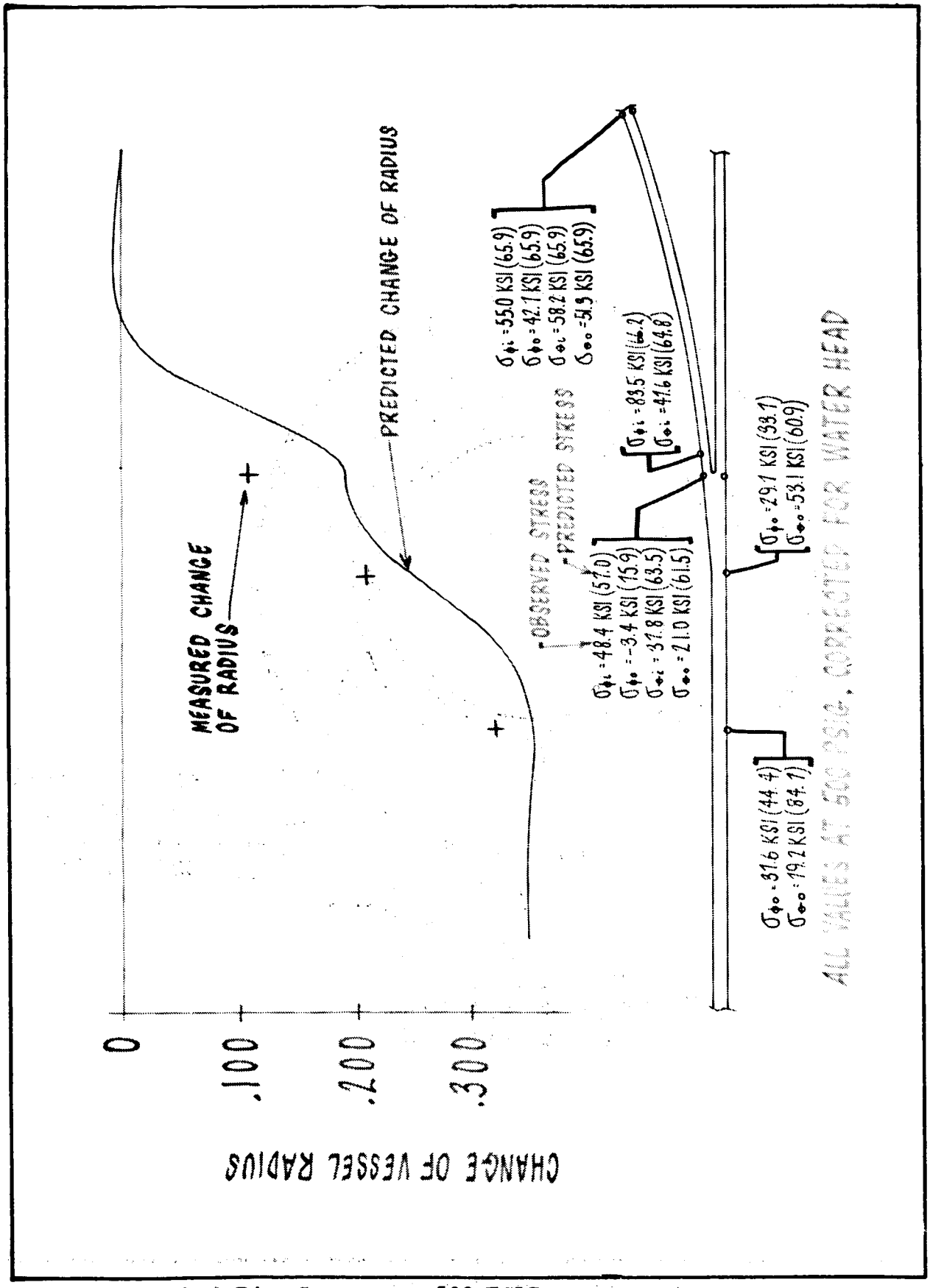


Figure 44 - Aft Y-Ring Stresses at 500 PSIG

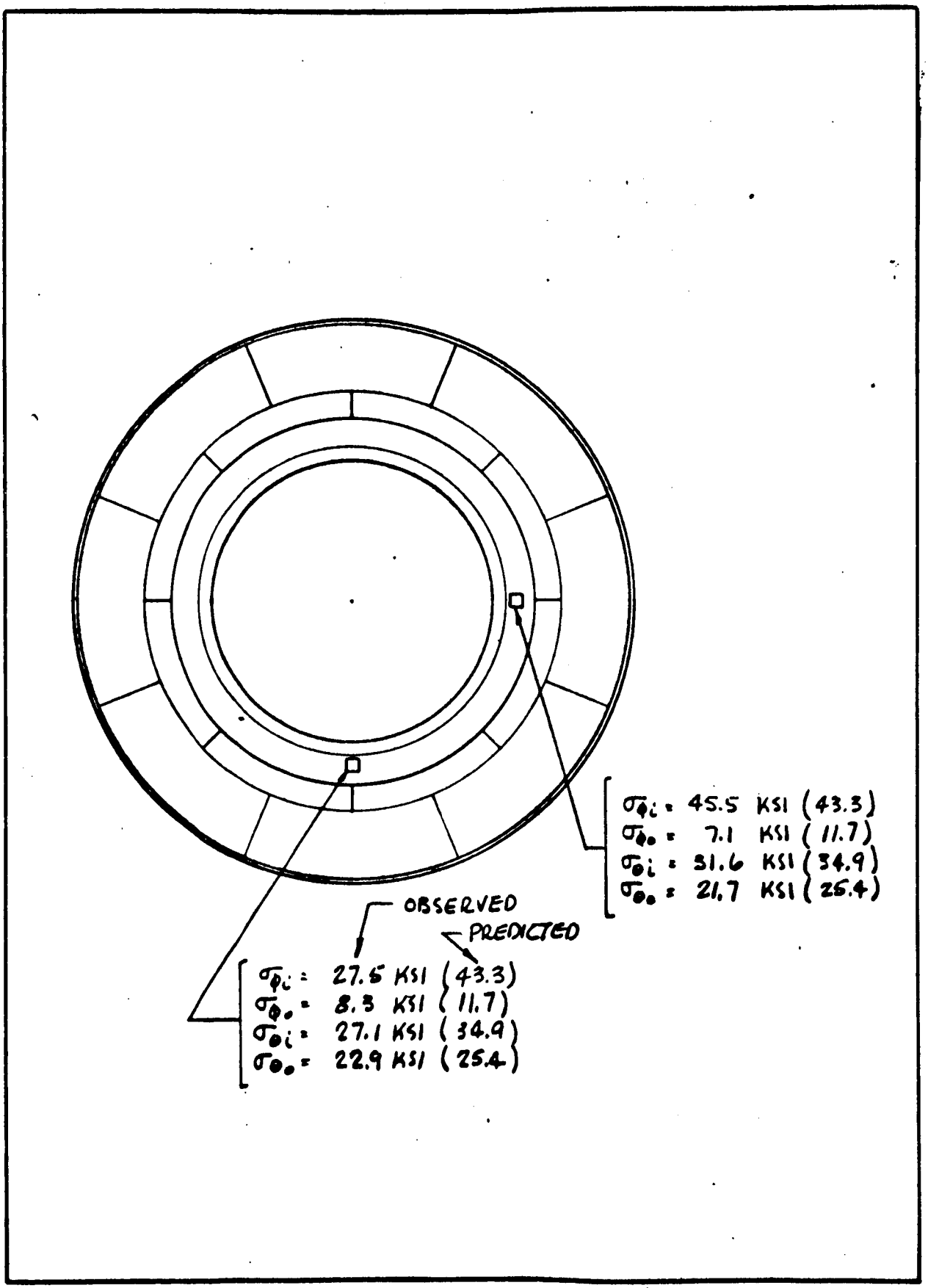


Figure 45 - Nozzle Attach Flange Stresses

APPENDIX - NASA FAILURE REPORT

by John E. Srawley and Jack B. Esgar

SUMMARY

The Thiokol Chemical Corporation 260-inch-diameter SL-1 motor case failed during hydrotest at a pressure of 542 pounds per square inch, which was about 56 percent of proof pressure. The motor case was constructed of 250 grade maraging steel plate joined mostly by submerged arc automatic welding. An investigation of the failure was conducted by a Committee composed of members from Industry and Government. Investigation showed that the failure originated from a defect that was not detected by nondestructive testing techniques prior to aging. Nondestructive testing was not conducted between aging and hydrotest. The defect causing the failure was in the heat-affected zone of a longitudinal submerged arc weld on the cylindrical section of the motor case. The area where the defect was located had been repaired by a manual gas-tungsten-arc (TIG) weld. The defect, which was submerged within the vessel wall and oriented longitudinally, was approximately 1.4 inches long and had a width of about 0.10 inch. Four other undetected defects of significant size were discovered after the motor case failure. All of these defects were also located beneath manual TIG weld repairs. One of these defects, which was in the same longitudinal weld as the defect causing the motor case failure, was involved in the fracture as a secondary origin. The other defects were discovered during reinspection of all welds by nondestructive testing techniques after hydroburst.

Although the detailed mechanism of the formation of these defects has not been established, it is reasonably certain that their formation was a consequence of the TIG weld repairs to the original welds.

The fracture toughness of the submerged arc welds was inadequate to tolerate crack-like defects as large as those that occurred in the motor case. It had been believed that much smaller defects could be detected with high reliability by the nondestructive inspection procedures that were used. The fracture toughness would have been sufficient if no defects had been present larger than what had been considered to be the detectable size.

As part of the failure investigation, a limited test program was conducted to determine the sensitivity of radiographic and ultrasonic procedures for detecting tight fatigue cracks in flat plate specimens. It was found that these nondestructive testing methods were much less sensitive and reliable than expected. It is concluded that much more research is required on nondestructive testing techniques for detection of small defects in thick pressure vessel walls before materials and weld procedures having the toughness found in the Thiokol motor case can be successfully utilized.

Reproduced from NASA Technical Memorandum X-1194 entitled "Investigation of Hydrotest Failure of Thiokol Chemical Corporation 260-Inch-Diameter SL-1 Motor Case", 1966, pp. 1-24

INTRODUCTION

In the course of a program to demonstrate the feasibility of 260-inch-diameter solid-rocket motors by Thiokol Chemical Corporation, a short-length case failed during hydrotest. An investigation of the failure was conducted by a Committee composed of technical representatives from Government and Industry. The findings of this Committee are reported herein.

The large solid-propellant rocket-motor program was initiated in 1963. Thiokol Chemical Corporation and the Aerojet-General Corporation were selected by the U. S. Air Force to demonstrate the feasibility of 260-inch-diameter solid-propellant rocket motors. NASA took over funding of the program on July 1, 1964 and assumed technical management March 1, 1965. Both Thiokol and Aerojet-General were under contract to build and test two motor cases of full diameter but only one-half the length required for the reference motor, which will produce 6 million pounds of thrust for 2 minutes. The two short-length motors scheduled to be built and tested by Thiokol were designated 260-SL-1 and 260-SL-2, and they were designed to produce 3 million pounds of thrust for 2 minutes.

During hydrotest of the Thiokol 260-SL-1 motor case on April 11, 1965, the case failed at an internal pressure of 542 pounds per square inch, which was about 56 percent of proof pressure. A failure investigating committee was formed to determine the cause of the failure and remedial actions that will prevent similar failures in other rocket motor cases. The first meeting of this Committee was held on April 26 and 27, 1965, after the failed motor case had been removed from the hydrotest tower, laid out in a protected area for inspection, and a preliminary inspection and mapping of the fracture paths had been performed by Mr. J. A. Kies from the U. S. Naval Research Laboratory and Mr. J. E. Srawley from the NASA Lewis Research Center. Although the investigation was not complete at that time, the origin and probable cause of the failure were determined. A preliminary report for NASA use was issued on May 7, 1965 listing the preliminary findings of the Committee. The investigation then continued with emphasis on a detailed metallographic study of the failure pieces in the region of the fracture origins and reinspection of most of the welds in the failed motor case to determine if previously undetected defects could be found. The metallographic investigation was conducted by the United States Steel Corporation, Applied Research Laboratories. Their report on the metallographic investigation, authored by A. J. Baker, A. J. Birkle, P. S. Trozzo, and R. P. Wei, is included as appendix A. Reinspection of motor case welds was conducted by the Newport News Shipbuilding and Dry Dock Company and the U. S. Naval Research Laboratory.

In addition to the regular committee members, several consultants with related experience in large, solid motor case problems were invited to inspect the case failure and provide comments to the Committee. The final findings of the Committee on the causes and factors relating to the motor case failure are presented in this report.

MOTOR CASE CONSTRUCTION

Design and Fabrication

The Thiokol cases were designed by the Space Booster Division of Thiokol Chemical Corporation and manufactured by the Newport News Shipbuilding and Dry Dock Company. The material specified in the USAF request for proposal was maraging steel (18 Ni-Co-Mo-Ti). Thiokol selected the 250 grade air-melted maraging steel. The term 250 grade refers to a nominal yield strength of 250 000 pounds per square inch (psi) for the material. The case design was based on a plate yield strength of 230 000 psi and a weld efficiency of 90 percent for a design strength in the welds of 207 000 psi. Using a factor of safety of 1.3 for the welds resulted in a nominal plate thickness of 0.730 inch in the cylindrical section and 0.477 inch in the hemispherical domes. In the weld area, a mismatch of 10 percent of the thickness was allowed, but it was not to exceed 0.060 inch. The eccentricity of membrane forces from this mismatch in a longitudinal weld results in an elastic stress magnification factor of 1.25.

The case fabrication procedure consisted of the buildup of three subassemblies, as shown in figure 1. The aft subassembly consisted of the aft closure, aft Y-ring, aft skirt, and one cylindrical section. The closure, skirt, and cylinder were welded to the Y-ring. The center subassembly consisted of two cylindrical sections. The forward subassembly consisted of the forward dome, forward Y-ring, forward skirt, and one cylindrical section.

All welds in the cylinder and the domes were accomplished by using the submerged arc process (hereinafter called subarc). The Y-rings were built up from four circumferential segments. The four longitudinal welds used to join the Y-ring segments were accomplished by using the vertical submerged arc process. This process was used because of the thickness of the part $\left(1\frac{7}{8}\text{ in.}\right)$ at the time of welding. The forward and aft skirts were welded to the respective Y-rings by using the multipass gas-tungsten-arc (TIG) process because the geometrical configuration permitted the weld to be deposited only along the outside circumference.

The three subassemblies of the motor case were aged separately at 835° F for 4 hours. The subassemblies were then joined to form the case by girth welds by using the two-pass subarc welding procedure. These welds were then locally aged with the same heat-treatment schedule as used for the subassemblies.

Several weld repairs were made during motor case construction. The weld repairs were all made by manual TIG welding, and they were made before aging. The welding records for the motor case showed the total weld length to be approximately 975 feet. Weld repairs were contained in 200 feet of this total length. In some cases, the weld repairs had to be re-repaired. The total length of weld repairs made during the construction was approximately 330 feet.

Nondestructive Testing

Nondestructive testing and inspection were generally carried out during the fabrication by four methods: (1) visual, (2) liquid penetrant (PT), (3) ultrasonic (UT), and (4) radiographic (RT). A very limited amount of magnetic particle (MT) inspection was also used for one weld joint. A brief description of the equipment and procedures used is given in this section. After the motor case failure, plate specimens containing fatigue cracks were prepared for evaluation of the sensitivity of the nondestructive testing methods (NDT), as discussed in the section Nondestructive Testing Sensitivity Evaluation.

Liquid penetrant (PT). - The Type II (nonfluorescent) penetrant materials, produced by the Magnaflux Corporation, for inspection are as follows:

Spot Check - Cleaner - SKC-NF

Spot Check - Penetrant - SKL-HF

Spot Check - Developer - SKD-NF

The procedure used called for cleaning the surface with SKC-NF, drying with clean cloths, then wetting the surface for at least 15 minutes with penetrant. Not more than 20 minutes after penetrant application (unless the penetrant was kept wet) the excess was wiped off and the penetrant film was removed with SKC-NF dampened cloths or absorbent paper. Developer was applied within 10 minutes by spraying or brushing if necessary. Inspection was to be made not sooner than 7 nor later than 30 minutes after the developer had dried.

The inspection rejection criteria varied somewhat during the time fabrication was in process. Generally, rounded indications up to 0.070 inch in diameter were acceptable in plate, and rounded indications 0.045 inch in diameter were accepted in the welds and adjacent areas 6 inches on either side of the welds. Linear indications, regardless of size or orientation and linearly disposed rounded indications were cause for rejection in all cases.

When defects were found by any of the NDT methods, the area was excavated by grinding for weld repair. These excavations were PT inspected prior to welding.

Radiography (RT). - Each weld was radiographically inspected over 100 percent of its length. The radiographic technique was based on military specification MIL-STD-453 with some modifications. The radiographic quality level was 2-2T, which indicates that a penetrameter whose thickness T is no greater than 2 percent of the welded joint thickness shall be visible in the radiograph. It also indicates that a hole drilled through the penetrameter with a diameter equal to twice the thickness of the penetrameter shall be visible.

All production exposures were made with X-ray equipment of the Triplett and Barton portable 275 or 300 maximum KVP - 10 maximum milliampere type. Some of the early exposures were made by using a 57-inch target to film distance,

but most exposures were made at a 36-inch distance to reduce fog and exposure times. Standard Kodak Type M film was used with 0.005-inch lead front screens and 0.010-inch lead back screens, except for thick sections such as the Y-ring welds, where Type AA film was used. Film was used in cassettes until about January 22, 1965. After that time Kodak "Ready Pack" was used because it saved interpretation time and virtually eliminated artifacts. Cassettes were used for about 65 percent of the total exposures taken during fabrication. The acceptance criteria for welds was as outlined in Standard I of MIL-R-11468 ORD dated September 24, 1951.

Ultrasonic (UT). - Two UT inspection procedures were developed; one for plates and forgings, and one for welds. The plate inspection procedure covered inspection for thickness, compressional wave (through thickness) for laminar oriented defects, and shear wave in longitudinal and transverse directions for nonlaminar defects. The weld inspection procedure called for compressional wave (through thickness) and shear wave in transverse and longitudinal directions.

Calibrations and rejectable flaw sizes for inspection of plates were changed several times during motor case fabrication. The final criteria for rejection are discussed in the following paragraphs.

Plate and forging inspection procedure: The equipment used was Branson Sonoray models 5, 50, or 51 for soundness testing, and model 14 Vidigage for thickness testing. The transducer frequency used for nearly all the testing was 2.25 or 4.0 megacycles. On occasions, however, other frequencies and/or dual transducers were used to improve sensitivity. Rejectable defect signals were determined from calibration plates with machined notches or flat-bottomed holes for use as standards. The following standards were set up:

Thickness:

Equipment calibrated from plates with thickness predetermined by micrometers. Calibration was checked before, during, and after tests on each plate.

Compressional wave:

For plates, signal size was calibrated for a 1/8-inch-diameter flat-bottom hole halfway through the plate thickness. When the signal amplitude exceeded that obtained from a 1/8-inch-diameter flat-bottomed calibration hole, the flaw was further examined to determine its area. The plate was rejected if the discontinuity equalled or exceeded 0.11 square inch.

For forgings and potential heat-affected zones (HAZ), calibrations were made by using 5/64-inch-diameter flat-bottomed holes at various depths to obtain a distance-amplitude line on the oscilloscope screen. Signals that exceeded this distance-amplitude line were a basis for rejection.

Shear wave:

Signal size was calibrated for a machined notch 1/32-inch deep and 1/4-inch long (or equivalent area). Signals exceeding that for the calibration notch, for equivalent distances to the defect and the calibration notch, were a basis for rejection.

Weld inspection procedure: The equipment used was Branson Sonoray models 5, 50, and 51. The transducer frequency was 2.25 megacycles for all the shear wave testing and was 4.0 megacycles (dual transducer) for compressional wave testing. On occasions it was necessary to utilize other frequencies to improve sensitivity. The standards for the rejectable defect sizes were as follows:

Compressional wave:

Calibrations were made for 5/64-inch-diameter flat-bottomed holes at various depths to obtain a distance-amplitude line on the screen. Signals exceeding this line were a basis for rejection and repair.

Shear wave:

For longitudinal defects (relative to weld direction) the rejection calibration standard was a machined circular segment notch 1/32-inch deep and 1/4-inch long.

For transverse defects (relative to weld direction) the rejection calibration standard was a machined circular segment notch 1/64-inch deep and 1/4-inch long.

Magnetic particle (MT). - Inspection by the MT technique was not used as a routine procedure for the 260-inch-diameter motor cases. As discussed in the section Reinspection of Weld Areas After Hydrotest Failure, MT was not considered to be a generally reliable NDT technique for welded maraging steel. It was utilized only in a limited way for special cases where the other techniques were not applicable. For example, a special technique was employed on the circumferential weld in the center of the assembled motor case to provide a survey of intermittent centerline surface cracking first indicated by PT. In this instance, PT was not fully reliable because cracking was partly subsurface, and the shallow, tight nature of the cracks prevented UT and RT from being successful. The magnetic field for the MT inspection was provided by strong permanent magnets with their poles contacting the opposite sides of the weld joint.

Repair Procedures

All the nondestructive testing (except for acceptance tests of parent material prior to fabrication) was conducted after welding, but before aging. If defects were found by any of the three methods (RT, PT, or UT) the defective material was removed by grinding, and the weld was repaired by the TIG method. The repaired area was reinspected by all three methods, and the process was continued until there was no further evidence of defects. During excavation of

the defect prior to repair welding PT was used to determine the amount of excavation required.

Past experience by Newport News Shipbuilding and Dry Dock Company had indicated that aging of the welds should not introduce new defects. As a result, a joint decision was made by Newport News Shipbuilding and Dry Dock Company and Thiokol Chemical Corporation on January 13, 1965 that nondestructive testing would not be repeated after aging of the welds. This decision received U. S. Air Force concurrence.

HYDROTEST PROCEDURE

The completed rocket motor case was readied for hydrotest by bolting on a nozzle adapter manufactured by the Rohr Corporation and a hydrotest nozzle cone manufactured by Newport News Shipbuilding and Dry Dock Company. These components are indicated in figure 1. The case was supported in a hydrotest tower by bolting the forward skirt to the forward lifting ring, which, in turn, was bolted to the base pedestal of the hydrotest tower (fig. 2). A piston attached to the hydrotest tower sealed the case as a pressure vessel and provided thrust loads on the forward skirt. Case growth during pressurization was accommodated by movement of the case in the longitudinal direction relative to the piston.

Twenty-four accelerometers were located on the case in the locations shown in figure 3 to detect stress waves generated during hydrotest. Procedures for interpreting the output of such accelerometers are being studied and are not completely developed at this time. Appendix B describes the use of accelerometers for determining stress-wave origins. The output of the accelerometers was to be fully analyzed after the test.

Strain gages were located on both the inside and outside surfaces of the case. Certain areas of the case were expected to experience relatively high stress because of plate-thin spots and out-of-contour areas near welds. These areas were strain gaged. The out-of-contour areas were of particular concern because of the difficulty in stress analyzing these areas. The strain gages in these critical areas were monitored during the test. The test was to be aborted if stress levels significantly exceeded analytic predictions.

The case was filled with water on Saturday, April 10, 1965. The water was inhibited by the addition of 0.73 pound of sodium dichromate in each 1000 gallons of water. In addition, caustic soda was introduced in sufficient amounts to achieve pH neutrality. The water was heated by addition of steam during filling to give a temperature of approximately 62° F. The inhibited and heated water was introduced into the case through the forward closure (bottom of case during hydrotest). Fluid was bled from the case top, through a bleed line in the fixed piston, initially and after each depressurization in order to ensure that the case was entirely filled with liquid.

The maximum hydrotest pressure planned was 960 psi, 10 percent above the maximum expected operating pressure of the motor. The actual pressure-time history for the case is shown in figure 4. The 300-psi pressurization on

April 10 permitted instrumentation and pressurization system checkout. The 350-psi pressurization on April 11 verified the status of the instrumentation. During the final pressurization there were 5-minute holds at 300 to 500 psi in order to record strain gage readings.

During hydrotest, the accelerometer system mounted on the motor case indicated eight stress waves, including the wave that occurred at failure. The predicted origins and the pressures at stress wave initiation are also shown in figure 3. The first stress wave occurred at a pressure of 242 psi. Previous experience in using a stress-wave detection system on hydrotest of motor cases has shown similar stress wave initiations in areas not related to final failure. Three of the stress wave origins were in the region of the lower skirt where the motor case was bolted to the hydrotest thrust stand. It is probable that some of these stress waves resulted from movement at the bolt holes.

As the pressure was increased to 542 psi another stress wave was detected. At the same time a loud report was heard from the direction of the hydrotest tower. Visual inspection revealed the case to have failed catastrophically. Prior to failure, two stress waves had originated in the general area of the fracture initiation location. At the present stage of development of the stress-wave detection system, however, it is not possible to determine the positions of these origins while the test is underway. The data are recorded during the hydrotest and played back later to determine stress wave arrival sequences at each accelerometer. These data are then fed into a computer to determine the origin locations by triangulation.

FAILURE INVESTIGATION

On failure at a gage pressure of 542 psi, the motor case had shattered into several large pieces and many smaller ones that fell into a precarious, interlocked pile within the test tower. Several days were required to remove the pieces to a large shop where they were laid out on the floor for detailed examination. Figure 5 is a photograph taken during this operation that shows the test tower site. A large piece consisting of the aft head and part of the cylindrical section is resting in the framework of the tower, and another large piece of the cylindrical section that had been removed from the tower is shown in the foreground. In spite of the lengthy exposure in the open air, the fracture surfaces were not visibly rusted; nor were they mechanically damaged in handling to any important extent. It was necessary to cut two of the larger pieces with a torch to facilitate removal, but these cuts did not impair the subsequent examination. Figure 6 shows the pieces laid out on the shop floor with the aft head in the center foreground and the other pieces arranged as nearly as possible in proper relation to one another.

While the pieces were being transferred to the shop, work was started on mapping the fracture paths throughout the entire vessel. The location and orientation of each piece could be ascertained either from the locations of welds in the piece, or by matching fracture surfaces of adjacent pieces. A reference grid related to the welds was marked out on the pieces, and their boundaries were then plotted on a 1:12 scale model of the motor case made of

Lucite. A plane development of the cylindrical section of the model map is shown in figure 7. This map was obtained by tracing the fracture paths onto a piece of tracing paper wrapped around the model. The arrowheads on this map show the directions of propagation of the fracture along the various branches, as ascertained from chevron markings on the fracture surfaces. Figure 8 is a photograph showing the typical chevron markings on either side of one of the fracture origins discussed in the next section. The chevrons point back to the origin, opposite to the direction of fracture propagation. Similarly well-defined markings were found on most of the fracture surfaces and, taken together with collateral information, these were sufficient to define the complete course of the fracture without ambiguity.

Fracture Origin Location

From the fracture map (fig. 7), it is clear that the fracture pattern developed from an origin close to the W7/302 longitudinal weld and somewhat forward of the W8/3 aft Y-ring weld. Although they are not shown here, the fracture paths in the skirts and the domes were completely mapped, and it was established that they had developed from cracks running out of the cylindrical section. There were no independent origins in these parts of the motor case, although there were one or two fracture branches that had run from the cylinder into one of the heads and then continued on back into the cylinder.

Independent confirmation of the general location of the fracture origin was obtained by triangulation based on the recorded accelerometer signals. As discussed in appendix B, the origin of the stress wave detected at the time of failure was estimated to be located within a 20-inch-diameter circle centered at a point 8 inches from the W7/302 weld and 29 inches forward of the W8/3 weld. This location, shown as a dashed circle in figure 7(b), is in good agreement with the position of the source of the fracture paths.

Two distinct fracture origins were discovered in the expected region, both associated with areas of TIG weld repair on the inside surface of the W7/302 weld. One origin was oriented parallel to the weld centerline, and the other transverse to it. The positions of these origins and sketches of their contours are shown in the detail fracture map (fig. 7(b)). Because of the obvious difference in appearance to the naked eye, the longitudinal defect was termed the "clean" origin, and the transverse defect the "black" origin. Photographs of the mating surfaces of the clean origin are shown in figure 9. The boundary is quite distinct except for two damaged places on one of the mating surfaces that must have rubbed against another piece of metal, but the appearance of the origin surface differs only in texture and tone from that of the surrounding fracture: there is no suggestion of a deposit on the surface. On the other hand, the black origin was covered with a tightly adhering, black deposit, as shown in figures 8 and 10. This deposit was eventually identified as essentially an iron oxide. This difference between the two origins is probably connected with the fact that, whereas the boundary of the black origin extends to the outer surface of the vessel wall, the clean origin is completely submerged within the wall.

The inner and outer faces of the pieces containing the two origins were

ground and etched to reveal the positions of the fusion lines and heat-affected zones of the W7/302 weld. It was then found that each origin was located beneath a separate manual TIG weld that had been deposited on the inside of the vessel to replace part of the original subarc weld. These locations are indicated in figures 11 and 12. The clean origin (fig. 11) was located near one edge of what appeared to be a fusion line TIG repair weld, and the black origin (fig. 12) was located near one end of a TIG repair, which covered the whole width of the weld and heat-affected zones. These locations are discussed in greater detail later. The TIG weld areas were identified by the responsible welding engineer as simulated repairs to an originally sound subarc weld. The simulated repairs had been made as part of an investigation concerned with cracking that had been encountered in TIG repair welding of meridional dome welds. Experimental TIG repairs had been made at three places on the W7/302 weld, but a total of four nondestructive inspections by PT, UT, and RT at times varying from 1 day to 19 weeks after the repairs were made had revealed no indications of defects in the repaired regions. The more detailed examination of the two origins is discussed in the next section, following discussion of the sequence of fracturing.

There is no doubt that both origins contributed to the overall development of the fracture. Fracturing in the aft head developed from a crack that ran longitudinally from the clean origin and branched just before it reached the W8/3 Y-ring junction weld (see fig. 7(b)). Fracturing in much of the cylindrical section, and throughout the forward head, developed from cracks that ran circumferentially for short distances from the black origin and then branched into spiral and longitudinal paths, as shown in figure 7. It is most unlikely, however, that the fracture started simultaneously and independently at both origins. It is almost certain that the stress redistribution associated with propagation of cracks from one origin brought about secondary crack propagation from the other origin.

In fact, the local fracture pattern in figure 7(b) can only be explained satisfactorily if it is assumed that fracture started first at the clean origin with the initial, longitudinal crack running both aft toward the head and forward toward the position of the black origin. The intensity of the stress field around the black origin would have increased with the approach of the crack, so that secondary crack propagation would have been triggered at the black origin before the primary crack reached it. The subsequent intersection of the developing transverse crack by the primary crack would then have disturbed the stress field in a way that would account for the early branching of both ends of the transverse crack. Since the velocity of propagation of brittle fracture in steel can approach 5000 feet per second, it is likely that the interval between primary and secondary crack initiation would be of the order of a millisecond.

The alternative hypothesis, that fracture started first at the black origin, does not lead to a satisfactory explanation of the observed fracture pattern. The development of the transverse crack from the black origin, and of the branches stemming from it, would not have increased the intensity of the stress field around the clean origin; if anything the stress intensity at the clean origin would have decreased as the crack pattern developed from the black origin. There would have been no reason, therefore, for secondary crack

propagation to start at the clean origin. In this case the complete fracture pattern should have been significantly different from that observed, and the clean origin should not have been involved at all.

Independent support for the conclusion that the clean origin was the primary origin of the fracture is provided by a comparison of the distances between the position of the stress wave origin calculated from the accelerometer data and the positions of the two fracture origins. As shown in figure 7(b), the distance from the center of the 20-inch-diameter circle representing the stress wave origin to the clean origin is about 12 inches, while the distance to the black origin is about 32 inches. Statistically, the probability of a triangulation error of 12 inches is significantly higher than the probability of an error of 32 inches.

In the absence of the clean origin it is quite likely that the vessel would have fractured, starting at the black origin, at some pressure less than the intended hydrotest proof pressure. In any event, under no circumstances would either origin have been considered a tolerable defect if its presence and magnitude had been detected prior to the hydrotest.

The Consultants reports, which are presented in appendix C, are in general agreement with the foregoing analysis of the origination and development of the fracture.

An investigation was conducted on other factors that may have been related to the failure. This investigation, reported in appendix D, further substantiated the preceding findings.

Metallographic Examination of Fracture Origins

Detailed metallographic examination of the fracture origins and neighboring regions of motor case fragments was undertaken by the Applied Research Laboratory of the U. S. Steel Corporation, under the direction of Mr. George Pellissier. The findings summarized in this section are discussed in greater detail in appendix A.

The locations of both origins with respect to weld deposits were established accurately by sectioning and etching. These locations are most readily visualized by reference to the simplified isometric drawings (figs. 11 and 12). The clean origin is located just below the intersection of the TIG weld interface with the interface of the inside, second pass of the subarc weld, in the grain-coarsened region of the subarc weld heat-affected zone. The black origin (fig. 12) is transverse to the W7/302 weld and crosses the inside, second pass of that weld, extending into the heat-affected zones on both sides of the weld deposit. The nearly straight boundary lies just below the fusion interface of the TIG weld repair, close to one end of the repair. The enlarged end of the origin extends to the outside surface of the vessel at about the position of the fusion interface of the first pass of the subarc weld. This end of the origin is within the combined heat-affected zones of the TIG and subarc welds, but its extremity probably reaches the limit of the austenite reversion region.

By optical microscopic examination of fracture profiles in polished sections, and electron microscopic examination of fracture replicas, it was ascertained that the fracture topographies of the two origins were quite similar to one another, but different from adjacent fracture surfaces. The origin surfaces were predominantly intergranular, with relatively flat facets that corresponded either to prior austenitic grain boundaries, or to dendrite interfaces in the case of that part of the black origin located within the weld. The surrounding fracture surfaces were predominantly of the noncrystallographic, dimpled type, which is indicative of more ductile rupturing.

The association of each of the origins with a TIG repair weld, and the nature of the origin surfaces, suggests that their formation was a consequence of TIG repair welding. This suspicion is reinforced by the finding of three other flaws associated with TIG weld repair regions. A tension test specimen taken from the W7/101 weld after hydrotest failure was used to examine one of these flaws shown in figure 13. This flaw and two flaws that were found in the W6/3 TIG weld are discussed further in the section Reinspection of Weld Repair Areas After Hydrotest Failure. The detailed mechanism of formation of the flaws has not been established, but it appears that the defects were generated by stresses set up during TIG repair welding in regions exhibiting microstructural inhomogeneity and grain coarsening.

The black deposit on the transverse origin was examined by glancing-angle X-ray diffraction, electron diffraction, and electron-probe microanalysis. The diffraction patterns corresponded to a mixture of ferrous oxide (Fe_2O_3) and ferric oxide (Fe_3O_4). The analysis showed that the metallic constituent was predominantly iron with small amounts of nickel, molybdenum, cobalt, and titanium. This oxide must have formed at a high temperature. Comparison of the color with oxidized crack surfaces obtained by heating in air at high temperatures suggests a formation temperature at least as high as 800° F. It would appear that at least some of the oxidation must have occurred during the aging cycle at 835° F.

Polished sections and fractographic replicas were examined to determine the location of the fracture surface at a representative position between the primary and secondary origins. Near the surfaces of the vessel wall the fracture is interdendritic, through the subarc weld metal in which the dendrites are normal to the surfaces. Further within the wall the fracture is intergranular, through the grain-coarsened region just adjacent to the fusion interface of the subarc weld, conforming macroscopically to the fusion interface. The path taken by the fracture suggests that the grain-coarsened region has a low fracture toughness associated with a highly sensitized microstructure. This observation is consistent with the occurrence of the clean and black origins in similarly grain-coarsened regions.

From the metallographic evidence it may be surmized that the high heat input during subarc welding caused grain coarsening and thermal embrittlement in the regions of the base plate adjacent to the weld deposit. Such regions would be expected to be susceptible to cracking under thermal stresses such as those generated by subsequent repair welding. To establish the mechanism of formation of the fracture origins more conclusively would require the undertaking of a research program directed toward duplicating the phenomenon in the laboratory.

Fracture Calculations and Fracture Toughness

Fracture mechanics background. - Engineering calculations concerning fracture are conducted currently on the basis of the mathematical theory of linear elastic fracture mechanics, which deals with the stress field singularities associated with cracks in ideal elastic bodies (refs. 1 and 2). While it is recognized that this mathematical model represents a considerable oversimplification of the situation in a real engineering material, the calculations are nevertheless often useful, particularly when applied to materials of high yield strength subjected to relatively low stress levels as in the present investigation.

The distribution of stresses and displacements near the edge of an elastic crack is dominated by the influence of the stress-free surfaces of the crack. The crack stress field system can be resolved into three basic component systems, each referring to a particular set of displacement discontinuities associated with a principal mode of crack extension. For simplicity only the first or opening mode of crack extension needs to be considered here, namely, that in which the relative displacement of corresponding points on the mating crack surfaces occurs in a direction normal to those surfaces. The other two component modes involve forward or sidewise sliding of the crack surfaces over one another. In the opening mode, the stress components near the crack edge are all proportional to the scalar stress intensity factor K_I. The magnitude of K_I is proportional to the loading forces acting on the body containing the crack and also depends upon the configuration of the body, including the crack shape and size. The dimensions of K_I are those of stress multiplied by the square root of length. The evaluation of K_I for configurations that are of practical interest is a primary task of linear elastic fracture mechanics (ref. 3).

For engineering application of linear elastic fracture mechanics some criterion for fracture of a material must be assumed. The assumption is that a material will exhibit a characteristic plane strain fracture toughness K_{Ic} such that a crack in the material will become unstable if the value of K_I anywhere along the crack boundary reaches the K_{Ic} value of the material. In practice, K_{Ic} values are measured by conducting fracture tests on appropriately designed specimens that incorporate cracks and that have been subjected to a sufficiently accurate K_I stress analysis (ref. 4). In a failure analysis, the K_I value calculated from the fracture origin dimensions and the loads can be compared with K_{Ic} values obtained from tests of the material involved. It is important to appreciate, however, that only approximate agreement is to be expected because of the simplifications involved in the underlying assumptions. Furthermore, there may be other sources of error or uncertainty, as will be noted in discussing the subject failure.

Accurate methods have not yet been developed for calculation of stress intensities of cracks of irregular contour such as the two origins involved in the hydrotest failure of the SL-1 motor case. Estimates of the upper and lower bounds can be obtained, however, from the analysis of cracks of elliptical contour published by Irwin (ref. 5). Figure 14 is a convenient working plot of the relevant results from this reference, showing the dimensionless quantity

$K_I/\sigma\sqrt{a}$ against the ratio a/c, where K_I is the maximum value of the stress intensity factor around the elliptical boundary, σ is the nominal stress acting across the crack, and a and c are the minor and major semiaxes of the ellipse, respectively. The stress intensity is greatest at the position of least curvature of the boundary, that is, at each end of the minor axis. Where part of the boundary of a crack has negative (concave) curvature, as is the case with the clean origin, the stress intensity will be higher than at a position of convex curvature, but the magnitude of the difference is not accurately known.

Stress intensity factors. - The nominal stress across the clean origin was estimated to be approximately 100 000 psi at the failure pressure of 542 psi. This estimate allows for the static pressure head and for a supplementary bending stress due to deviation of the shell contour from the ideal cylinder. This bending stress supplement corresponds to the position of the inner boundary of the origin where K_I should have been greatest because of the negative curvature of the boundary. The stress values used in this fracture toughness analysis are in substantial agreement with the values quoted by the consultants (appendix C). The differences are small and the values used herein are best estimates. The estimate of nominal stress is probably accurate to within 5 percent.

The estimates of the upper and lower bounds of the stress intensity corresponding to this nominal stress are based on fitting ellipses to the clean origin as shown in figure 15. The lengths of the ellipses are equal to that of the origin. For the lower bound, the width of the ellipse is 0.10 inch, equal to the minimum width of the origin. For the upper bound, the width of the ellipse is 0.22 inch, equal to the distance from the convex boundary of the origin to the tangent spanning the opposite boundary. The estimated K_I bounds for the clean origin are then 39 000 and 57 000 psi$\sqrt{\text{in.}}$

The nominal stress across the black origin is estimated to have been 46 000 psi at the failure pressure of 542 psi. This estimate allows for the static pressure head and the thrust on the fixed piston, but assumes the bending stress to be zero. The estimate of the lower bound of the K_I value for the black origin is based on an ellipse 1.6 inches long by 0.2 inch wide; these dimensions correspond to those of the black origin if the enlarged end is neglected. The estimated lower bound K_I value for the black origin is then 25 000 psi$\sqrt{\text{in.}}$, and this is probably a good estimate of the correct value for the narrow limb of the origin that crosses the subarc weld proper (fig. 12).

Estimation of the upper bound K_I value for the black origin is much more uncertain. The K_I value should be greatest at the sharp corner in the origin boundary (figs. 10 and 12), but advance of the crack front from this point would produce a smoother contour and, temporarily, a lower K_I value. Since there is no better basis for estimation, it will be assumed that the K_I value for this origin is unlikely to be greater than that based on an ellipse 1.6 inches long by 0.5 inch wide (this width being equal to the distance from the outer surface of the wall to the far boundary of the origin). The upper bound K_I value calculated on this basis is then 37 000 psi$\sqrt{\text{in.}}$ The fact that the black origin was open to the surface over a short distance will hardly

affect the K_I estimates because this distance amounts to less than 10 percent of the total length of the origin. This is a somewhat subtle point that is inferred from reference 5.

Residual stress effects. - The contributions of any residual stresses that may have existed in the origin regions have been neglected in the preceding K_I calculations. Experiments at the Newport News Shipbuilding and Dry Dock Company during the period when the motor case was under construction did reveal the existence of substantial residual stresses in the heat-affected zone of a subarc weld. A relaxation technique involving hole drilling was used. Substantial tensile stresses in the circumferential direction were measured in that part of the heat-affected zone just below the outside surface of the case. Compressive stresses occurred in the longitudinal direction. Unfortunately, there is no way of knowing the magnitudes and distributions of residual stresses in the regions of the clean and black origins at the time of the hydrotest. This uncertainty is aggravated by the somewhat contrary findings of the Boeing Company, who also conducted residual stress studies, as discussed in appendix C. Under the circumstances, the question of residual stresses can only be regarded as an additional factor of uncertainty of unknown magnitude affecting the accuracy of the K_I calculations.

Fracture toughness. - Measurements of K_{Ic} toughness were made at the NASA Lewis Research Center by using crack-notch bend specimens obtained from the W7/301 weld and adjacent plate material. This weld was made by the same welding procedure and joined the same two plates as the W7/302 weld where the failure originated. Unfortunately none of the K_{Ic} specimens were obtained from a region that had been repaired by TIG welding, and therefore the fracture toughness values were not properly representative of the material in the vicinity of the fracture origins. Because of a misunderstanding, the only part of the W7/301 weld that had been repaired by TIG welding was cut up in such a manner that it could not be used for fracture toughness specimens.

The types of four-point bend specimens used for the K_{Ic} tests are shown in figure 16. All the specimens had 90° notches that terminated in fatigue cracks. The crack notches in specimen types WT and HT were located so that the direction of crack propagation was from the inside to the outside of the original vessel wall. The crack notches in specimen types WL and HL were located so that the direction of crack propagation was along the weld. The cracks in types WT and WL were located in the center of the weld, and those in types HT and HL were located in the heat-affected zone to correspond approximately with the position of the clean origin. Base plate specimens, type BT, were also tested and were similar to types WT and HT.

Crack extension during the K_{Ic} tests was sensed by two independent methods. In one method a constant current is maintained through the specimen during the test, and the difference of electrical potential between two points located symmetrically on either side of the crack is detected, amplified, and used to drive one axis of an X-Y recorder. The other axis of the recorder is driven by the output of a load cell so that the resulting record is a plot of load as a function of a measure of the change in crack length. In the other method, acoustic vibrations emitted during crack extension are picked up by a

sensitive transducer attached to the specimen and recorded on magnetic tape together with a record of the load. Both methods are described in detail in reference 4. In most of the tests there was no ambiguity about the results because the specimens fractured completely at the maximum recorded loads without appreciable crack extension at lower loads. In the tests of three of the five HT specimens, however, small increments of abrupt crack extension did occur at loads well below the maximum. Nevertheless, the maximum loads were taken as corresponding to the K_{Ic} values in these cases as well as in the other cases because the increments of crack extension were isolated, that is, there was no further appreciable crack extension up to maximum load. It is considered that the explanation for the behavior of the three HT specimens is that the crack tips in these specimens were located in highly heterogeneous regions, low in toughness in the grain-coarsened part of the heat-affected zones, but higher in toughness in the finer grained part of the heat-affected zones slightly farther from the crack tips.

TABLE I. - FRACTURE TOUGHNESS VALUES FROM FOUR-POINT BEND SPECIMENS TAKEN FROM W7/301 WELD REGION

Specimen type[a]				
WT[b]	HT[c]	WL[d]	HL[e]	BT[f]
Fracture toughness, K_{Ic}, psi$\sqrt{\text{in.}}$				
45 000	77 700	38 800	54 400	83 100
55 400	77 500	38 900	50 400	81 000
50 300	75 400	40 500	53 000	83 000
43 400	84 500			69 800
51 900	75 000			81 000
Average K_{Ic}				
49 200	78 000	39 400	52 900	79 600

[a]See fig. 16.
[b]Weld centerline, through thickness crack propagation.
[c]HAZ, through thickness crack propagation.
[d]Weld centerline, longitudinal crack propagation.
[e]HAZ, longitudinal crack propagation.
[f]Base plate, through thickness crack propagation.

The results of the K_{Ic} tests are given in table I. The locations and directions of propagation of the cracks in the type HT specimens most nearly correspond to those of the clean origin. The average of the K_{Ic} values for these specimens is nearly as high as that for the base-plate specimens, and the lowest of the five values, 75 000 psi$\sqrt{\text{in.}}$, is considerably higher than the upper bound of the K_I estimated for the clean origin, which was

57 000 psi$\sqrt{\text{in.}}$. It is quite possible that the actual K_I level was greater than this upper bound if there were substantial residual tensile stresses at the clean origin, but is unlikely that the K_I level could have been as high as 75 000 psi$\sqrt{\text{in.}}$ On the other hand, it is quite reasonable to suppose that the K_{Ic} toughness of the material adjacent to the clean origin boundary could have been substantially lower than the values determined with the type HT specimens from the W7/301 weld. The very existence of the origin suggests the possibility of a locally embrittled region, not necessarily restricted to the actual origin. The effect of TIG weld repairs on the toughness of the underlying material is an unknown factor that would require a considerable program of welding and testing to clarify adequately.

An alternative possibility is that the K_{Ic} toughness of the material adjacent to the convex boundary of the clean origin may have been sufficiently low that propagation started first at this boundary rather than at the concave boundary. The material immediately adjacent to the convex boundary is subarc weld metal of low toughness (fig. 11). However, the bulk of the material between the convex boundary of the origin and the inside surface of the wall is TIG weld deposit, which is presumably of high toughness.

Taking into consideration the uncertainty regarding the actual K_I level at the clean origin at 542 psi pressure and also the uncertainty regarding the K_{Ic} toughness of the material adjacent to the clean origin indicates that the fracture mechanics analysis is not inconsistent with the conclusion from the evidence of the fracture pattern that the hydrotest failure started from this origin.

The K_{Ic} values listed in table I for the specimens of types WT, WL, and HL, in which the cracks propagated wholly or partly through the subarc weld material, are considerably lower than those for the heat-affected zone, type HT, and base plate, type BT, specimens. If these weld material K_{Ic} values are to be compared with the K_I value for the black origin, it must be remembered that only part of the narrow limb of the origin is located in the W7/302 weld deposit (fig. 12). As stated previously, the lower bound K_I value of 25 000 psi$\sqrt{\text{in.}}$ is probably a good estimate of the correct value for this part of the origin at 542 psi pressure. This K_I value is considerably lower than any of the K_{Ic} values reported in table I. On the other hand, the corresponding K_I value for the hydrotest proof pressure of 960 psi is 45 000 psi$\sqrt{\text{in.}}$, which is higher than the K_{Ic} values for the WL specimens in table I. There is, therefore, a distinct possibility that premature failure would have started at the black origin if the clean origin had not been present.

A transverse defect was also found in the W7/101 weld, as discussed in the section Reinspection of Weld Areas After Hydrotest Failure. A large, longitudinal tension specimen containing this defect was tested and failed at a gross stress of 115 000 psi. The defect is clearly defined in the fracture surface, shown in figure 13, and is 0.6 inch long by 0.12 inch wide. It is located in the heat-affected zone of the TIG repair weld, which was also in the center of the subarc weld deposit, and oriented transverse to the weld centerline. The K_{Ic} value calculated from this test result is 47 500 psi$\sqrt{\text{in.}}$, which is in good agreement with the values for the WT specimens listed in table I.

Reinspection of Weld Areas After Hydrotest Failure

Since the clean and black origins were undetected by nondestructive testing techniques prior to aging, the question arose as to whether the defects were caused by aging, and if they would have been detected if additional nondestructive testing had been conducted subsequent to aging. It was further reasoned that if these defects were caused by the aging cycle, additional defects, which would have been at subcritical size at the hydrotest failure pressure, may have been present in other welds in the motor case. As a result, the Failure Investigating Committee asked Newport News Shipbuilding and Dry Dock Company to reinspect all welds in the 260-SL-1 motor case by using the inspection procedures previously used (PT, RT, and UT) plus magnetic particle (MT). In addition the U. S. Naval Research Laboratory was asked to inspect independently some of the weld areas by using UT. About 85 percent of the nondestructive testing of welds was completed before contract termination on June 5, 1965.

It was determined during this investigation that magnetic particle testing was of questionable value in the examination of welds in the 18 percent nickel maraging steel alloy. Similar conclusions were drawn in research conducted by Excelco Developments, Inc. under NASA contract NASw - 687. All welds in this alloy exhibit narrow but significant bands of reverted metastable austenite in the parent material heat-affected zones, and in such zones created in the weld metal by the deposition of subsequent weld beads. Since such bands impose a change in magnetic permeability in a uniform magnetic field impressed across them through adjacent fully martensitic material, small magnetic leakage fields result. The austenitic areas are therefore clearly defined when magnetic particle powder is applied, and any small flaws in or near these zones will be masked. The problem proved to be even more acute when an attempt was made to apply the testing technique to weld areas that were repaired by the TIG process. In such cases, each repair weld bead was outlined by fine but distinct powder adherence lines parallel to the repair bead progression sequence. Reliable delineation of a tight surface crack (or one just beneath the surface) under such conditions was questionable.

During the postfailure inspection of welds, eleven defect areas were found that had not been evident, or not rejectable, by the applicable standards prior to hydrotest. Of these defect areas, seven were found by UT, two by PT, and two by RT. It is not certain how many of these defects may have been present or how big they were during prehydrotest inspection. It is possible that some of the defects may have enlarged during pressurization or at burst so that they were more easily detectable in the posthydrotest inspection.

Four of the seven defects found by UT could not be discerned by RT. Two of the remaining three defect areas had such faint RT indications that preknowledge of the presence of the defect was required to locate the indication. These two flaws were not rejectable based on the film indications. A defect area found on W7/101 weld was detected by both UT and RT and will be discussed in more detail subsequently.

The two defects determined by PT could not be detected by other NDT

methods. One of these defects was removed by a light sanding indicating that it was a probable surface scratch.

Two defect areas were determined by RT on the W6/3 TIG weld (aft skirt). One of the defect areas also proved to be on the prehydrotest film, but it was so faint that preknowledge of its existence was necessary to locate it on the film. In the other defect area, which was not detected by NDT until after hydrotest, two defects 1/4- to 3/8-inch long were found under a TIG repair. The defects under the TIG repair to this TIG weld were the only known instances of thermal-shock cracking of a TIG weld in the welding program of the 260-SL-1 motor case.

In addition to the abovementioned defects, three other defects were found by RT that had been missed by the film interpreter on the original films taken before hydrotest. In all cases the flaws showed very faintly on the original film.

The most serious defect found in the posthydrotest NDT investigation was in the W7/101 weld beneath a TIG weld repair. This defect area was investigated by personnel from both the Newport News Shipbuilding and Dry Dock Company and the U. S. Naval Research Laboratory. Conflicting indications by RT and UT were given on the size and location of the defect. It was indicated by RT that the defect was a transverse crack located and oriented relative to the subarc and TIG welds similar to the black origin found on weld W7/302, but somewhat smaller. The UT investigation did not pick up the defect as well as RT, but indicated that the defect was not of rejectable size, in contrast to the large apparent size indicated by RT. A section of the motor case containing the defect was shipped to the U. S. Naval Research Laboratory. Again, UT was used to locate the suspected defect. A tensile specimen was cut with the apparent position of the defect in the middle of a 4-inch-wide test section. Instead of the failure originating at the defect indicated by UT, the failure originated from a defect that was displaced from the center of the specimen and not indicated by UT inspection at the Naval Research Laboratory, as shown in figure 13. The failure origin defect was approximately 0.6 inch long and 0.12 inch wide and similar in appearance to the clean origin in weld W7/302. After the tensile test, the radiograph was again examined and it was determined that the fracture origin had, indeed, been indicated on the radiograph, but it was not indicated by UT. The defect that was giving the UT response has not been found. In the section Nondestructive Testing Sensitivity Evaluation it is shown that, for fatigue-cracked specimens, UT is much more sensitive than RT for finding surface cracks. On first thought, it would therefore seem strange that the defect in the W7/101 weld was not indicated by UT as readily as it was by RT. A brief description of the mechanics of defect detection by UT will help clarify the reason for surface cracks to be detected more easily than submerged cracks.

Cracks that are approximately normal to the surface are detected by UT by transmission of pulsed waves of acoustic energy into the plate at an oblique angle, as illustrated rather idealistically in figure 17. When the transmitted wave intersects a defect, the wave is reflected. If this reflected wave returns to the transducer, the reflected signal can be observed on an oscilloscope. Figures 17(a) and (b) show that defects near the surface readily re-

flect the energy waves back to the transmitter. It is possible, however, for reflected waves from submerged defects to miss the transducer as illustrated in figure 17(c) so that the defect may not be detected. Reflections generally scatter much more than illustrated in figure 17, but the use of single transducers may not permit detection of all submerged defects in relatively thick plate. It appears that the defect in the W7/101 weld may have been missed for this reason. In addition, very tight cracks may not be detectable in all cases by UT. It has been determined that when accurately machined gage blocks are held closely together, the signal obtained from UT that indicates the discontinuity between the blocks is quite low. Very tight cracks are not detectable by RT either. It therefore appears possible to have submerged cracks of a type similar to the clean origin that may not be detectable by presently available nondestructive testing techniques.

The lessons learned from both the original and reinspection of weld areas before and after the hydrotest failure are: (1) reinspection of welds by NDT is required after aging as indicated by the number of defects that were found - at least some of which were present at the time of inspection prior to aging, but were not detected at that time; (2) all applicable NDT inspection techniques must be utilized since no single one is infallible, as indicated by the very carefully inspected defect in the W7/101 weld where conflicting information was obtained by RT and UT; and (3) it appears possible to have submerged defects within welds that are not detectable by NDT methods now available.

Nondestructive Testing Sensitivity Evaluation

No indication of the existence of either the clean or the black origin had been obtained from the nondestructive inspection of the W7/302 weld region that followed the experimental TIG repair welding. The TIG repair regions had been inspected by radiography on the day after the repairs were made, by dye penetrant 1 week and 19 weeks later, and ultrasonically 16 weeks after making the repairs. The procedures followed were those described earlier in the section Nondestructive Testing. These inspections were conducted before the aging heat treatment of the part, and no further inspection was conducted after aging, which was approximately 20 weeks after the TIG repairs were made on the W7/302 weld. Under these circumstances it was considered important to ascertain the sensitivity of radiographic (RT) and ultrasonic (UT) procedures for detecting cracks (as distinguished from the usual penetrameter or calibration notch sensitivities). For this purpose, five small test plates were prepared from motor case plate stock at the NASA Lewis Research Center. One of these plates was a blank, and each of the others was provided with a surface fatigue crack. The five plates were circulated for either RT or UT or both by each of the following organizations:

(a) Newport News Shipbuilding and Dry Dock Company (RT and UT)

(b) Sun Shipbuilding and Dry Dock Company (RT and UT)

(c) U. S. Naval Ordnance Laboratory (RT only)

(d) U. S. Naval Research Laboratory (UT only)

(e) NASA Lewis Research Center (UT only)

The test plates were each about 12 inches long, 3 inches wide, and 0.7 inch thick, and were aged at 900° F for 3 hours before fatigue cracking. The surface fatigue cracks were generated from small crack-starter notches, located at the centers of the plate faces, by repeated cantilever bending so that the nominal maximum fiber stress was approximately one-half the yield strength. The size of each crack was controlled by observing the length at the plate surface with a microscope mounted on a micrometer slide. After completion of fatigue cracking, the faces of the plates were ground to remove any trace of the starter notches. It was still possible, however, to detect the crack traces visually under proper illumination. The cracks were readily detectable by liquid penetrant or magnetic particle methods, and the test plates were not intended to be used for evaluating these methods.

After the plates had been circulated to all five participants for inspection, they were aged in air at 900° F for 1 hour with the object of heat tinting the crack surfaces. They were then cooled with liquid nitrogen and broken in tension to reveal the cracks, which are shown in figure 18. The purpose of cooling with liquid nitrogen was simply to enhance the brittleness of the fracture so that the cracks would be readily distinguishable in the photographs. These cracks are perpendicular to the long axes of the plates, extending into the plate thickness from the center of one face.

The dimensions of crack C (fig. 18) are about the same as those in the standard part-through-crack specimens used for evaluating toughness of test modules representing motor case material throughout the course of fabrication. Based on penetrameter and calibration notch sensitivities, it was assumed that cracks of this size and larger would be detectable with a high degree of confidence by the inspection procedures. To provide some indication of the relative severities of the cracks in the test panels, the calculated fracture stresses for a K_{Ic} fracture toughness of 50 000 psi$\sqrt{\text{in.}}$ are 210 000 psi for B, 180 000 psi for C, 147 000 psi for D, and 105 000 psi for E. For other K_{Ic} values the fracture stresses would be proportionate.

The results of the cooperative inspection program did not justify the confidence that had been placed in the ability of RT and UT to detect cracks. None of the radiographs obtained by the three organizations that used this method showed a rejectable indication of any of the cracks. In two cases, faint indications of what appeared to be a crack were discernable in the correct location in plate E, but it is doubtful that these indications would have been noticed in the normal course of the radiographic inspection procedure. The report by Newport News stressed the point that, under no circumstances, could the indication that they obtained for plate E be construed as a rejectable radiographic indication.

The ultrasonic methods proved to be somewhat more successful in detecting the cracks. The two shipbuilding companies and the U. S. Naval Research Laboratory employed ultrasonic testing at a level of sensitivity equivalent to that

specified for the inspection of the motor case. This specified level of sensitivity was limited by the need to keep indications reflected from the weld centerline grain structure to a reasonably low level. As a matter of interest, the U. S. Naval Research Laboratory repeated their inspection of the test plates at a higher level of sensitivity, and the NASA Lewis Research Center also inspected the plates with experimental equipment of high sensitivity that was designed for research studies of fatigue crack growth. These high sensitivity methods employed 5-megacycle crystals. In both cases, all the cracks were detected by the high-sensitivity equipment, but it would be unwise to assume that this sensitivity could always be put to practical use in shop testing of weld regions.

The three participants that used ultrasonic inspection at the sensitivity level employed during motor case fabrication all detected crack E as a rejectable defect. Crack D was reported as rejectable by one participant, not rejectable by another, and not detected by the third. Cracks B and C were reported as not rejectable by one participant and not detected by the other two. Thus, the ultrasonic method at the specified sensitivity appears to be reliable for detecting cracks of size E and larger, but doubtful for cracks of smaller size. Since the clean and black fracture origins were both larger than crack E, the question of why these origins were not discovered by UT inspection is still not resolved. If the origins existed as definite discontinuities at the time the UT was conducted, the gaps between their mating surfaces must have been considerably less than the gaps between the surfaces of the fatigue cracks in the test plates. Since the clean origin was entirely subsurface and the black origin almost entirely so, the possibility cannot be dismissed that they were present in the form of very tight cracks at the time of the UT inspection.

The results of this nondestructive testing sensitivity evaluation program were somewhat confounded by the inspections of the defect in the W7/101 weld discussed in the section Reinspection of Weld Areas After Hydrotest Failure. This defect is shown in figure 13, near one edge of the fracture surface of the tension specimen taken longitudinally from the weld region. The defect is about 0.6 inch long and 0.12 inch wide - somewhat larger than the crack in test plate E. It is actually located near the centerline of the subarc weld, but that weld was close to the edge of the 4-inch-wide test section of the tension specimen. The defect is closer to the outer surface than to the inner surface of the weld, and there were two TIG weld repair areas on the outer surface that intersected at the position of the defect.

Of the radiographs taken of this region after the hydrotest failure, two taken with the source on the outer side of the weld showed the defect distinctly, but a third, taken from the other side of the weld, showed only a vague indication. Radiographs taken in August and September of 1964, prior to the hydrotest, showed no indication in this region. As mentioned earlier, the UT examinations conducted after the hydrotest did not give indications of rejectable size.

The fact that this defect was detected by RT after the hydrotest failure, but was not detected some months earlier by the same means, should be considered in relation to the fact that the somewhat smaller crack in test plate E could not be detected definitely by radiography, although it was unquestionably

present. The most reasonable explanation would seem to be that the sensitivity of radiography for detecting cracks depends very strongly on the gaps between the crack faces as well as crack orientation. Between prehydrotest and post-hydrotest inspection there must have been an increase in the size of the gap in the defect in the W7/101 weld sufficient to make it detectable.

The main conclusion to be drawn from this minimal, exploratory program of evaluation of nondestructive inspection sensitivity is that there is a serious and urgent need for a much more comprehensive evaluation program.

SUMMARY OF FINDINGS

The significant findings from the hydrotest failure of the Thiokol Chemical Corporation 260-inch-diameter motor case can be summarized as follows:

1. The failure originated from an undetected defect in a region of the heat-affected zone of the W7/302 longitudinal weld that had been covered by a manual TIG repair weld. The defect, which was submerged within the vessel wall and oriented longitudinally, was approximately 1.4-inches long and had a width of about 0.10 inch.

2. A second undetected defect associated with the W7/302 weld was involved as a secondary fracture origin. This defect was also located beneath a TIG repair weld. It was somewhat larger than the primary origin, but was oriented transversely so that the nominal stress acting across it was only about one-half that acting across the primary origin. In the absence of the primary origin, fracture might have originated from this secondary origin at a pressure closer to the intended proof pressure.

3. Three other undetected defects were discovered under manual TIG repair welds when the weld regions were reinspected by nondestructive test methods after the failure. One of these defects was transverse to the W7/101 subarc weld. A large tension specimen that was tested to determine the severity of this defect fractured at a gross stress of 115 000 psi. The other two defects of substantial size were submerged under a TIG weld repair to the W6/3 TIG weld.

4. The association of severe defects with four separate TIG weld repair regions strongly suggests that the formation of these defects was a consequence of the TIG repair welding over a grain-coarsened material structure resulting from the high thermal input of the welding processes used. The detailed mechanism of formation of the defects has not been established because an extensive research program would probably be required for this purpose.

5. The fracture toughness of the submerged arc welds in this 250 grade maraging steel motor case was inadequate to tolerate crack-like defects as large as those that actually occurred in the motor case. It had been believed previously that much smaller defects could be detected with high reliability by the nondestructive inspection procedures that were used. The fracture toughness would have been sufficient to tolerate defects of a size that had been considered to be detectable.

6. Because none of the critical defects had been discovered by nondestructive testing prior to the hydrotest, a limited investigation was undertaken to ascertain the sensitivity of radiographic and ultrasonic procedures in detecting cracks. The results of this study showed that the NDT methods as used in motor case inspection are much less sensitive and reliable than had been expected, and that there is more to be learned about nondestructive inspection for the detection of cracks. The criticality of the sensitivity of inspection depends, of course, on the toughness of the materials involved. In the present state-of-the-art, the materials and welding processes selected should provide the highest attainable toughness consistent with the requirements of the application. In general, the tougher materials will be among those that have the lower yield strengths consistent with the requirements of the application. The sensitivity of the nondestructive inspection procedures should be evaluated for any specific application in relation to the toughness of the materials used.

7. For new motor case projects it is recommended that the sensitivity of the selected nondestructive testing procedures be thoroughly evaluated to determine if defects of a critical size for the design loads and materials used can be detected with confidence.

8. There is a possibility that the defects that were not detected during the inspection of the motor case prior to aging might have been detected if the motor case had been reinspected just before hydrotest. The aging heat treatment may have caused the defects to "open up" and thus become more detectable. It is therefore recommended that pressure vessels that are to be hydrotested should be thoroughly inspected immediately prior to the hydrotest, regardless of any previous inspections that may have been performed.

9. There is no evidence that any external factors or inadvertent loads contributed to the failure. It was a straightforward example of the weakening of a structure by a severe flaw.

Lewis Research Center,
National Aeronautics and Space Administration,
Cleveland, Ohio, October 19, 1965.

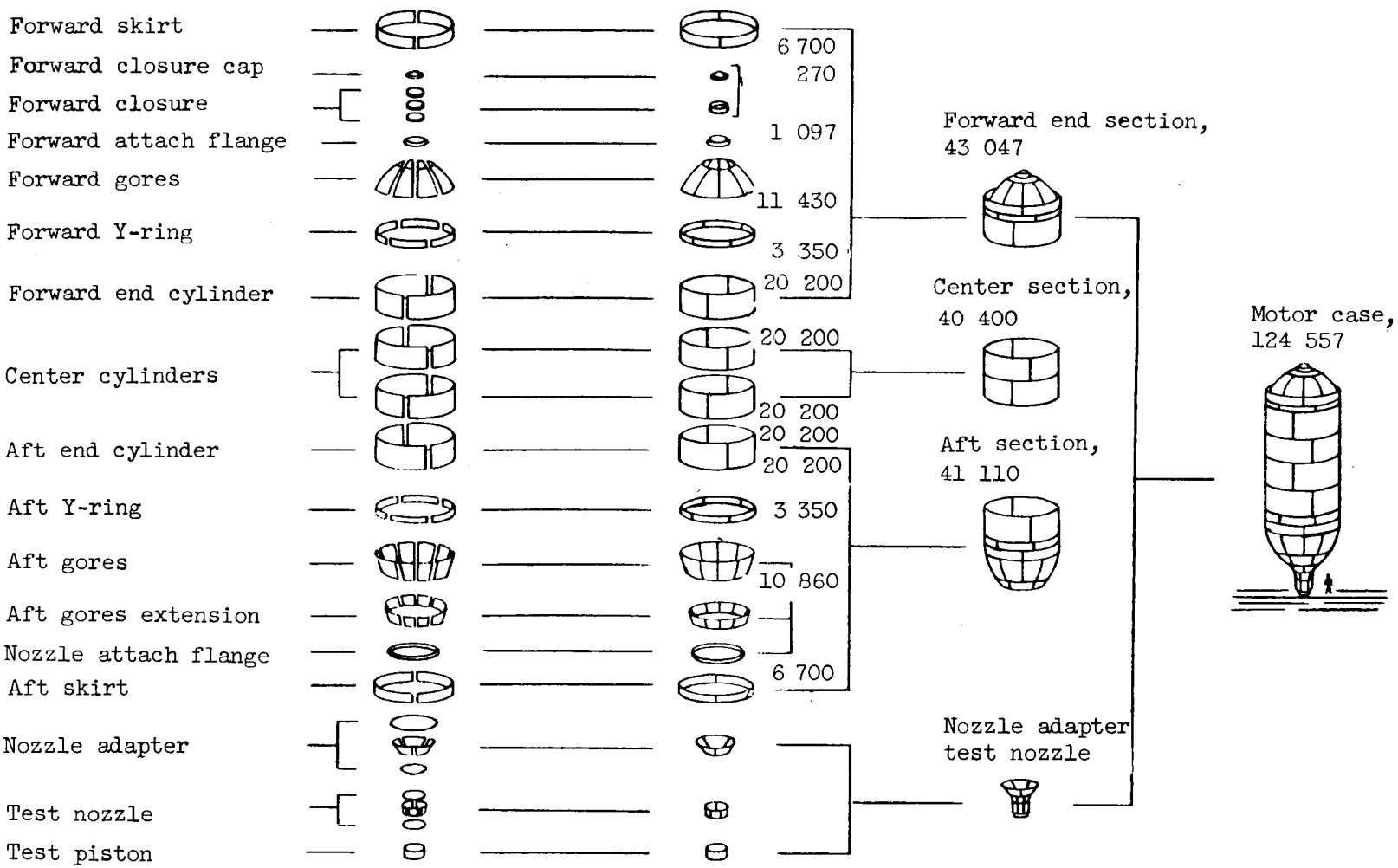


Figure 1. - Fabrication sequence for 260-inch-diameter solid-fuel rocket motor case. (All values are weight in pounds.

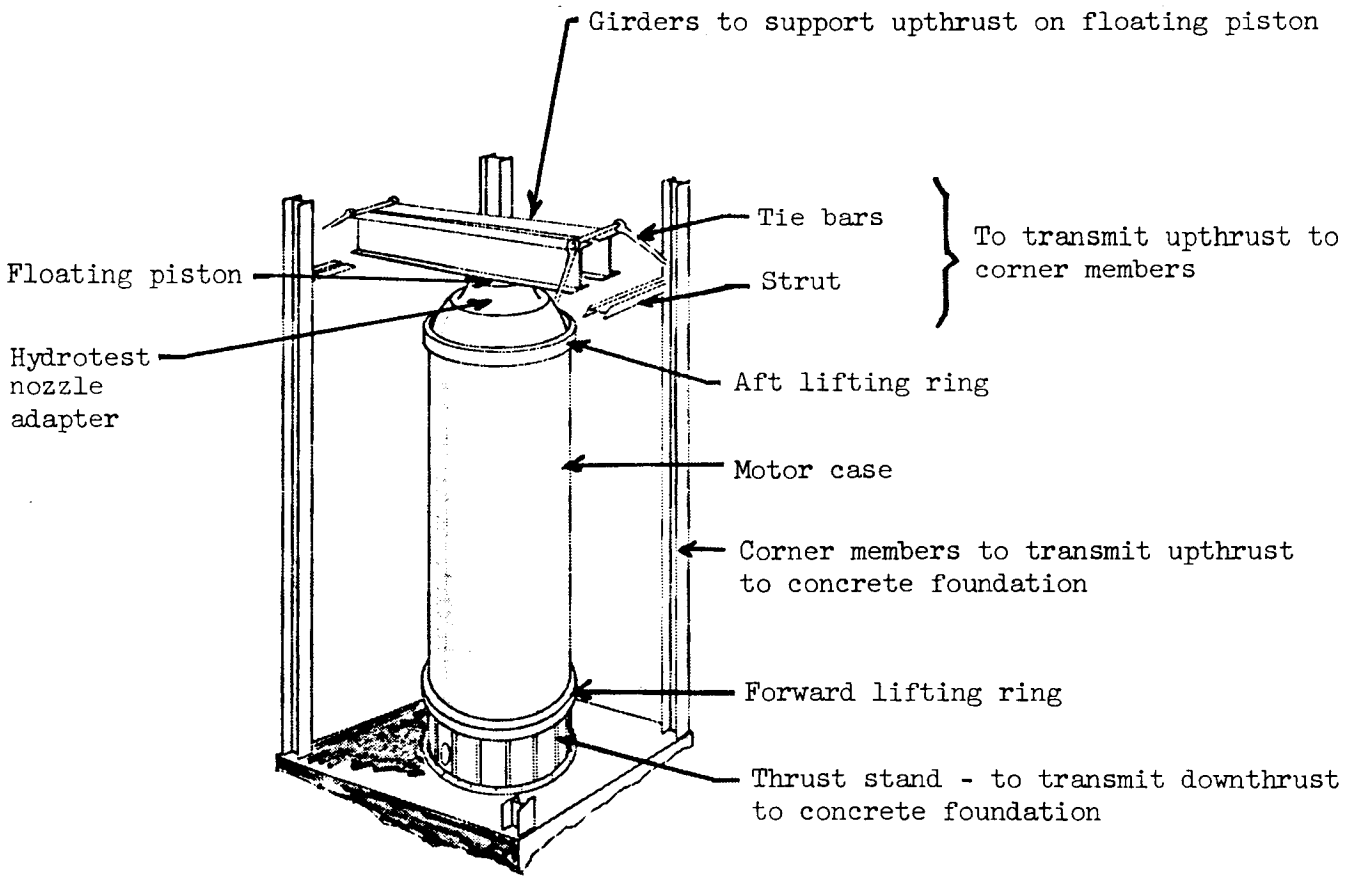


Figure 2. - Motor case installation in hydrotest tower.

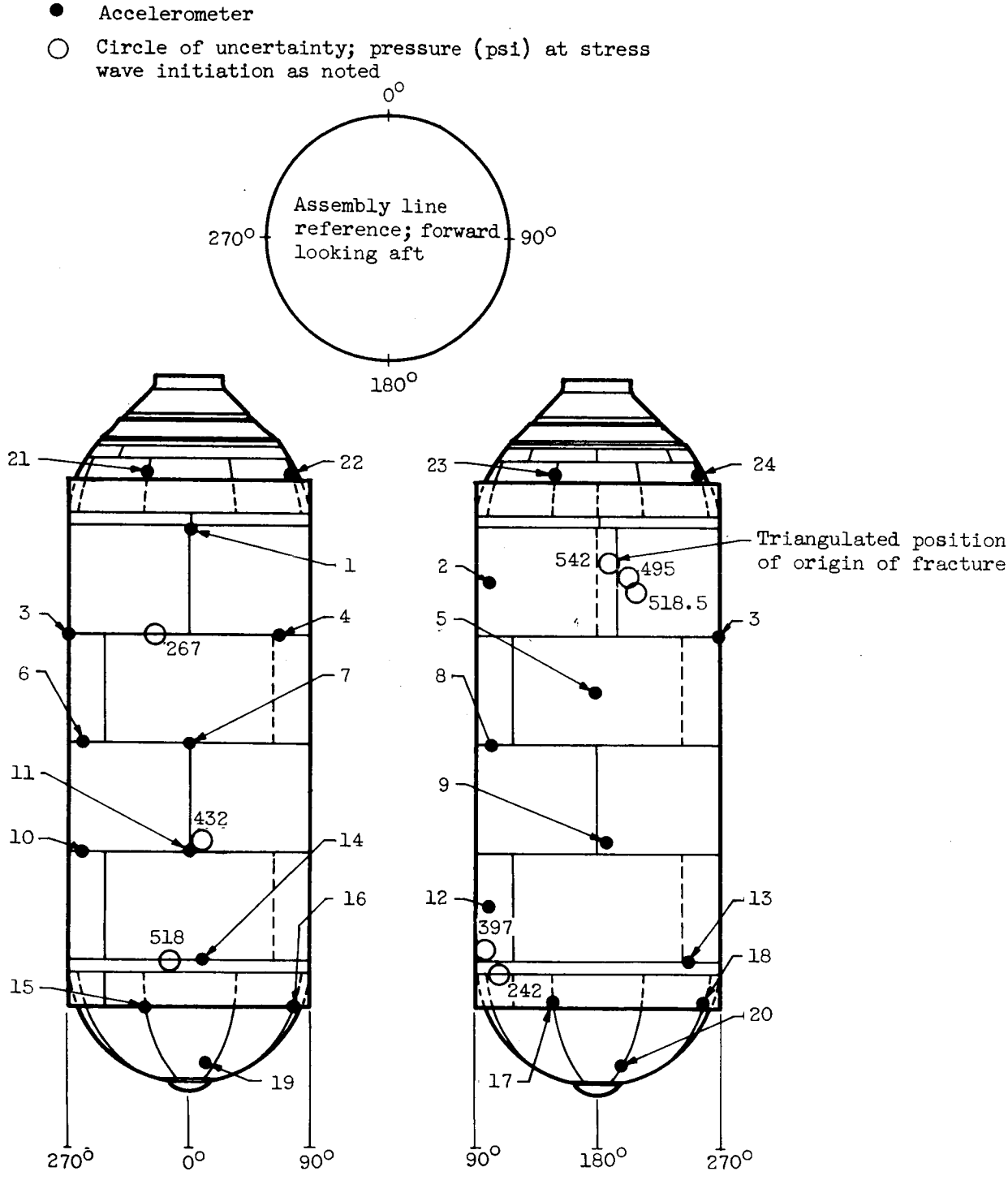


Figure 3. - Locations of accelerometers and stress wave origins on 260-inch-diameter SL-1 motor case.

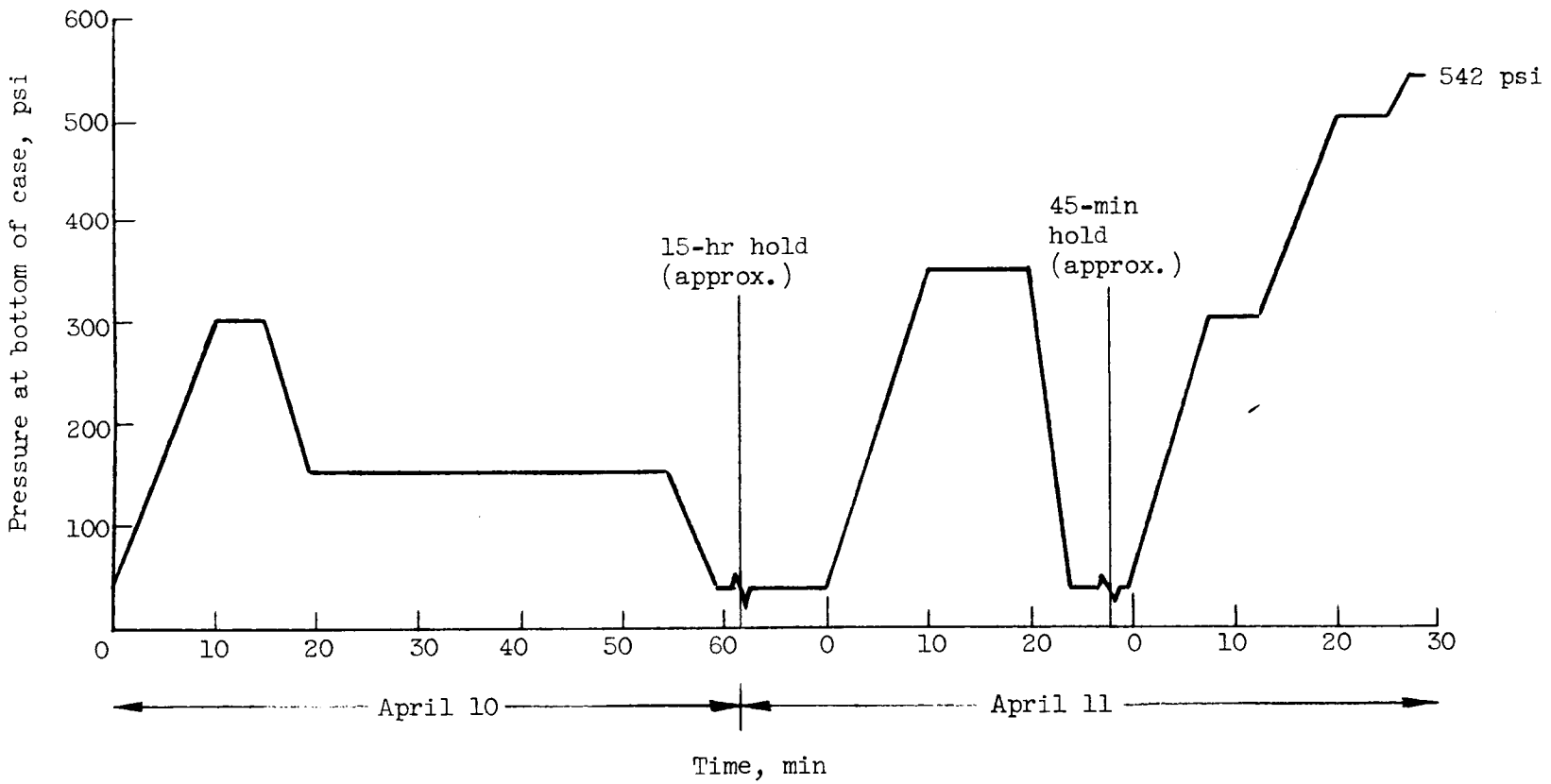


Figure 4. - Pressure-time history during hydrotest.



Figure 5. - Portion of failed motor case as it was being removed from hydrotest tower.

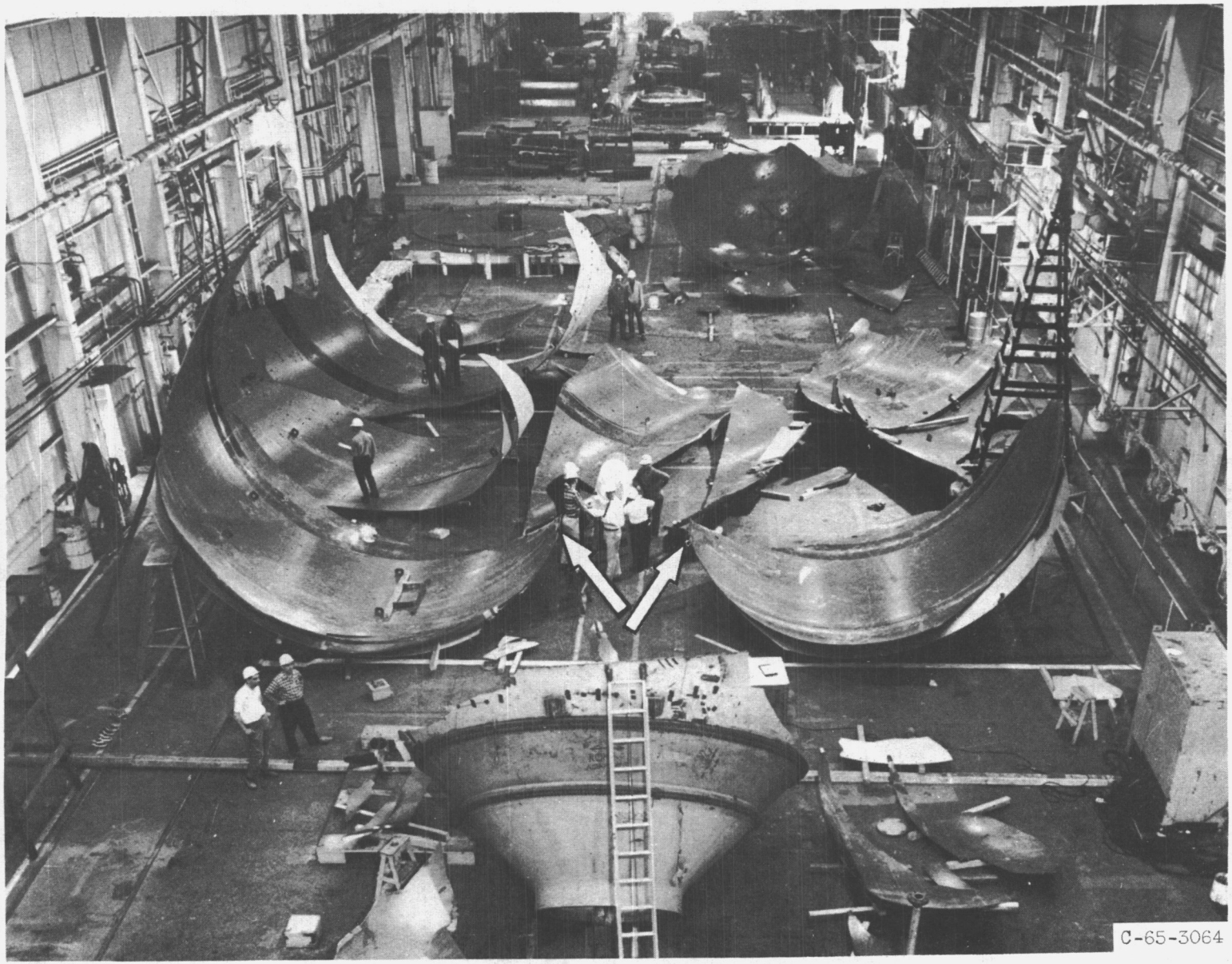
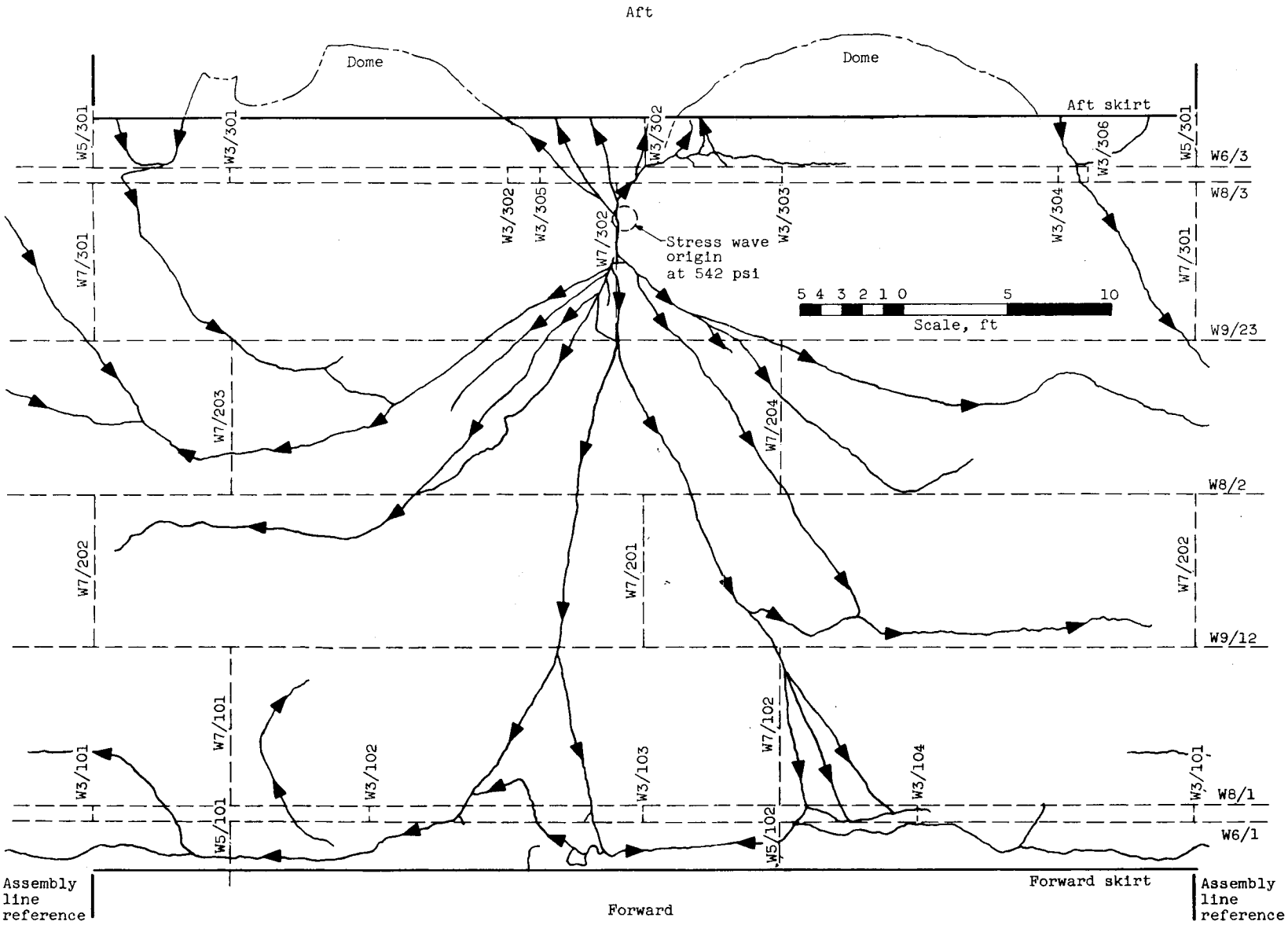
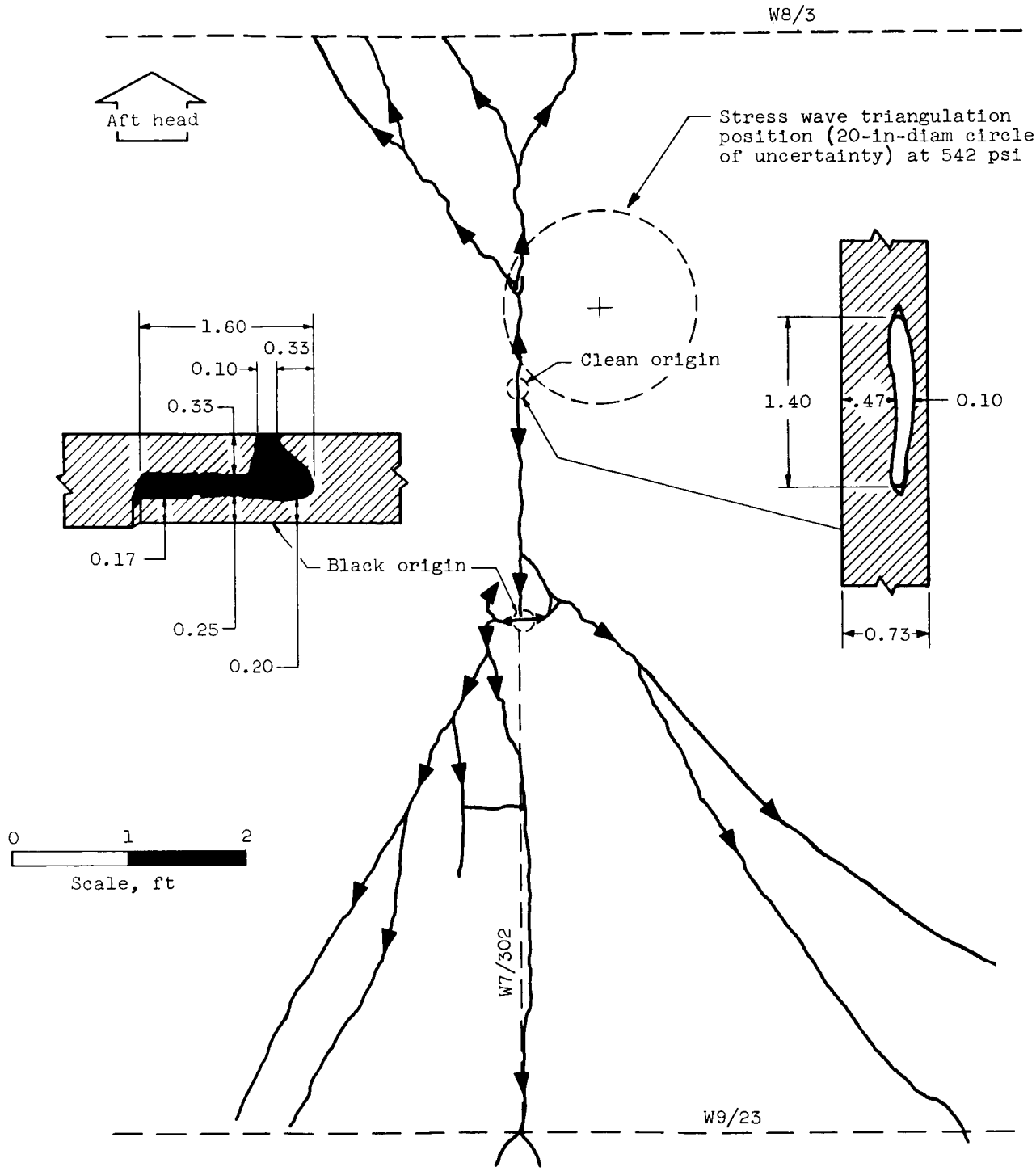


Figure 6. - Failed motor case with pieces laid out in approximately the proper relation to each other. View is looking forward with aft head in foreground. Origin of fracture indicated by arrows.



(a) Cylinder and skirts.

Figure 7. - Map of fracture paths as viewed when looking at inside surface developed onto plane obtained by unrolling cylinder. Arrowheads indicate directions of fracture propagation.



(b) Detail in immediate vicinity of primary and secondary origins. Inset sketches show shapes and dimensions of the two origins.

Figure 7. - Concluded.



Figure 8. - Typical chevron markings on fracture surface showing directions of fracture propagation away from black origin.

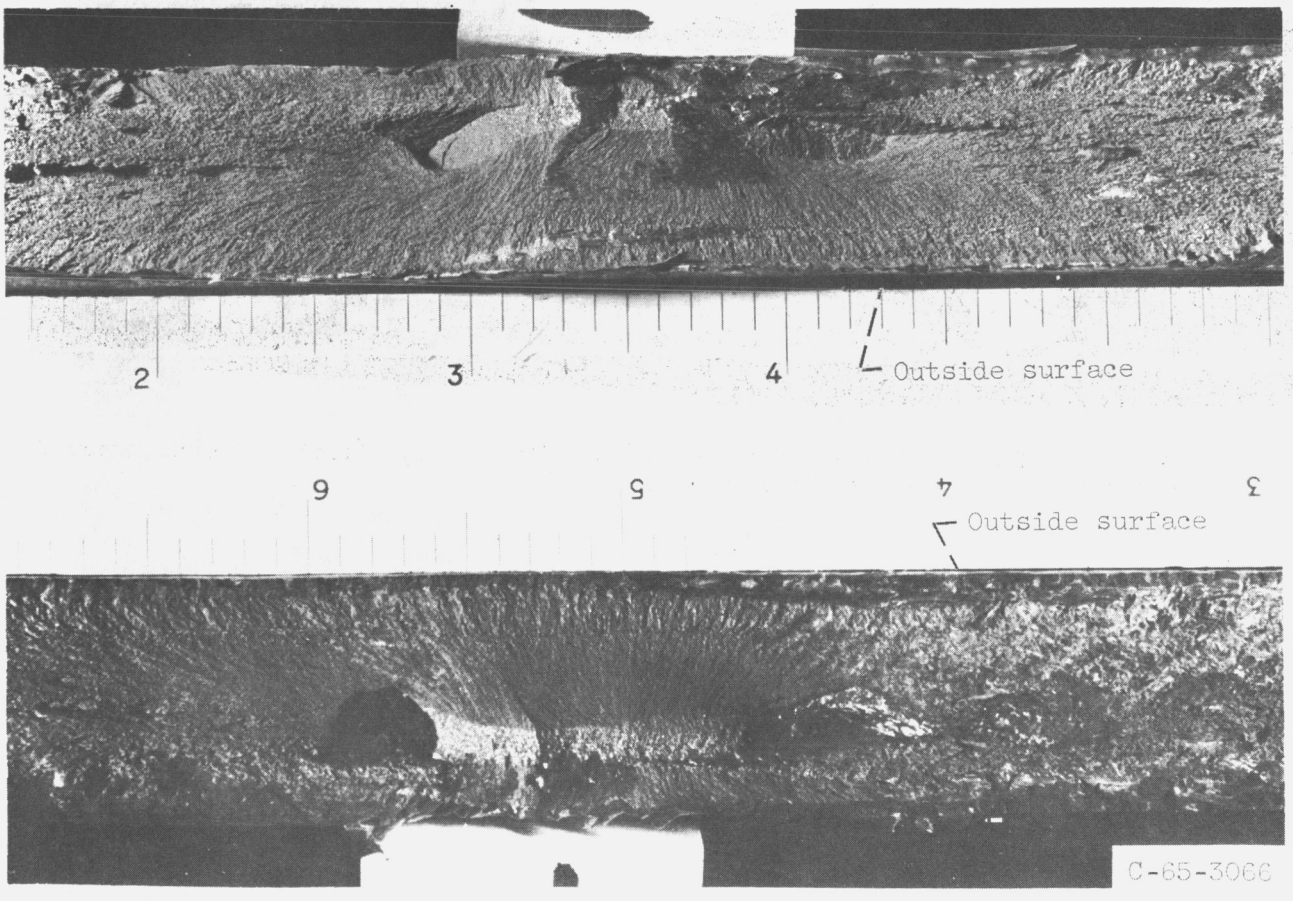


Figure 9. - Mating surfaces of clean origin on W7/302 weld.

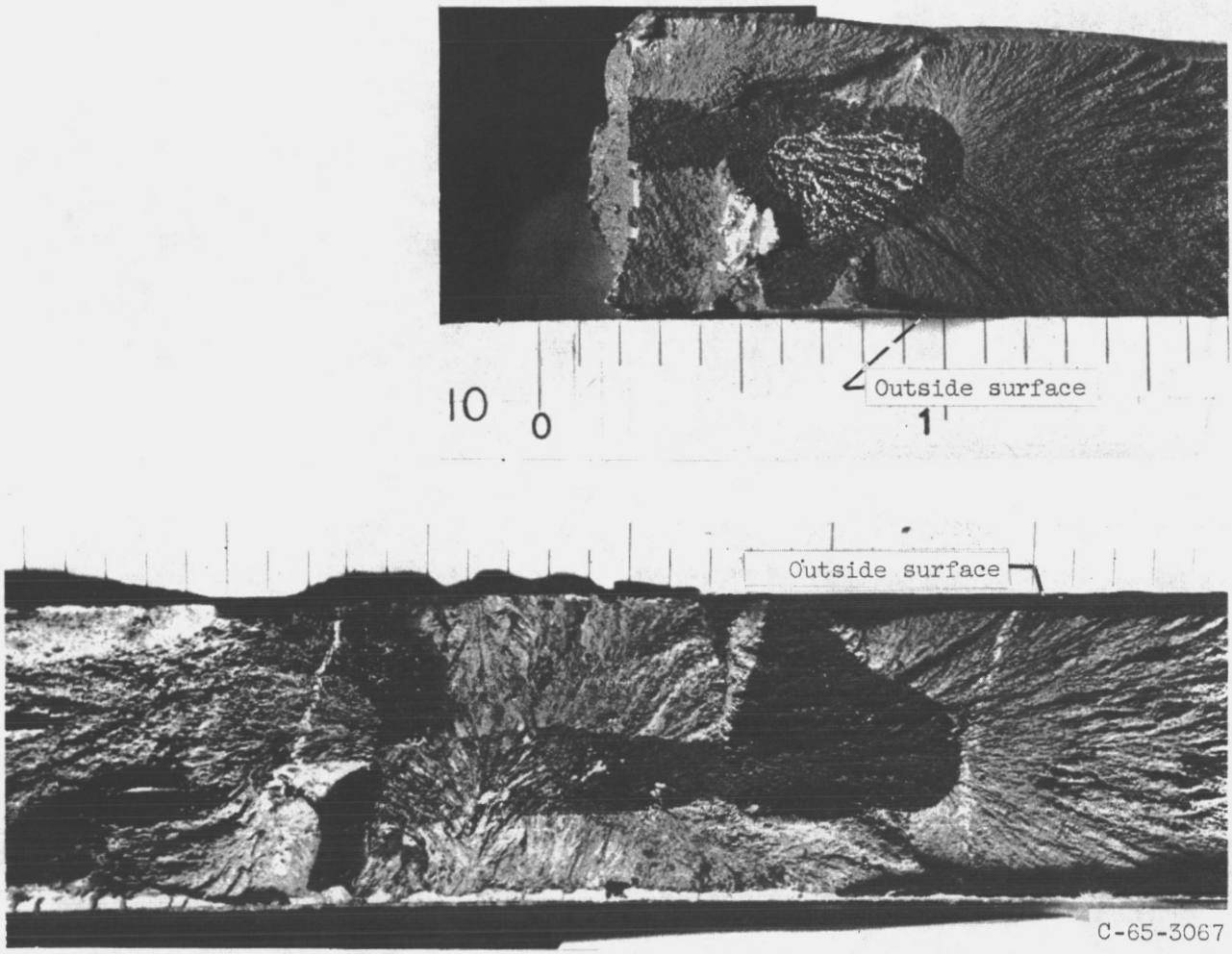


Figure 10. - Mating surfaces of black origin on W7/302 weld. (Part of black material has been removed from one surface for analysis.)

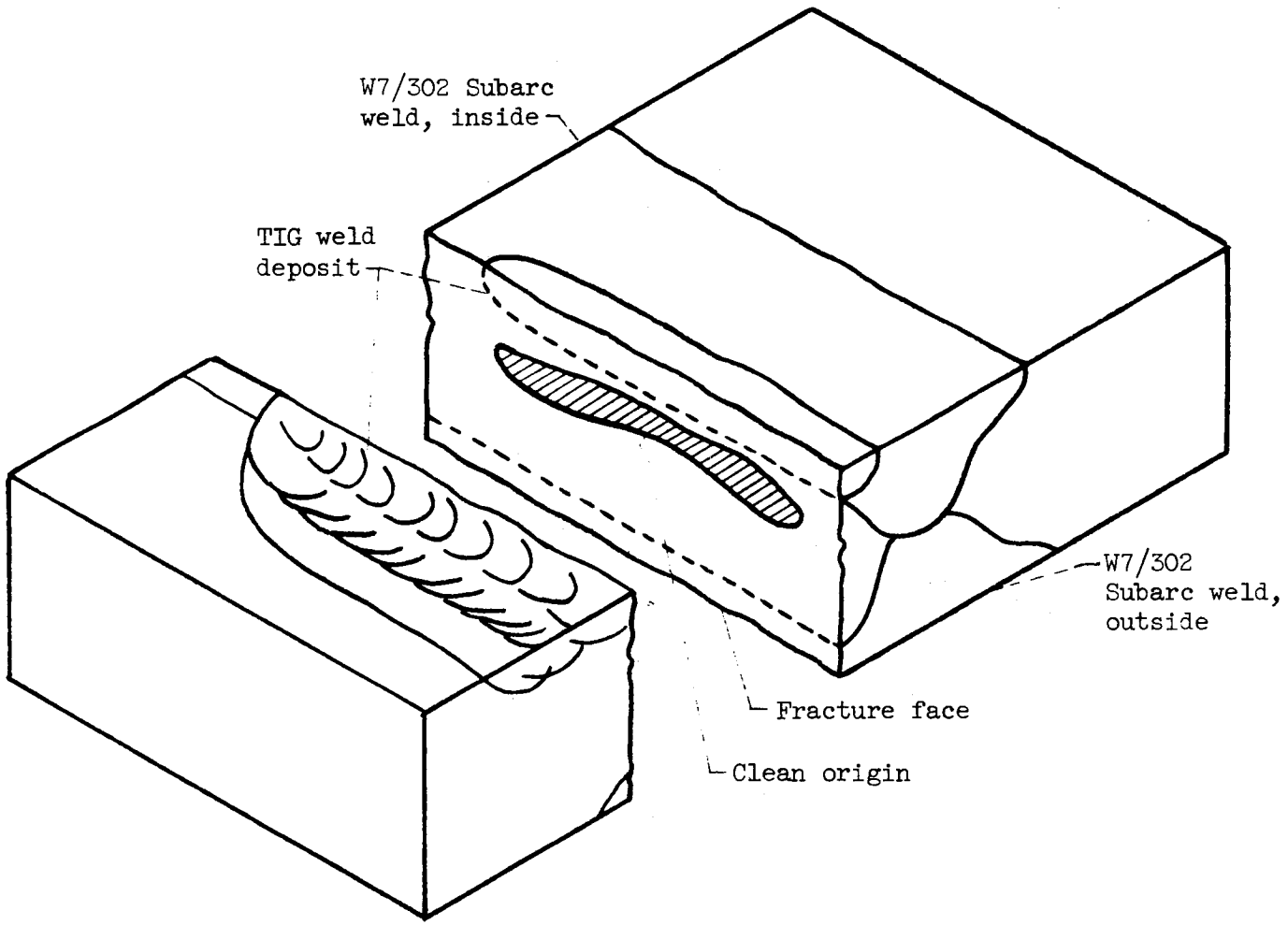


Figure 11. - Isometric drawing showing relation of clean origin to weld deposits.

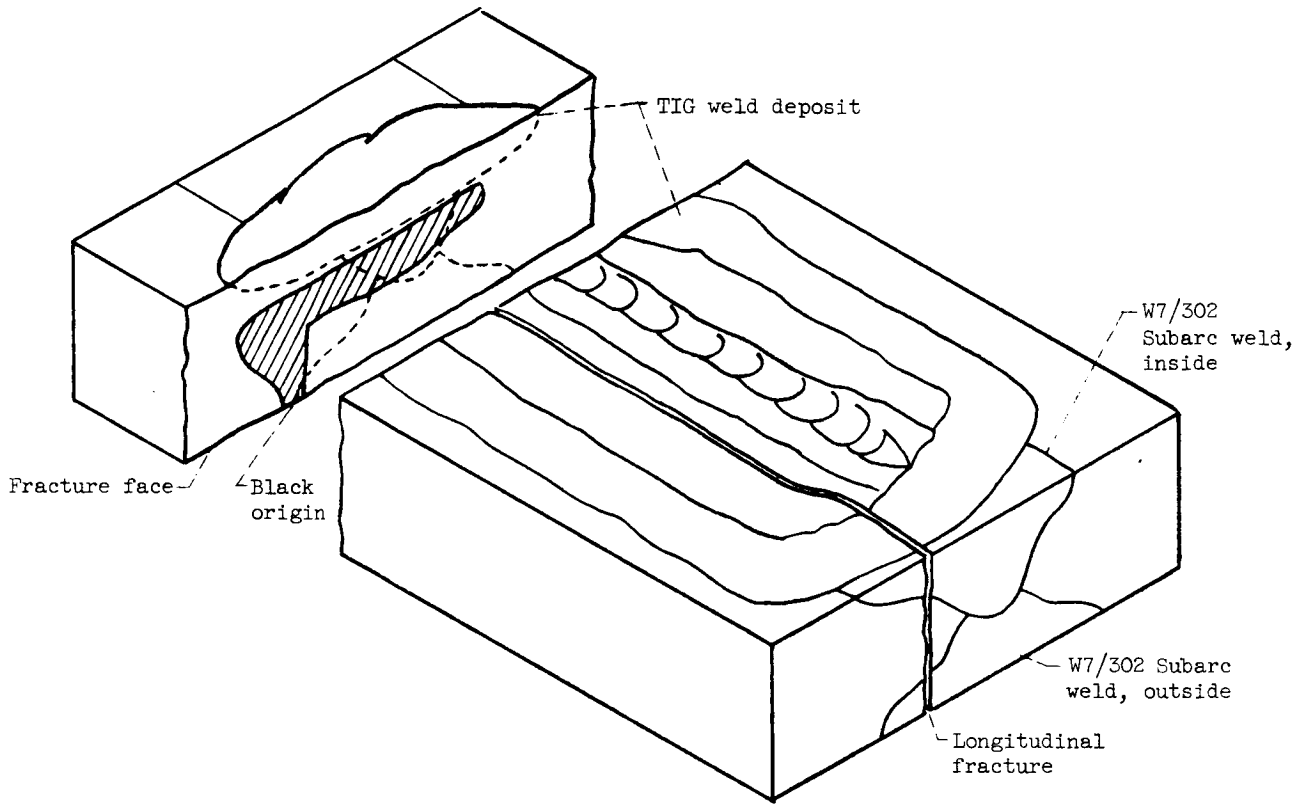


Figure 12. - Isometric drawing showing relation of black origin to weld deposits.

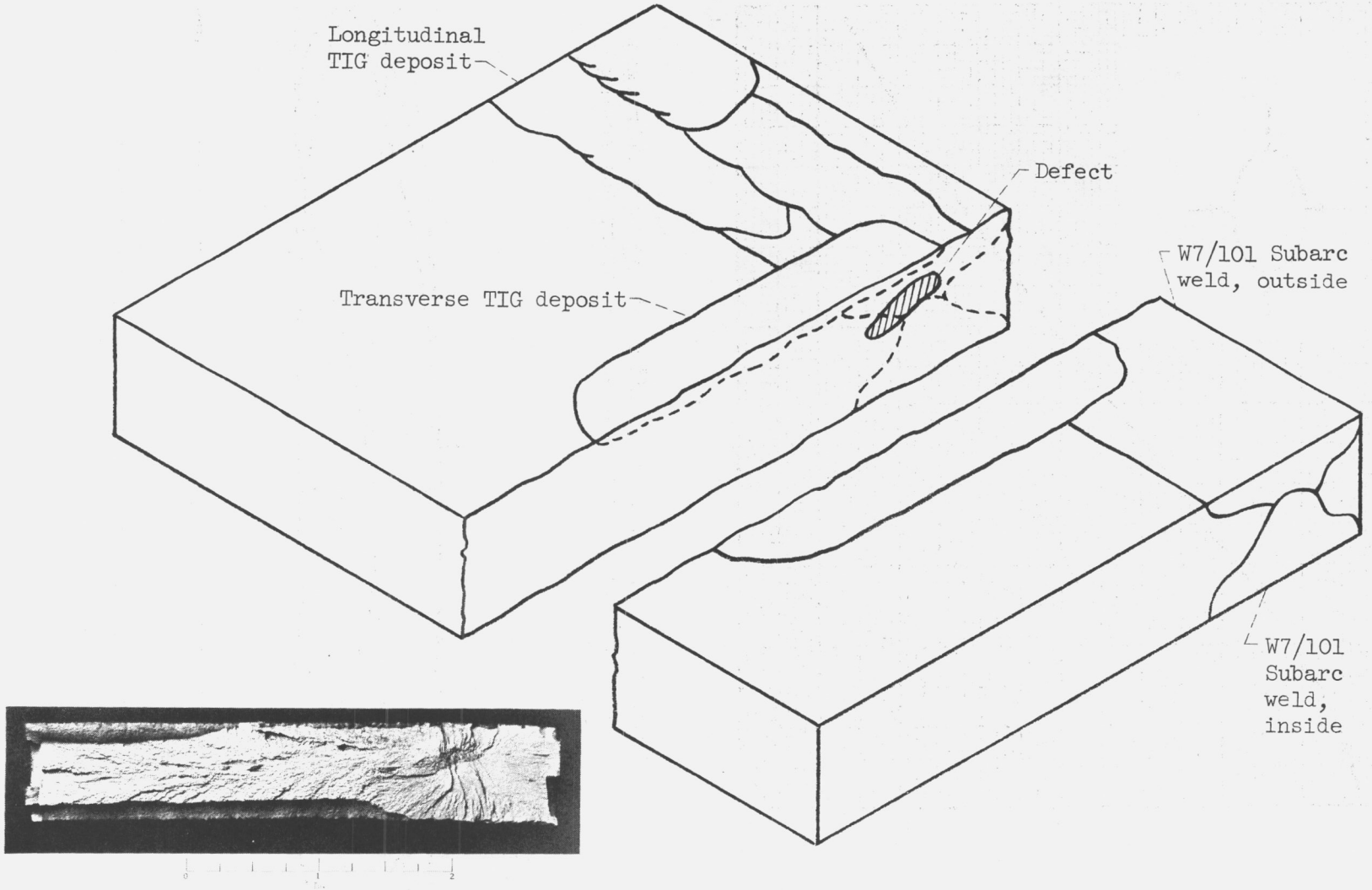


Figure 13. - Isometric drawing and photograph of fracture surface of longitudinal tension specimen from W7/101 weld region showing defect related to weld deposits.

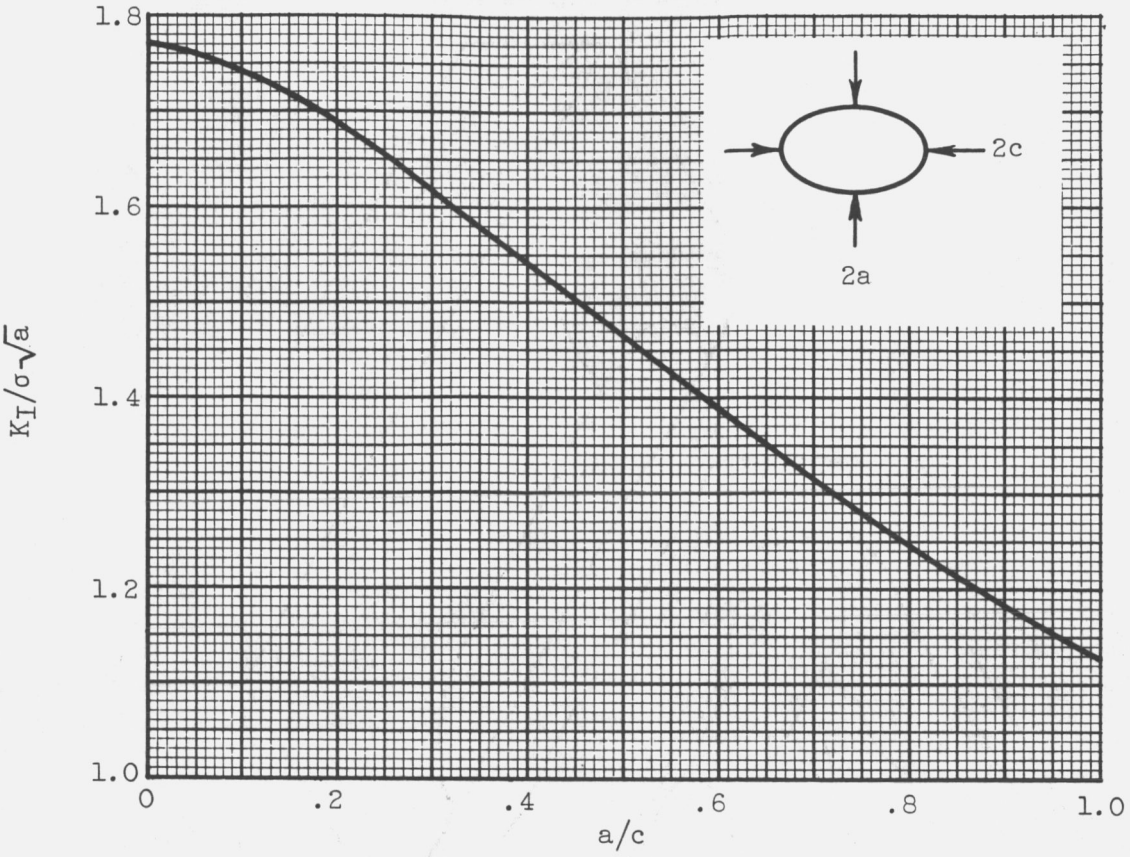


Figure 14. - Plot for calculation of K_I for submerged elliptical crack where σ is nominal stress acting across crack.

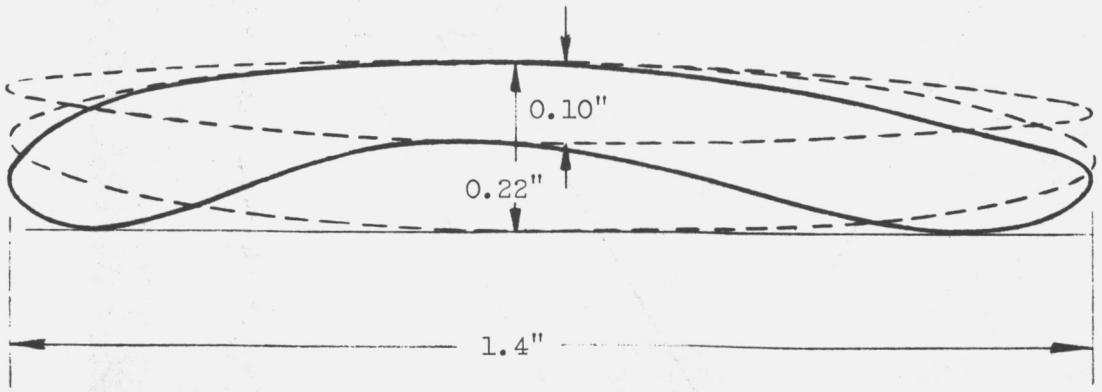


Figure 15. - Ellipses used to calculate upper and lower bounds of K_I for clean origin.

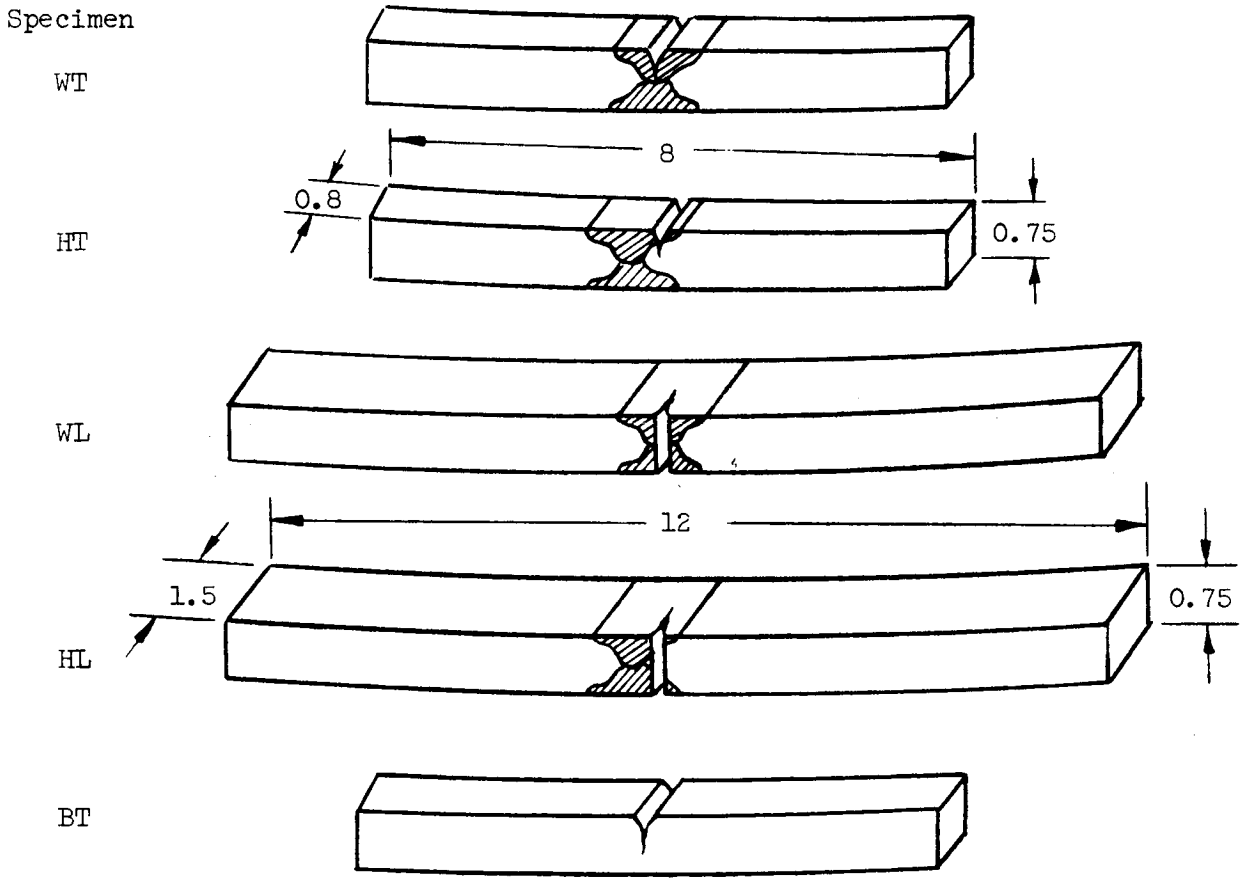
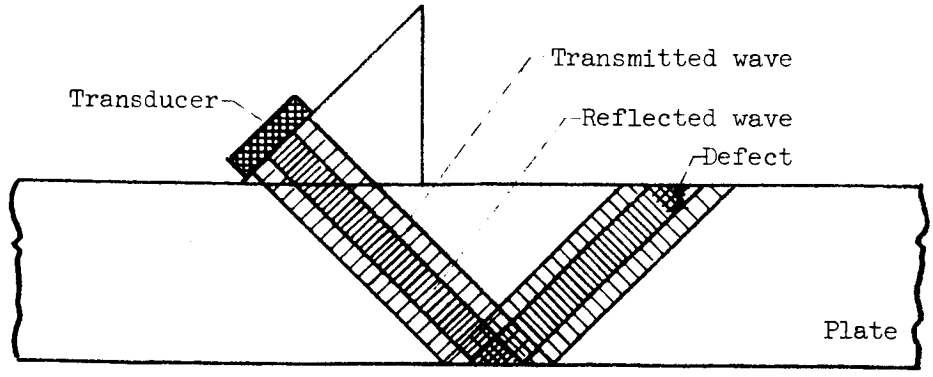
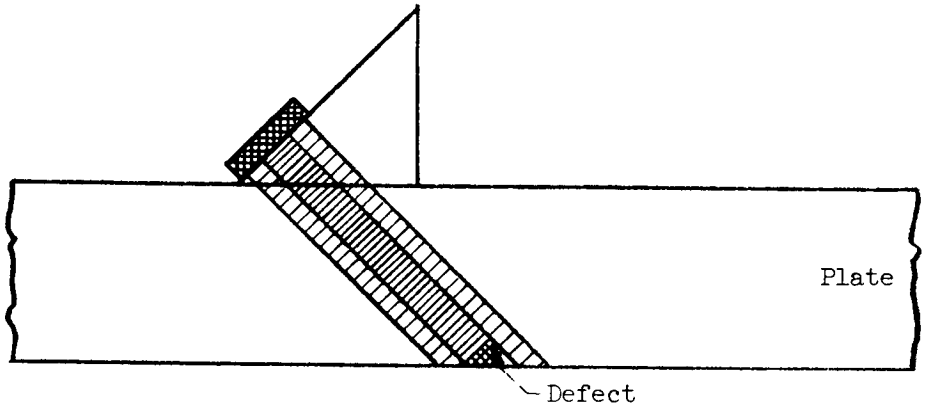


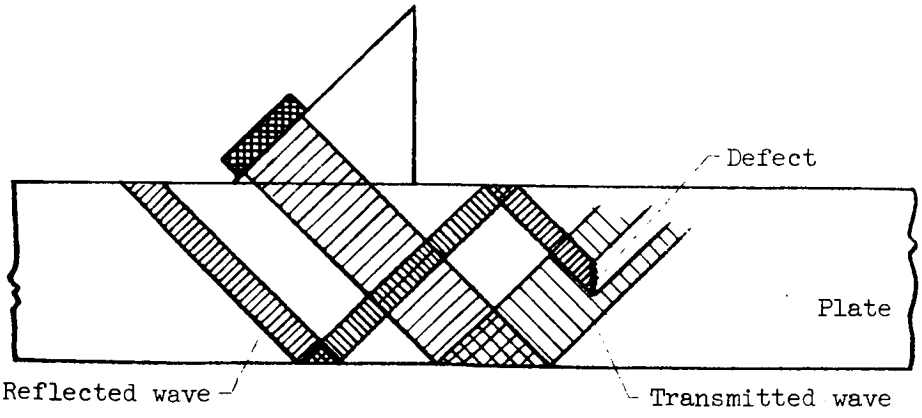
Figure 16. - Types of specimens used for K_{Ic} bend tests. Widths and thicknesses shown are nominal.



(a) Defect on same surface as transducer.

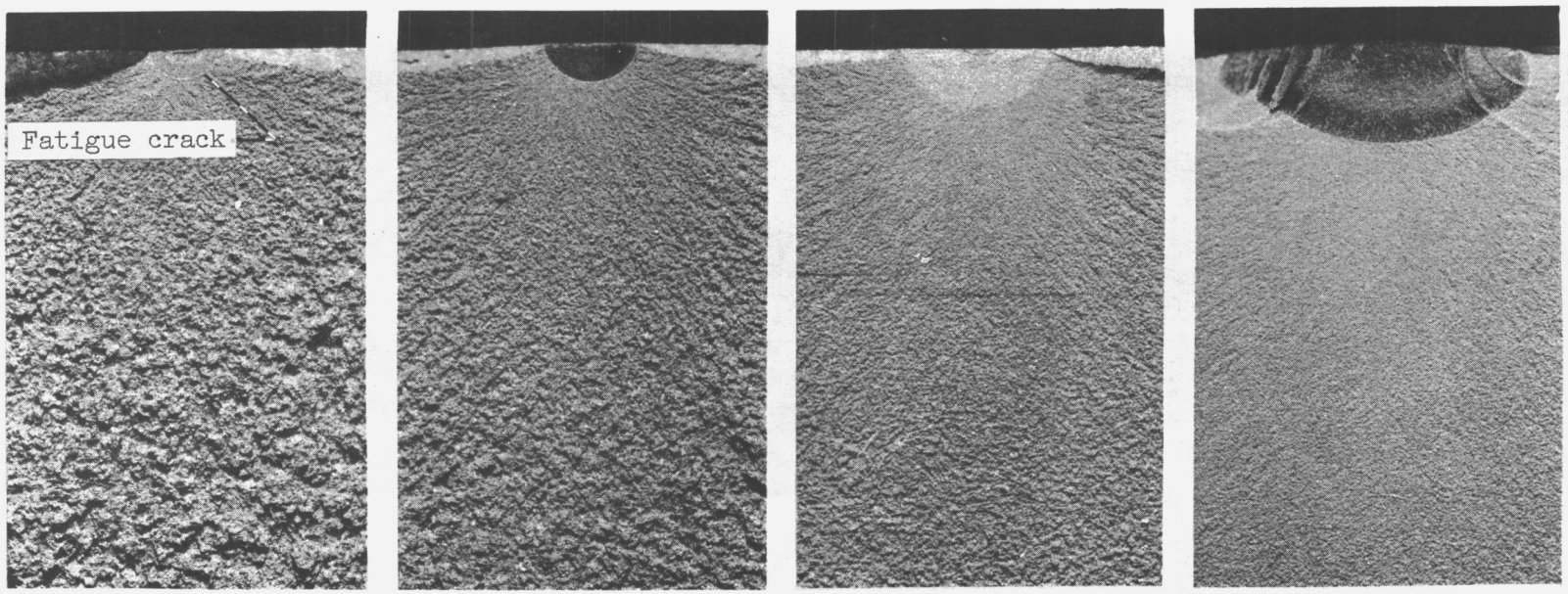


(b) Defect on surface opposite to transducer.



(c) Defect submerged within plate.

Figure 17. - Effect of defect location on detectability by ultrasonic techniques.



Specimen:	B	C	D	E
Fatigue crack depth, in.:	0.030	0.041	0.063	0.106
Fatigue crack surface length, in.:	0.075	0.100	0.155	0.309
Thickness, in.:	0.743	0.747	0.713	0.737

C-65-1147

Figure 18. - Fatigue cracks in test plates for nondestructive inspection evaluation program. ×5. (Specimen A had no fatigue cracks.)

FINAL REPORT DISTRIBUTION LIST

SOLID ROCKET TECHNOLOGY

NASA Lewis Research Center
21000 Brookpark Road
Cleveland, Ohio 44135
Attn: Contracting Officer
Mail Stop 500-313 (1)
Solid Rocket Technology Branch
Mail Stop 500-205 (8)
Technical Library
Mail Stop 60-3 (2)
Tech. Report Control Office
Mail Stop 5-5 (1)
W. E. Roberts
Mail Stop 3-17 (1)

National Aeronautics and
Space Administration
Washington, D. C. 20546
Attn: RPM/William Cohen (3)
RPS/Robert W. Ziem (1)
ATSS-AL/Technical Library (2)

NASA Western Support Office
150 Pico Boulevard
Santa Monica, California 90406
Attn: Eugene F. Wyszpolski (1)
Harry Williams (1)

NASA Ames Research Center
Moffett Field, California 94035
Attn: Technical Library (1)

NASA Langley Research Center
Langley Station
Hampton, Virginia 23365
Attn: Robert L. Swain (1)
Technical Library (1)

NASA Goddard Space Flight Center
Greenbelt, Maryland 20771
Attn: Technical Library (1)

NASA Manned Spacecraft Center
2101 Webster Seabrook Road
Houston, Texas 77058
Attn: Technical Library (1)

NASA George C. Marshall Space
Flight Center
Redstone Arsenal
Huntsville, Alabama 35812
Attn: Technical Library (1)
R-P&VE-PA/K. Chandler (1)

Jet Propulsion Laboratory
California Institute of Technology
4800 Oak Grove Drive
Pasadena, California 91103
Attn: Richard Bailey (1)
Technical Library (1)

Scientific and Technical Information
Facility
NASA Representative
Post Office Box 33
College Park, Maryland 20740
Attn: CRT (1)

GOVERNMENT INSTALLATIONS

AF Space Systems Division
Air Force Unit Post Office
Los Angeles, California 90045 (1)
Attn: Col. E. Fink

AF Research and Technology Division
Bolling AFB, D. C. 20332
Attn: Dr. Leon Green, Jr. (1)

AF Rocket Propulsion Laboratory
Edwards AFB, California 93523
Attn: Norman Hirsch (1)
RPM/Col. R. Harned (2)

AF Materials Laboratory
Wright-Patterson AFB, Ohio 45433
Attn: MANC/D. Schmidt (1)
MAAE (1)

AF Ballistic Missile Division
Post Office Box 262
San Bernardino, California
Attn: WDSOT (1)

Structures Division
Wright Patterson AFB, Ohio 45433
Attn: FDT/R. F. Hoener (1)

Army Missile Command
Redstone Scientific Information Ctr.
Redstone Arsenal, Alabama 35809
Attn: Chief, Document Section (1)

Ballistic Research Laboratory
Aberdeen Proving Ground,
Maryland 21005
Attn: Technical Library (1)

Picatinny Arsenal
Dover, New Jersey 07801
Attn: Technical Library (1)

Navy Special Projects Office
Washington, D. C. 20360
Attn: H. Bernstein (1)

Naval Air Systems Command
Washington, D. C. 20360
Attn: AIR-330/Dr. O. H. Johnson (1)

Naval Propellant Plant
Indian Head, Maryland 20640
Attn: Technical Library (1)

Naval Ordnance Laboratory
White Oak
Silver Spring, Maryland 20910
Attn: Technical Library (1)

Naval Ordnance Test Station
China Lake, California 93557
Attn: Edward W. Price (1)
Technical Library (1)
C. J. Thelen (1)

Naval Research Laboratory
Washington, D. C. 20390
Attn: Technical Library (1)

Chemical Propulsion Information
Agency
Applied Physics Laboratory
8621 Georgia Avenue
Silver Spring, Maryland 20910 (1)

Defense Documentation Center
Cameron Station
5010 Duke Street
Alexandria, Virginia 22314 (1)

Defense Materials Information
Center
Battelle Memorial Institute
505 King Avenue
Columbus, Ohio 43201 (1)

Materials Advisory Board
National Academy of Science
2101 Constitution Avenue, N. W.
Washington, D. C. 20418
Attn: Capt. A. M. Blamphin (1)

Institute for Defense Analyses
1666 Connecticut Avenue, N. W.
Washington, D. C.
Attn: Technical Library (1)

Advanced Research Projects Agency
Pentagon, Room 3D154
Washington, D. C. 20301
Attn: Technical Information Office (1)

INDUSTRY CONTRACTORS

Aerojet-General Corporation
Post Office Box 1168
Solid Rocket Plant
Sacramento, California 94086
Attn: Dr. B. Simmons (1)
Technical Information Ctr. (1)

Aerojet-General Corporation
Post Office Box 296
Azusa, California 91702
Attn: Technical Library (1)

Aerospace Corporation
2400 East El Segundo Boulevard
El Segundo, California 90245
Attn: Technical Library (1)
Solid Motor Dev. Office (1)

Aerospace Corporation
Post Office Box 95085
Los Angeles, California 90045
Attn: Technical Library (1)

Atlantic Research Corporation
Shirley Highway at Edsall Road
Alexandria, Virginia 22314
Attn: Technical Library (1)

Battelle Memorial Library
505 King Avenue
Columbus, Ohio 43201
Attn: Edward Unger (1)

Boeing Company
Post Office Box 3999
Seattle, Washington 98124
Attn: Technical Library (1)

Chrysler Corporation
Space Division
Michoud Operations
New Orleans, Louisiana
Attn: Technical Library (1)

Douglas Missiles and Space Systems
Huntington Beach, California
Attn: T. J. Gordon (1)

Hercules Company
Allegany Ballistics Laboratory
Post Office Box 210
Cumberland, Maryland 21502
Attn: Technical Library (1)

Hercules Company
Bacchus Works
Post Office Box 98
Magna, Utah 84044
Attn: Technical Library (1)

Lockheed Missiles and Space Company
Post Office Box 504
Sunnyvale, California
Attn: Technical Library (1)

Lockheed Propulsion Company
Post Office Box 111
Redlands, California 92373
Attn: Bud White (1)

Martin Marietta Corporation
Baltimore Division
Baltimore, Maryland 21203
Attn: Technical Library (1)

Mathematical Sciences Corporation
278 Renook Way
Arcadia, California 91107
Attn: M. Fourney (1)

Philco Corporation
Aeronutronics Division
Ford Road
Newport Beach, California 92660
Attn: F. C. Price (1)

Rocketdyne
Solid Propulsion Operations
Post Office Box 548
McGregor, Texas
Attn: Technical Library (1)

Rocketdyne
6633 Canoga Avenue
Canoga Park, California 91304
Attn: Technical Library (1)

Rohm and Haas
Redstone Arsenal Research Division
Huntsville, Alabama 35807
Attn: Technical Library (1)

Rohr Corporation
Space Products Division
8200 Arlington Boulevard
Riverside, California
Attn: H. Clements (1)

Space Technology Laboratories, Inc.
5730 Arbor Vitae Street
Los Angeles, California 90045
Attn: Technical Library (1)

Thiokol Chemical Corporation
Wasatch Division
Brigham City, Utah 84302
Attn: B. L. Petty (1)

Thiokol Chemical Corporation
Elkton Division
Elkton, Maryland 21921
Attn: Technical Library (1)

Thiokol Chemical Corporation
Huntsville Division
Huntsville, Alabama 35807
Attn: Technical Library (1)

Thompson, Ramo, Wooldridge, Inc.
Structures Division
23444 Euclid Avenue
Cleveland, Ohio 44117
Attn: L. Russell (1)

United Technology Center
Post Office Box 358
Sunnyvale, California 94088
Attn: Technical Library (1)